Journal of Structural Geology xxx (2011) 1–30

Contents lists available at ScienceDirect

Journal of Structural Geology

journal homepage: www.elsevier.com/locate/jsg

Quantifying internal strain and deformation temperature in the eastern Himalaya, Bhutan: Implications for the evolution of strain in thrust sheets

Sean Long*, Nadine McQuarrie, Tobgay Tobgay, Jessica Hawthorne

Department of Geosciences, Princeton University, Princeton, NJ 08544, USA

ARTICLE INFO

Article history:
Received 3 June 2010
Received in revised form
10 December 2010
Accepted 31 December 2010
Available online xxx

Keywords:
Himalaya
Bhutan
Strain
Rf-phi method
Normalized Fry method
Quartz microstructure
Balanced cross-section

ABSTRACT

Quartz microstructural analysis together with quantification of 3-D crystal–plastic strain of quartz clasts (Normalized Fry and Rf-φ methods) constrain deformation temperature ranges and internal strain magnitude/orientation within Himalayan thrust sheets in Bhutan. Lesser Himalayan (LH) thrust sheets display an inverted deformation temperature gradient, from ~250 to 310 °C at the Main Boundary Thrust to ~500–670 °C at the Main Central Thrust (MCT), attributed primarily to stacking of LH thrust sheets deformed at progressively higher temperatures toward the hinterland. The 'hot-iron' effect of the MCT hanging wall only affects the upper few hundred meters of hinterland LH thrust sheets. Frontal thrust sheets exhibit ~7% layer-parallel shortening (LPS) strain. All other thrust sheets exhibit layer-normal flattening (LNF) strain, with 1.9:1.8:1.0 (LH rocks) and 2.1:1.8:1.0 (Greater and Tethyan Himalayan rocks) median ellipsoids (*X* parallel to lineation). We propose that LPS strain developed foreland-ward of the thrust deformation front, and that LNF strain resulted from later tectonic loading. The LPS to LNF transition occurs at minimum temperatures for quartz plasticity (ca. 250–270 °C). LNF ellipsoids are folded along with strata within thrust sheets, indicating that internal strain preceded thrust imbrication and translation. At the scale of 10's of meters structural distance, strain magnitude of hanging wall rocks does not increase near thrusts, which supports the existence of discrete faults with large translations, as generally depicted in balanced cross-sections Strain magnitudes in low-grade Greater and Tethyan Himalayan rocks in central Bhutan indicate that the top-to-the-north component of channel-flow extrusion is most likely less than 19 km.

1. Introduction

Accurate quantification of orogenic deformation requires examination at multiple scales. Studies that focus on macroscopic deformation of entire fold-thrust belts generally consider translation across major thrust faults and map-scale folding as the most significant quantifiable components of deformation (e.g. Dahlstrom, 1969; Boyer and Elliott, 1982; Woodward et al., 1989; Wilkerson and Dicken, 2001). In most orogen-scale balanced cross-sections, the contributions of meso- and microscopic deformation, including minor faults and folds, and internal strain from cleavage development and/or grain-scale fabrics, are not included. However, internal strain may constitute a significant component of total deformation, and must be understood to accurately assess mass balance in orogens (e.g. Mitra, 1994).

Internal deformation can exhibit significant variability as a function of multiple factors, such as spatial position within the fold-thrust belt, material properties of fault zones and hanging wall rocks (e.g. lithology, rheology, mineralogy, grain size), environmental conditions (e.g. deformation temperature, fluid pressure), and boundary conditions (e.g. displacement rate), among others (e.g. Sanderson, 1982). In addition, internal deformation and bulk translation magnitudes can be decoupled; for example, it is possible to have thrust sheets with large bulk displacement and minor internal deformation as well as minor displacement and significant internal deformation (e.g. Elliott, 1977; Mitra, 1994). As a consequence, there is no unique "mode" of internal deformation within orogens, requiring characterization and integration of strain patterns at multiple scales within a fold-thrust-belt. This integration is required to understand the mechanisms and contribution of internal strain of thrust sheets to the total amount of deformation, as well as the relative contributions of large- and small-scale deformation mechanisms during the evolution of a fold-thrust belt.

In the frontal thrust sheets in many orogenic belts, cleavage and grain-scale fabrics often indicate that internal strain is dominated by

* Corresponding author. Present address: Nevada Bureau of Mines and Geology, University of Nevada, Reno, NV 89557, USA. Tel.: +1 775 682 8750; fax: +1 775 784 1709.
E-mail address: splong@unr.edu (S. Long).

0191-8141/$ – see front matter © 2011 Elsevier Ltd. All rights reserved.
doi:10.1016/j.jsg.2010.12.011

low-magnitude, layer-parallel shortening (LPS) that forms early in the deformation history (e.g. Geiser and Engelder, 1983; Mitra, 1994; Ong et al., 2007; Yonkee and Weil, 2009). However, reported LPS strain magnitudes vary significantly, typically between ca. 5 and 30%, and depend strongly on the mechanical strength of the strata being deformed (Crosby, 1969; Engelder, 1979; Nickelsen, 1983; Gockley, 1985; Craddock, 1992; Mitra, 1994; McNaught and Mitra, 1996; Mukul and Mitra, 1998; Faill and Nickelsen, 1999; Yonkee and Weil, 2009). Studies that account for LPS strain in deformation restoration indicate that balanced cross-sections that consider macroscopic structures alone can underestimate cumulative shortening (e.g. Mitra, 1994; McNaught and Mitra, 1996; Yonkee and Weil, 2009).

In hinterland thrust sheets, which are typically deformed at higher temperatures, more widely-varying internal deformation patterns are observed that include components of layer (or thrust)-parallel simple shear, and layer (or thrust)-normal pure shear (e.g. Sanderson, 1982). Sub-simple shear dominated deformation has been documented in many thrust sheets (e.g. Coward and Kim, 1981; Mitra, 1994; Seno et al., 1998; Yonkee, 2005), and the component of simple shear has been observed to increase toward the base in some thrust sheets, possibly reflecting deformation of more viscous hanging wall rocks just above the thrust (Mitra, 1994; Yonkee, 2005). Alternatively, pure shear dominated deformation resulting in thrust-normal thinning accompanied by thrust-parallel extension and/or volume loss has also been observed in many thrust sheets, and is often associated with higher deformation temperatures (e.g. Kligfield et al., 1981; Sanderson, 1982; Mukul and Mitra, 1998; Ring et al., 2001), most likely indicating plastic deformation after significant loss of shear strength of quartz- or mica-rich rocks (Means, 1989; Yonkee, 2005). Several studies have explored the implications of this type of strain on the restored geometry of thrust sheets (e.g. Mitra, 1994; McNaught and Mitra, 1996), and on orogenic taper (Mitra, 1994). However, 3-D geometric complications can arise from multiple factors, including non-plane strain, heterogeneous ductile deformation, uncertainty of the relative contributions of simple- and pure shear (e.g. Yonkee, 2005), volume change accompanying thinning (e.g. Ring et al., 2001) and/or metamorphism, and can add considerable difficulty and uncertainty to assessment of bulk strain of thrust sheets with simple geometric models.

In order to better understand the three-dimensional evolution of deformation, illuminate the sequential development of internal strain mechanisms, magnitudes, and spatial patterns, and to assess the relative contribution of internal strain to large-scale deformation, we have collected extensive thin-section scale data that quantify deformation temperature ranges and 3-D internal strain of Himalayan thrust sheets in the country of Bhutan. The objectives of this paper are to: 1) present quartz and K-feldspar deformation microstructure data that constrain the deformation temperature ranges of Subhimalayan (SH) and Lesser Himalayan (LH) thrust sheets in eastern and central Bhutan, and 2) present an extensive dataset quantifying 3-D crystal–plastic quartz strain in SH and LH thrust sheets in eastern and central Bhutan and a low-grade Greater Himalayan-Tethyan Himalayan section in central Bhutan. These two datasets illuminate multiple aspects of micro-scale deformation, including the role of plane versus 3-D strain, the relative contributions of pure and simple shear (kinematic vorticity), and the sequential development and spatial variation of strain patterns as a function of lithologic, structural, and deformation temperature controls. Recent work in Bhutan that has illustrated the map-scale geometry of the Himalayan fold-thrust belt, and estimated crustal shortening and displacements on major thrust structures (McQuarrie et al., 2008; Long et al., 2011b), facilitates this complementary study focused on micro-scale deformation.

2. Himalayan geologic background

Tertiary collision and continued convergence between the Indian and Eurasian plates have formed the Himalaya–Tibetan Plateau orogenic system (Heim and Gansser, 1939; Gansser, 1964; LeFort, 1975; Hodges, 2000), together the world's highest mountain range and largest elevated plateau. The Himalaya accommodates crustal shortening of the northern part of the Indian plate, and is composed of a south-vergent fold-thrust belt, which detaches and translates thrust sheets of Paleoproterozoic to Recent sedimentary and igneous rocks, that have been metamorphosed to varying extents (Gansser, 1964; Powell and Conaghan, 1973; LeFort, 1975; Mattauer, 1986; Hodges, 2000; DeCelles et al., 2002; Murphy and Yin, 2003; Yin, 2006). Crustal shortening accommodated by the Himalayan fold-thrust belt has been estimated from studies that utilize retro-deformable balanced cross-sections, and shortening estimates range between ca. 400 and 900 km (see compilations in DeCelles et al., 2002 and Long et al., 2011b).

The Himalayan fold-thrust belt is divided into the Subhimalayan (SH), Lesser Himalayan (LH), Greater Himalayan (GH), and Tethyan Himalayan (TH) tectonostratigraphic zones (Fig. 1), which have been imbricated and thrust to the south since the Tertiary collision of the Indian and Asian plates (Heim and Gansser, 1939; Gansser, 1964; Powell and Conaghan, 1973; LeFort, 1975; Mattauer, 1986; Hodges, 2000; Murphy and Yin, 2003; Yin, 2006). The LH, GH, and TH zones are packages of pre-Himalayan sedimentary and igneous rocks of Greater India, and the SH zone represents synorogenic deposits of the Himalayan foreland basin. The SH zone is thrust over modern foreland basin sediments across the Main Frontal Thrust (MFT), the LH zone is thrust over the SH zone across the Main Boundary Thrust (MBT), and the GH zone is thrust over the LH zone across the Main Central Thrust (MCT) (Heim and Gansser, 1939; Gansser, 1964). In most places, the TH zone sits structurally above the GH zone across the South Tibetan Detachment (STD) system (Burg, 1983; Burchfiel et al., 1992), but in several localities the GH–TH contact is interpreted as stratigraphic (Stocklin, 1980; Gehrels et al., 2003; Robinson et al., 2006; Long and McQuarrie, 2010).

3. Bhutan tectonostratigraphy and structural geometry

In the country of Bhutan, which lies in the eastern quarter of the Himalaya (Fig. 1), recent studies have examined the metamorphic and deformational history of the GH zone (Grujic et al., 1996, 2002; Davidson et al., 1997; Daniel et al., 2003; Hollister and Grujic, 2006; Long and McQuarrie, 2010), defined the original stratigraphy of the SH and LH zones (Richards et al., 2006; McQuarrie et al., 2008; Long et al., 2011a), and illustrated the large-scale fold-thrust belt geometry and provided crustal shortening estimates, using detailed mapping and balanced cross-sections (Long et al., 2011b). In this study, we show two areas (Figs. 2 and 3) of the detailed geologic map of eastern and central Bhutan and smaller-scale versions of four balanced cross-sections (Fig. 4), the Trashigang (A-A'), Kuru Chu (B-B'), Bhumtang Chu (C-C'), and Mandge Chu (D-D') sections, originally presented in Long et al. (2011b). For additional details on the geologic map, and the methods, constraints, and shortening estimates obtained from the cross-sections, please refer to Long et al. (2011b).

3.1. Subhimalayan zone

The SH zone consists of the Miocene-Pliocene Siwalik Group, which coarsens upward from siltstone and claystone to sandstone and conglomerate, and has been divided into informal lower, middle, and upper members (Nautiyal et al., 1964; Jangpangi, 1974; Gansser, 1983; Lakshminarayana and Singh, 1995; Long et al., 2011a).

Please cite this article in press as: Long, S., et al., Quantifying internal strain and deformation temperature in the eastern Himalaya, Bhutan: Implications for the evolution of strain in thrust sheets, Journal of Structural Geology (2011), doi:10.1016/j.jsg.2010.12.011

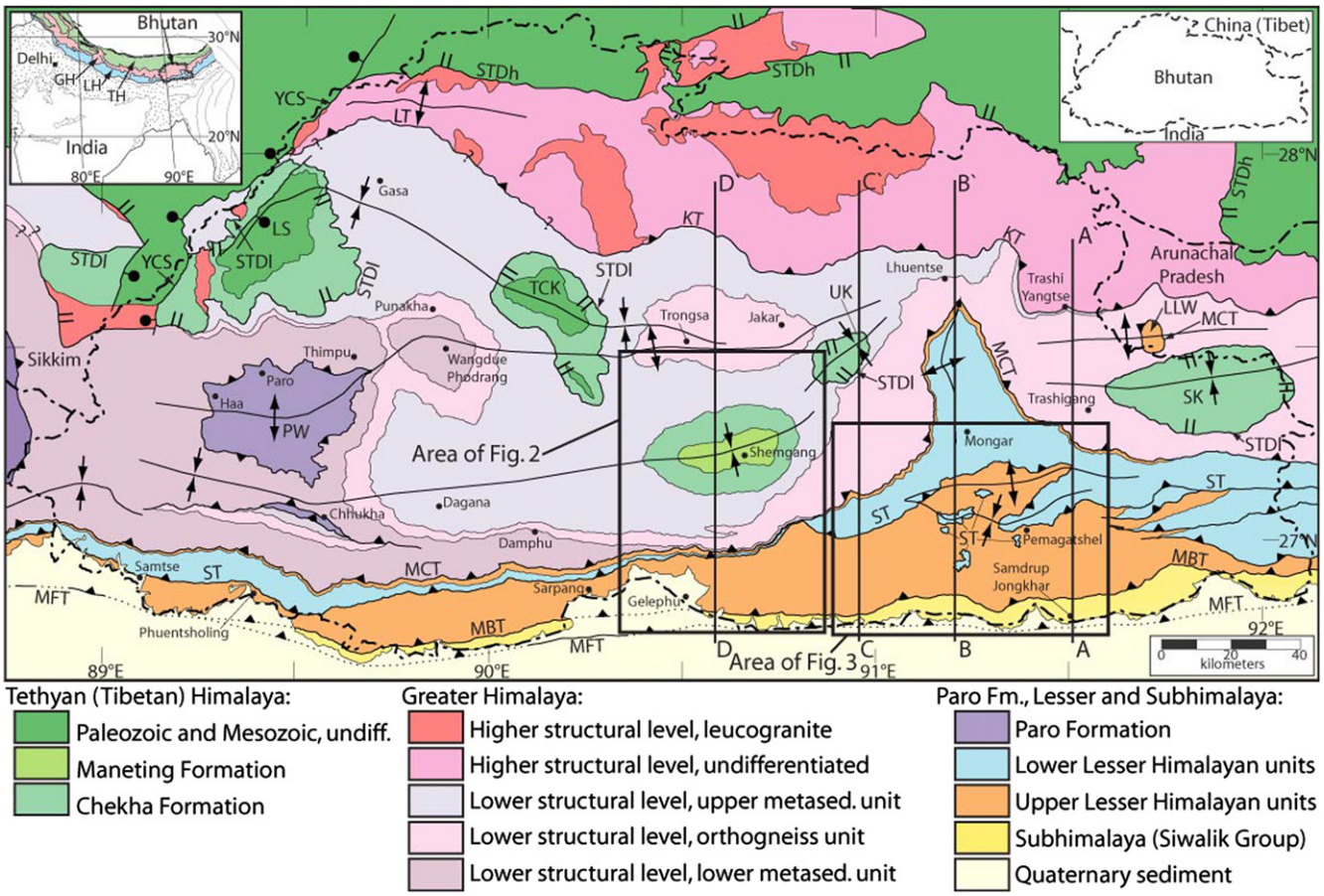

Fig. 1. Simplified geologic map of Bhutan and surrounding region, after Gansser (1983), Bhargava (1995), Grujic et al. (2002), and our own mapping. Area of detailed geologic maps (Figs. 2 and 3) shown, along with lines of section of the four balanced cross-sections (Fig. 4) from Long et al. (2011b). Upper left inset shows generalized geologic map of central and eastern Himalayan orogen (modified from Gansser, 1983). Structural detail from TH section north of central Bhutan compiled from Edwards et al. (1999); map patterns of NE-striking normal faults northwest of Bhutan (Yadong Cross-Stucture) compiled from Wu et al. (1998). Abbreviations: 1) inset: GH: Greater Himalaya, LH: Lesser Himalaya, TH: Tethyan Himalaya: 2) structures from north to south: YCS: Yadong Cross-Structure, STDh: structurally-higher South Tibetan Detachment, LT: Laya Thrust (location from Chakungal et al., 2010), KT: Kakhtang Thrust, STDl: structurally-lower South Tibetan Detachment, MCT: Main Central Thrust, MBT: Main Boundary Thrust, MFT: Main Frontal Thrust; 3) windows and klippen from west to east: LS: Lingshi Syncline, PW: Paro Window, TCK: Tang Chu Klippe, UK: Ura Klippe, SK: Sakteng Klippe, LLW: Lum La Window (location from Yin et al., 2010).

The SH zone consists of a single thrust sheet, uplifted along the MFT (Figs. 2–4) (Long et al., 2011b).

3.2. Lesser Himalayan zone

The Bhutan LH zone consists of 6 map units (Long et al., 2011a): the 1) Shumar Formation and, 2) Daling Formation, which comprise the Paleoproterozoic Daling–Shumar Group, which we refer to as the lower LH section, and the 3) Neoproterozoic-Cambrian(?) Baxa Group, 4) Neoproterozoic–Ordovician(?) Jaishidanda Formation, 5) Permian Diuri Formation, and 6) Permian Gondwana succession, which we refer to as the upper LH section.

The Paleoproterozoic Daling–Shumar Group displays a consistent 2-part stratigraphy of quartzite of the Shumar Formation (1–6 km thick) below schist, phyllite, and quartzite of the Daling Formation (2.2–3.2 km thick) (Nautiyal et al., 1964; Jangpangi, 1974, 1978; Sengupta and Raina, 1978; Gansser, 1983; McQuarrie et al., 2008; Long et al., 2011a). In Bhutan, the lower contact is always a thrust which either repeats the Daling–Shumar Group, or places the Daling–Shumar Group over the Baxa Group (the Shumar Thrust [ST]) (Figs. 2 and 3) (Ray et al., 1989; Ray, 1995; McQuarrie et al., 2008). The upper contact of the Daling–Shumar Group is an unconformity with the overlying Jaishidanda Formation (Long et al., 2011a). An upper stratigraphic contact with the Baxa Group is not observed in Bhutan, but is documented along-strike in Sikkim (Bhattacharyya and Mitra, 2009; Mitra et al., 2010). The combined Daling–Shumar Group and Jaishidanda Formation sections are repeated in a duplex system with the MCT acting as the roof thrust (Fig. 4), which we call the lower LH duplex (Long et al., 2011b).

The Neoproterozoic-Cambrian(?) Baxa Group (1.5–2.6 km thick) consists of coarse-grained to conglomeratic quartzite, interbedded with phyllite and dolomite (Nautiyal et al., 1964; Sengupta and Raina, 1978; Gansser, 1983; Tangri, 1995a; McQuarrie et al., 2008; Long et al., 2011a), and is exposed beneath the ST across Bhutan (Figs. 2 and 3). The Baxa Group is repeated by a series of intraformational thrust faults, creating a duplex system with the ST acting as the roof thrust (Figs. 2–4), which we call the upper LH duplex (Long et al., 2011b). In the southern portions of the duplex, upper stratigraphic contacts with the Diuri Formation and Gondwana succession are exposed (Long et al., 2011a, 2011b).

The Neoproterozoic–Ordovician(?) Jaishidanda Formation (500–1700 m thick) is only exposed under the MCT (Figs. 2 and 3), and consists of biotite-rich, locally garnet-bearing schist interbedded with biotite-rich quartzite (Bhargava, 1995; Dasgupta, 1995; Long et al., 2011a).

Please cite this article in press as: Long, S., et al., Quantifying internal strain and deformation temperature in the eastern Himalaya, Bhutan: Implications for the evolution of strain in thrust sheets, Journal of Structural Geology (2011), doi:10.1016/j.jsg.2010.12.011

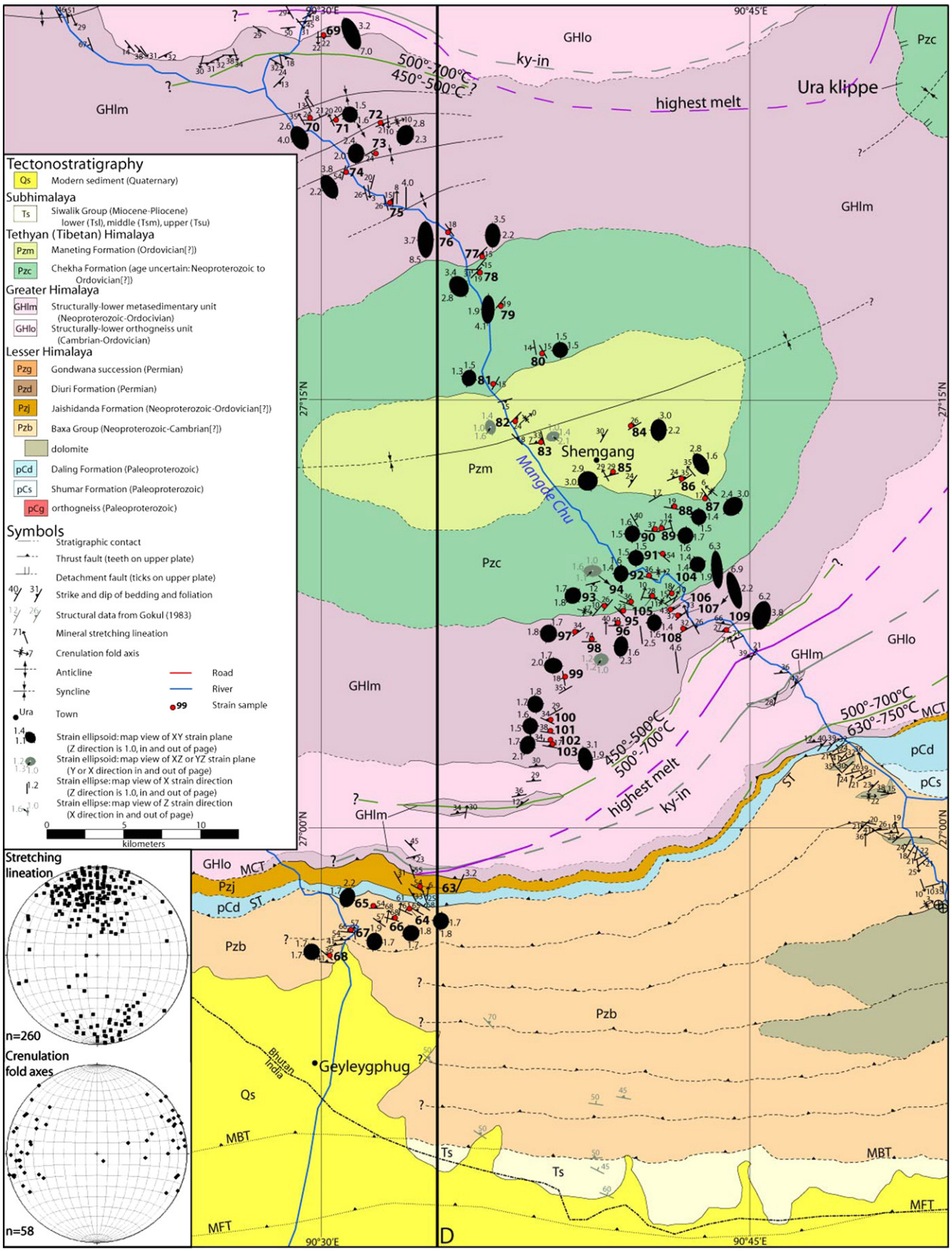

Please cite this article in press as: Long, S., et al., Quantifying internal strain and deformation temperature in the eastern Himalaya, Bhutan: Implications for the evolution of strain in thrust sheets, Journal of Structural Geology (2011), doi:10.1016/j.jsg.2010.12.011

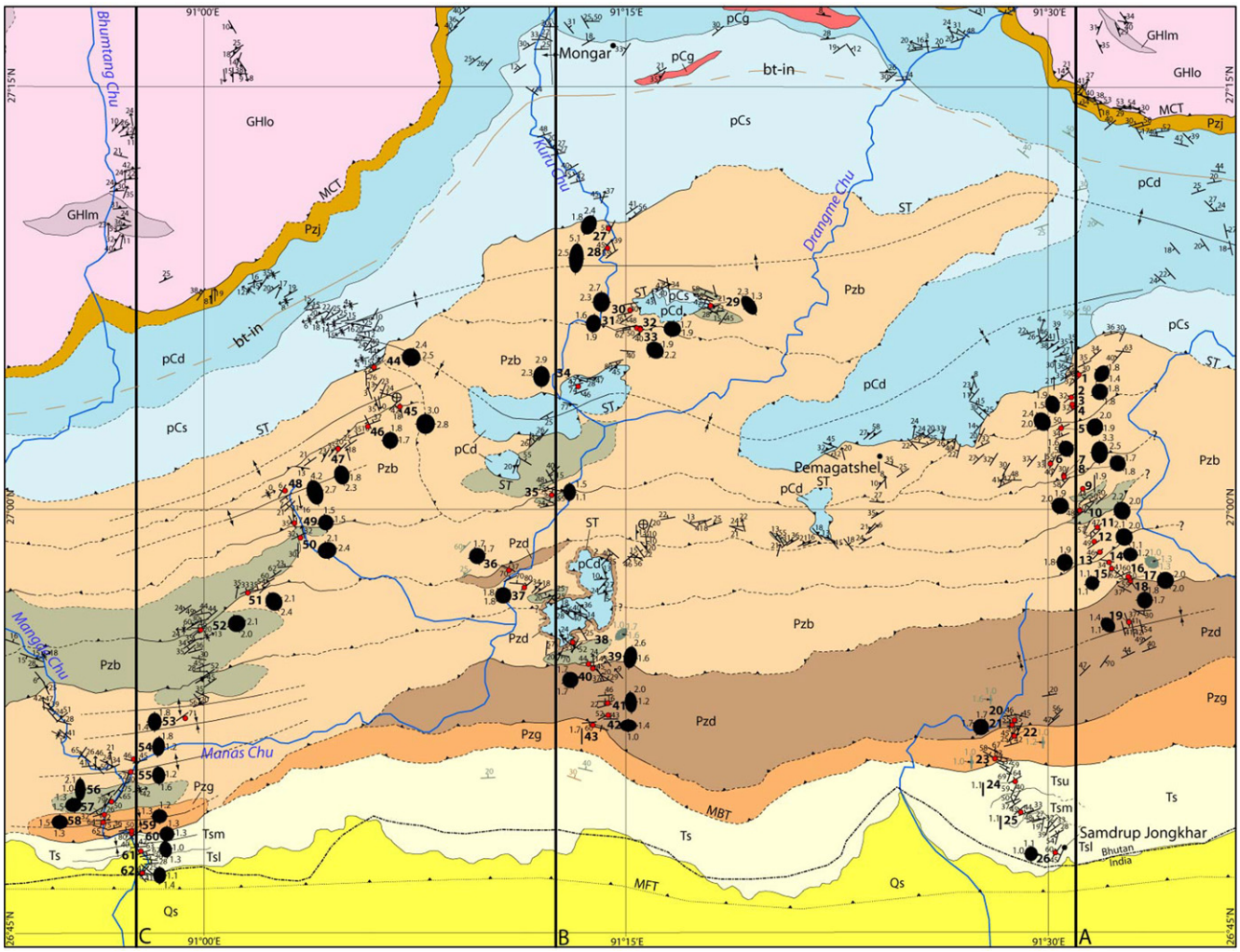

Fig. 3. Geologic map of part of southeast Bhutan; location shown on Fig. 1 (simplified from Fig. 2 of Long et al., 2011b). Black lines with A, B, and C at southern end represent lines of section of Trashigang, Kuru Chu, and Bhumtang Chu cross-sections, respectively (Fig. 4A–C). Stratigraphic position of biotite-in line (solid = observed, dashed = inferred) in Daling–Shumar Group shown. See Fig. 2 and caption for unit abbreviations, map symbols, and description of strain ellipsoids/ellipses; see Fig. 1 caption for structure abbreviations.

The Permian Diuri Formation (2.4–3.0 km thick) consists of pebble-clast diamictite (Jangpangi, 1974; Gansser, 1983; Bhargava, 1995; Tangri, 1995b; McQuarrie et al., 2008; Long et al., 2011a). The Permian Gondwana succession (1.2–2.5 km thick) consists of sandstone, carbonaceous siltstone and shale, and coal (Gansser, 1983; Gokul, 1983; Bhargava, 1995; Joshi, 1995; Lakshminarayana, 1995; McQuarrie et al., 2008; Long et al., 2011a). The Diuri Formation and Gondwana succession are each carried by thrust faults in southeast Bhutan (Fig. 3).

3.3. Greater Himalayan zone

The GH zone is divided into a lower structural level above the MCT and below the Kakhtang Thrust (KT), and a higher structural level above the KT (Figs. 1 and 4) (Grujic et al., 2002). The structurally-higher GH section consists of migmatitic orthogneiss and metasedimentary rocks, and Miocene leucogranite (Fig. 1) (Gansser, 1983; Swapp and Hollister, 1991; Davidson et al., 1997; Grujic et al., 2002). The structurally-lower GH section consists of a lower, Cambrian–Ordovician granitic orthogneiss unit and an upper metasedimentary unit, comprised of quartzite, schist, phyllite, and paragneiss (Long and McQuarrie, 2010) (Fig. 1). Detrital zircon ages indicate a Neoproterozoic to Cambrian–Ordovician (or younger) deposition age range for the GH metasedimentary unit (Richards et al., 2006; Long and McQuarrie, 2010).

Subparallel bedding and tectonic foliation above and below the MCT indicate a hanging wall flat over footwall flat relationship over LH rocks (Fig. 4), and that the hanging wall cutoff for the GH section has passed through the erosion surface (Long et al., 2011b). Tectonic foliation in orthogneiss, schist, and phyllite are approximately parallel

Fig. 2. Geologic map of part of south-central Bhutan; location shown on Fig. 1 (simplified from Fig. 2 of Long et al., 2011b). See Fig. 1 caption for structure abbreviations. Black line with 'D' at southern end represents line of section of Mandge Chu cross-section (Fig. 4D). Temperature constraints from quartz recrystallization microstructure (630°–750 °C – GBM recrystallization with chessboard extinction; 500°–700 °C – GBM recrystallization; 450°–500 °C – SGR recrystallization with K-feldspar recrystallization; from Long and McQuarrie, 2010; see Section 4.6 and Fig. 7) are indicated by solid (observed) and dashed (inferred) lines; also shown are stratigraphic positions of highest occurrence of partial melt texture (lower limit is MCT), and kyanite-in line (from Long and McQuarrie, 2010). 3-D strain ellipsoids and 2-D strain ellipses are projected onto the map by rotating bedding/foliation of each sample to horizontal (Table SM1 caption). The strain plane that most closely approximates horizontal after rotation is projected. Black ellipsoids represent the *XY* strain plane (*Z* axis is in and out of page, and has Rs of 1.0), and gray ellipsoids represent either the *XZ* or *YZ* strain plane (*X* or *Y* axis is in and out of page). The Rs and azimuth of the *X* axis of the 2-D strain ellipse are shown for three samples (*Z* axis is in and out of page). Ellipsoids and ellipses are all scaled to constant volume. Lower left inset shows equal-area stereonet plots of orientations of mineral stretching lineation and crenulation fold axes for LH, GH, and TH units in eastern and central Bhutan (from Long et al., 2011b).

Please cite this article in press as: Long, S., et al., Quantifying internal strain and deformation temperature in the eastern Himalaya, Bhutan: Implications for the evolution of strain in thrust sheets, Journal of Structural Geology (2011), doi:10.1016/j.jsg.2010.12.011

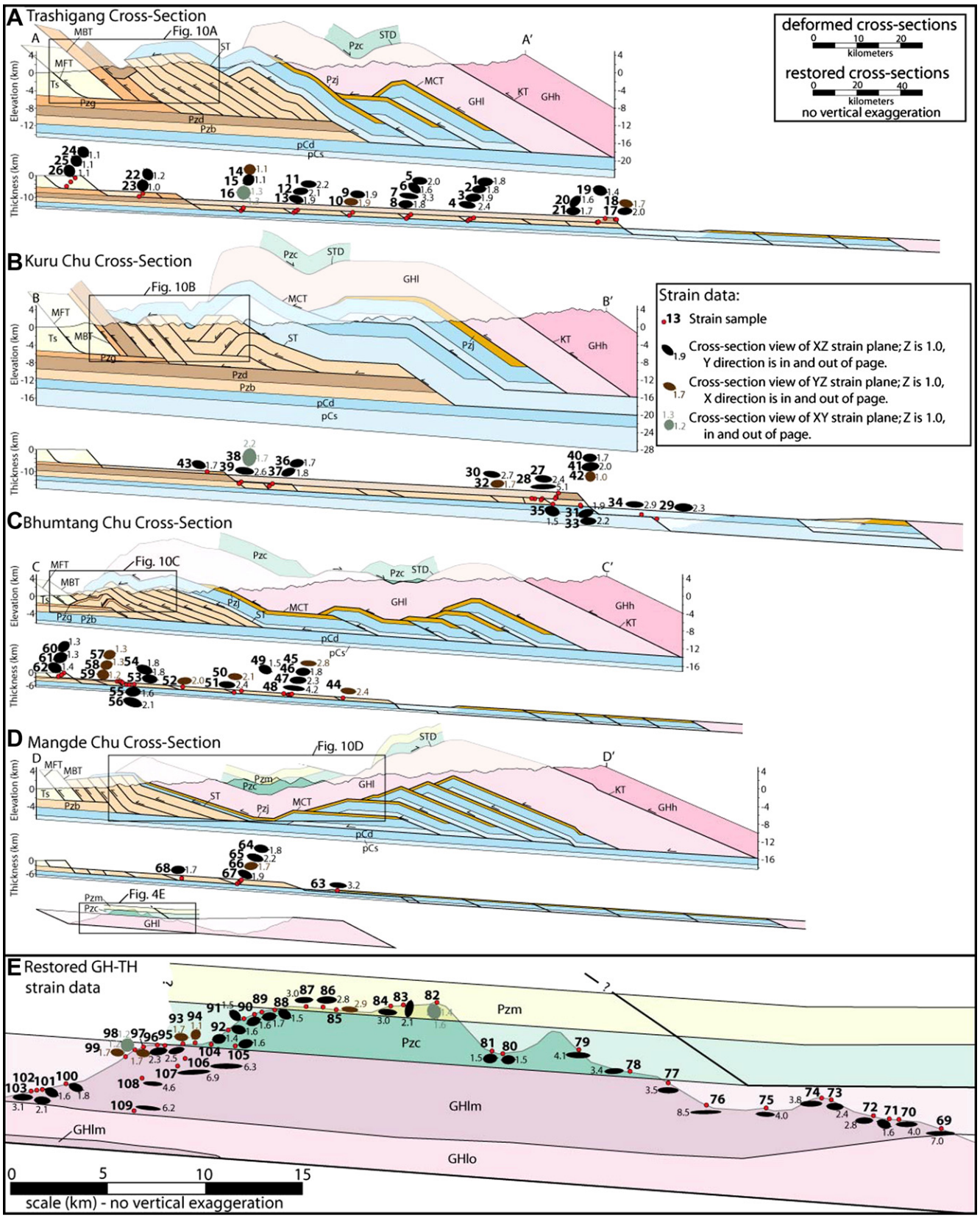

Fig. 4. A–D) Deformed and restored balanced cross-sections of Bhutan fold-thrust belt (simplified from Fig. 3 of Long et al., 2011b; readers are referred to this paper for details on methods of construction, constraints, and details on shortening estimates). Locations of lines of section shown on Figs. 1–3. Note that restored sections are shown at a smaller scale than deformed sections. Translucent areas represent rock that has passed above the modern erosion surface. Insets on deformed sections are referenced to Fig. 10. See Fig. 2 for unit abbreviations; see Fig. 1 caption for structure abbreviations. Note that the stratigraphy of the structurally-lower and higher GH sections are simplified to GHl and GHh, respectively. Strain ellipses from thin sections that approximate N-S (lineation-parallel, crenulation fold axis-perpendicular, dip direction-parallel, or N-S; see Section 5.1) are projected directly onto the restored cross-sections. The 3-D ellipsoids defined by these analyses are all scaled to constant volume (see Figs. 2 and 3), and the 2-D ellipses on this figure are scaled

Please cite this article in press as: Long, S., et al., Quantifying internal strain and deformation temperature in the eastern Himalaya, Bhutan: Implications for the evolution of strain in thrust sheets, Journal of Structural Geology (2011), doi:10.1016/j.jsg.2010.12.011

to quartzite bedding (Long and McQuarrie, 2010; Long et al., 2011b), and exhibit regional-scale, east-west trending folds attributed to growth of the underlying lower LH duplex (Figs. 1 and 4). The lower GH section is ~8 km thick across eastern Bhutan (Fig. 4A–C), and in central Bhutan the section thickens to the north, from 5.3 km above the MCT and below TH units to 10.5 km below the KT (Fig. 4D) (Long et al., 2011b).

3.4. Tethyan Himalayan zone

Several isolated exposures of greenschist-facies Precambrian (inferred) through Mesozoic metasedimentary rocks of the TH zone lie above the GH section in the axes of synforms (Fig. 1) (Gansser, 1983; Bhargava, 1995; Edwards et al., 1996; Grujic et al., 2002). The basal TH unit consists of quartzite and biotite–muscovite-garnet schist and is referred to as the Chekha Formation. The overlying Maneting Formation (>1.0 km thick) consists of biotite–garnet phyllite (Tangri and Pande, 1995; Long and McQuarrie, 2010). In our study area, these are the only TH units exposed; Paleozoic and Mesozoic TH units are limited to western Bhutan (Gansser, 1983; Bhargava, 1995).

Four of the five isolated TH exposures have been interpreted as klippen above the STD (Grujic et al., 2002), based on field evidence for top-to-the-north sense shear zones at the base of the Chekha Formation. However, in the Shemgang region the Chekha Formation is in interfingering depositional contact above GH metasedimentary rocks (Long and McQuarrie, 2010), requiring the GH and TH sections there to be part of the same thrust sheet (Fig. 4D). The maximum permissible northern and southern locations for footwall and hanging wall ramps through the Chekha Formation are shown on Fig. 4C and D, and these geometries constrain displacement on the STD to ~20 km (Long and McQuarrie, 2010; Long et al., 2011b).

4. Deformation temperature constraints

One of the most intriguing characteristics of the LH zone is its inverted metamorphic gradient, which is defined by the general upsection progression to higher temperatures and pressures as the MCT is approached, with metamorphic isograds approximately parallel to the MCT (Heim and Gansser, 1939; Gansser, 1964; LeFort, 1975; Pecher and LeFort, 1986; Harrison et al., 1998; Hodges, 2000; Robinson et al., 2003). This is documented in multiple field-based studies across the orogen (e.g. Arita, 1983; Gansser, 1983; Hubbard, 1989; Harrison et al., 1997; Stephenson et al., 2000; Catlos et al., 2001; Kohn et al., 2001; Dasgupta et al., 2004), and has been an important constraint in several models of Himalayan deformation (e.g. LeFort, 1975; Harrison et al., 1998; Robinson et al., 2003).

In Bhutan, previous research has documented an inverted metamorphic gradient at the scale of the entire LH section, with metamorphic isograds approximately parallel to the MCT (Gansser, 1983). The metamorphic map of Gansser (1983) (simplified in Grujic et al., 1996) shows an S–N increase from lower greenschist facies at the MBT, to upper greenschist facies, to lower amphibolite facies in the northern Kuru Chu valley just under the MCT.

The most influential hypothesis for the origin of inverted LH metamorphism is that it represents footwall contact metamorphism from the hot GH rocks in the hanging wall of the MCT ('hot-iron' effect; LeFort, 1975). Alternatively, studies in central Nepal argue that inverted metamorphism is not observed within individual LH thrust sheets, but rather is the result of stacking multiple LH thrust sheets, with each structurally-higher sheet carrying progressively higher-grade rocks (Robinson et al., 2003; Martin et al., 2005, 2010). In order to differentiate between the 'hot-iron' and thrust sheet-stacking hypotheses, to estimate the depths of deformation of individual LH thrust sheets, and to compare temperature trends with the magnitudes, spatial patterns, and mechanisms of strain that we document below, we have performed extensive analysis of quartz and K-feldspar microstructure to semi-quantitatively constrain deformation temperature ranges. This data is presented below for each individual LH and SH map unit in Bhutan that has been deformed as a unique structural package, including the Siwalik Group thrust sheet, Gondwana succession thrust sheet, Diuri Formation thrust sheet, and Baxa Group thrust sheets in the upper LH duplex (Long et al., 2011b). We discuss the Daling–Shumar Group and Jaishidanda Formation sections together, because these rock units were detached and translated together in individual thrust sheets to form the lower LH duplex (Long et al., 2011b).

4.1. Daling–Shumar Group and Jaishidanda Formation (lower Lesser Himalayan duplex)

4.1.1. Metamorphic mineral assemblages

In the Kuru Chu valley, metamorphism in the Daling–Shumar–Jaishidanda section increases from upper greenshist facies at the base, to biotite-zone upper greenschist facies in mid structural levels, to lower amphibolite facies just beneath the MCT (Gansser, 1983; Grujic et al., 1996). The lower amphibolite facies LH rocks correspond with garnet-bearing Jaishidanda Formation schist (Daniel et al., 2003; Long et al., 2011a).

We observe foliation-parallel muscovite neoblasts in all lithologies, including quartzite (typically between ~0.1 and 0.5 mm-long; Fig. 5A and D), and phyllite and schist (typically multiple-mm size; Fig. 5E and J) of the Jaishidanda Formation and the Daling–Shumar Group. These include all strata that are structurally above the ST and below the MCT (Fig. 5A,D and E). Foliation-parallel biotite neoblasts, typically between 0.1 and1.0 mm long (Fig. 5D and E), are lacking at the base of the section, but are present in stratigraphically-higher parts of the section, closer to the MCT (Gansser, 1983). The first appearance of biotite neoblasts in the two Kuru Chu valley sections is in the upper part of the Shumar Formation, and is repeated in both thrust sheets (Fig. 6C). To the east and west of the Kuru Chu, the first appearance of biotite neoblasts is within the Daling Formation (Figs. 5D, E, J and 6A, D, E). The biotite-in line varies between ~1300 and 2600 m structural distance below the MCT east and west of the Kuru Chu valley (Fig. 6A,D and E), to a maximum of ~5800–6000 m beneath the MCT in the Kuru Chu valley (Fig. 6C).

Garnet porphyroblasts (typically ~1–3 mm in diameter; Fig. 5J) first occur within Jaishidanda Formation schist, and the garnet-in line varies between ~200 and 500 m structural distance beneath the MCT east and west of the Kuru Chu valley (Fig. 6B,D and E), to a maximum of ~1000 m beneath the MCT in the northern Kuru Chu thrust sheet (Fig. 6C). Garnet was not observed along the

accordingly. All map units are restored to a regional dip of 4°N (Long et al., 2011b), and all strain ellipses are rotated so that they differ from this regional dip by θ' (the angle between bedding/foliation and the long direction of the strain ellipse in the view plane; see Section 5.1 and Table SM1 caption), which restores them to an undeformed orientation. Black ellipses ($n = 87$) represent the *XZ* strain plane (*Y* axis is in and out of page), with Rs of *X* shown. Brown ellipses ($n = 18$) represent the *YZ* strain plane (*X* axis is in and out of page), with Rs of *Y* shown. Gray strain ellipsoids ($n = 4$) represent the *XY* strain plane (*Z* axis in and out of page). E) Inset showing strain ellipses from GH and TH rocks on the Mandge Chu cross-section restored to an undeformed orientation. Samples 69–82 are on Trongsa transect, samples 83–103 are on Sure transect, and samples 104–109 are on Gonphu transect of Long and McQuarrie (2010). Strain ellipsoids are scaled to constant volume. (For interpretation of the references to colour in this figure legend, the reader is referred to the web version of this article).

Please cite this article in press as: Long, S., et al., Quantifying internal strain and deformation temperature in the eastern Himalaya, Bhutan: Implications for the evolution of strain in thrust sheets, Journal of Structural Geology (2011), doi:10.1016/j.jsg.2010.12.011

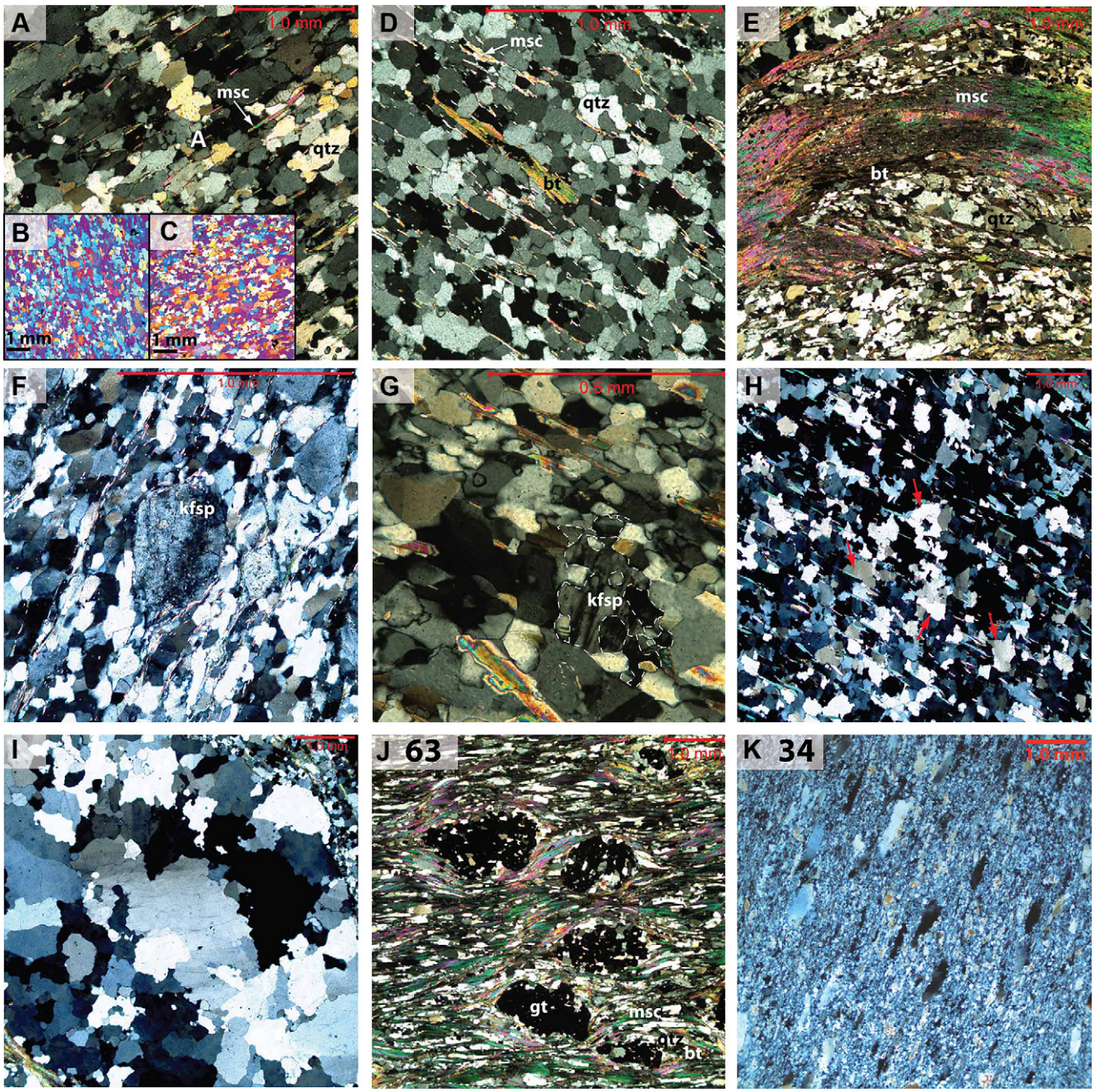

Fig. 5. Photomicrographs of Daling–Shumar Group and Jaishidanda Formation thin-sections (cross-polarized light). All thin sections cut perpendicular to quartzite bedding or schist tectonic foliation, and parallel to mineral stretching lineation. Photomicrographs A–G display granoblastic texture of equigranular, polygonal, ~0.1–0.2 mm diameter, recrystallized quartz subgrains, interpreted as evidence for SGR recrystallization in which all relict grains (porphyroclasts) have been completely recrystallized. A) Quartzite from lower Shumar Formation section in Kuru Chu valley, displaying ~0.1–0.5-mm muscovite neoblasts; note lack of biotite neoblasts. B, C) Quartzite from Jaishidanda Formation west of Mongar; photos taken with gypsum plate inserted; C is same area of sample as B, but rotated 90° counterclockwise. Dominance of blue in B and yellow in C illustrates crystallographic preferred orientation, which is present in most Daling, Shumar, and Jaishidanda quartzite samples. D) Quartzite from Daling Formation east of Mongar, displaying ~0.05–0.5-mm neoblastic muscovite and biotite. E) Biotite–muscovite-quartz schist from upper Shumar Formation in northern Kuru Chu valley. F) Quartzite from lower Daling Formation south of Trashigang; note ductile elongation and sweeping extinction of K-feldspar porphyroclast. G) Quartzite from middle Daling Formation in northern Kuru Chu valley; note recrystallization of K-feldspar porphyroclast into multiple subgrains (outlined). H) Quartzite from upper Jaishidanda Formation on Bhumtang Chu transect exhibiting variable grain size and formation of amoeboid 'island' grains up to ~0.5-mm in diameter, surrounded by smaller subgrains; this is interpreted as a transitional texture between GBM and SGR recrystallization. I) Quartzite from top of Daling Formation in southern Kuru Chu valley thrust sheet. Exhibits 'amoeboid' grain microstructure and multiple-mm grain size characteristic of GBM recrystallization. J) Strain sample 63: garnet–muscovite–biotite schist of Jaishidanda Formation, north of Geylegphug. Note isolated, plastically-elongated, non-recrystallized quartz clasts surrounded by muscovite–biotite matrix. K) Strain sample 34: Quartzite from Daling Formation klippe in southern Kuru Chu valley. Note ~90% volume proportion of recrystallized quartz subgrains, which form a matrix surrounding elongated ribbon porphyroclasts up to ~1.0 mm long. (For interpretation of the references to colour in this figure legend, the reader is referred to the web version of this article).

Please cite this article in press as: Long, S., et al., Quantifying internal strain and deformation temperature in the eastern Himalaya, Bhutan: Implications for the evolution of strain in thrust sheets, Journal of Structural Geology (2011), doi:10.1016/j.jsg.2010.12.011

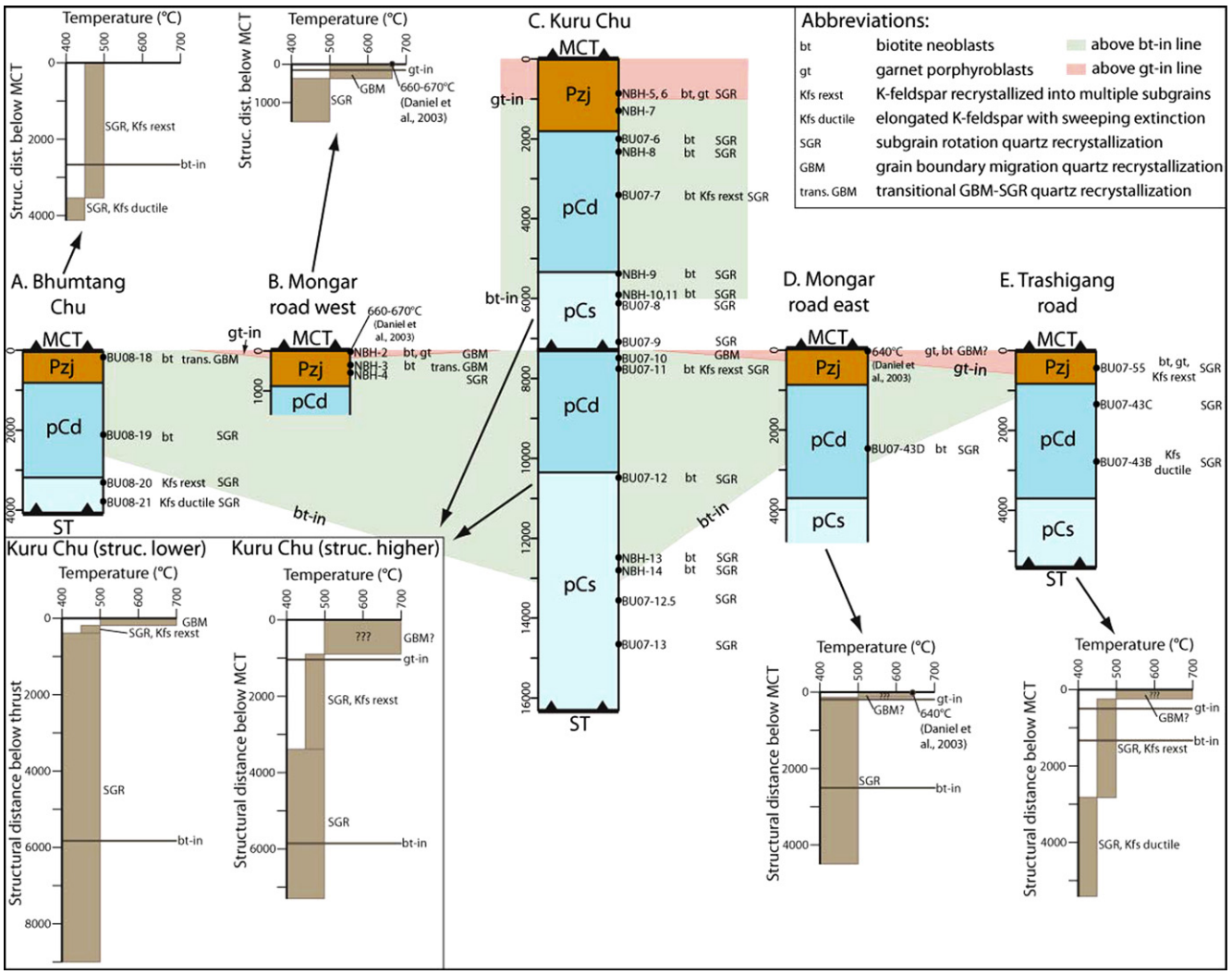

Fig. 6. Stratigraphic columns of transects through the Shumar–Daling–Jaishidanda section in eastern Bhutan, from west (left) to east (right). Text to the right of each column shows stratigraphic locations of thin sections, metamorphic minerals (note: neoblastic muscovite is present at all stratigraphic levels), quartz recrystallization mechanism, and K-feldpsar deformation mechanism. Green shaded area represents part of section above biotite-in line, and red shaded area represents part of section above garnet-in line. Temperature profiles for each column show constraints from quartz and feldspar deformation microstructure, and peak metamorphic temperatures of garnet obtained just beneath the MCT (Daniel et al., 2003). (For interpretation of the references to colour in this figure legend, the reader is referred to the web version of this article).

Bhumtang Chu or at the top of the structurally-lower thrust sheet in the Kuru Chu valley (Fig. 6A and C), but this may be due to the abundance of quartzite and lack of schist at the top of these sections. Daniel et al. (2003) reported peak metamorphic conditions of 640°–670 °C and 9–13 kbar from Jaishidanda Formation garnets, collected from samples within 20 m structural distance below the MCT east and west of Mongar (Fig. 6B and D).

4.1.2. Quartz and feldspar microstructure

Quartz microstructure throughout the Daling–Shumar and Jaishidanda sections exhibits a granoblastic or 'foam' texture (Schmid, 1994), with equigranular, polygonal porphyroclasts, typically ~0.1–0.2 mm in diameter (Fig. 5A–G). This texture is indicative of dynamic recrystallization through progressive subgrain rotation (SGR) (Poirier and Nicolas, 1975; White, 1977; Guillope and Poirier, 1979), in which all relict grains have been completely consumed. SGR recrystallization indicates deformation at temperatures between ca. 400° and 500 °C (Stipp et al., 2002). SGR deformation corresponds with the higher-temperature part of dislocation creep regime 2 of Hirth and Tullis (1992) (Stipp et al., 2002). Recrystallized quartz subgrains show a weak shape-preferred orientation with aspect ratios generally less than 2:1. Many Daling, Shumar, and Jaishidanda quartzite samples exhibit a crystallographic preferred orientation when viewed with a gypsum plate (Fig. 5B and C).

An upsection change from ductile elongation of K-feldspar (Fig. 5F) to recrystallization of K-feldspar into subgrains (Fig. 5G) is observed in two transects. On the Bhumtang Chu transect, this transition occurs in the Shumar Formation (Fig. 6A), and south of Trashigang this transition occurs in the middle of the Daling Formation (Fig. 6E). Recrystallization of K-feldspar indicates a minimum deformation temperature of ca. 450 °C (Voll, 1976; Tullis and Yund, 1980; Pryer, 1993).

Quartz microstructure indicative of recrystallization through grain boundary migration (GBM), which occurs between ~500° and 700 °C (Stipp et al., 2002), is observed at the top of the lower LH section on three transects (Fig. 6A–C). Irregular grain size distribution with incipient nucleation of 'island' grains up to ~0.5 mm in diameter (Fig. 5H), which we interpret as a transitional GBM-SGR texture (e.g. Stipp et al., 2002), is observed within 350 m structural distance below the MCT west of the Kuru Chu (Fig. 6A and B). The SGR-GBM transition corresponds with dislocation creep regime 3 of Hirth and Tullis (1992) (Stipp et al., 2002). 'Amoeboid' grains with

Please cite this article in press as: Long, S., et al., Quantifying internal strain and deformation temperature in the eastern Himalaya, Bhutan: Implications for the evolution of strain in thrust sheets, Journal of Structural Geology (2011), doi:10.1016/j.jsg.2010.12.011

highly-irregular, interfingering boundaries and multiple-mm grain size characteristic of GBM recrystallization (Fig. 5I) (Stipp et al., 2002) are observed at 10 m structural distance below the MCT west of Mongar (Fig. 6B), and at 100 m structural distance below the Shumar over Daling thrust in the Kuru Chu valley (Fig. 6C).

4.1.3. Summary of deformation temperature

The quartz and feldspar deformation microstructure summarized above (Fig. 6) combined with peak metamorphic temperature estimates of garnet at the MCT (Daniel et al., 2003) constrain a composite deformation temperature profile of the Shumar–Daling–Jaishidanda section (Fig. 7). At the base of the section, SGR quartz recrystallization combined with a lack of K-feldspar recrystallization indicates deformation at ca. 400°–450 °C. Higher in the section, SGR quartz recrystallization combined with K-feldspar recrystallization indicates deformation at ca. 450°–500 °C. Within 350 m below the MCT, transitional GBM-SGR recrystallization indicates deformation at ca. 500 °C. Above this level, GBM recrystallization indicates deformation above 500 °C and below 640°–670 °C, the peak metamorphic temperature range of garnet at the MCT (Daniel et al., 2003).

These temperature ranges correspond very well with ca. 450°–510 °C deformation temperatures (from bottom to top of section) obtained from Raman spectroscopy on carbonaceous material in Daling–Shumar–Jaishidanda rocks south of Trashigang (Whynot et al., 2010).

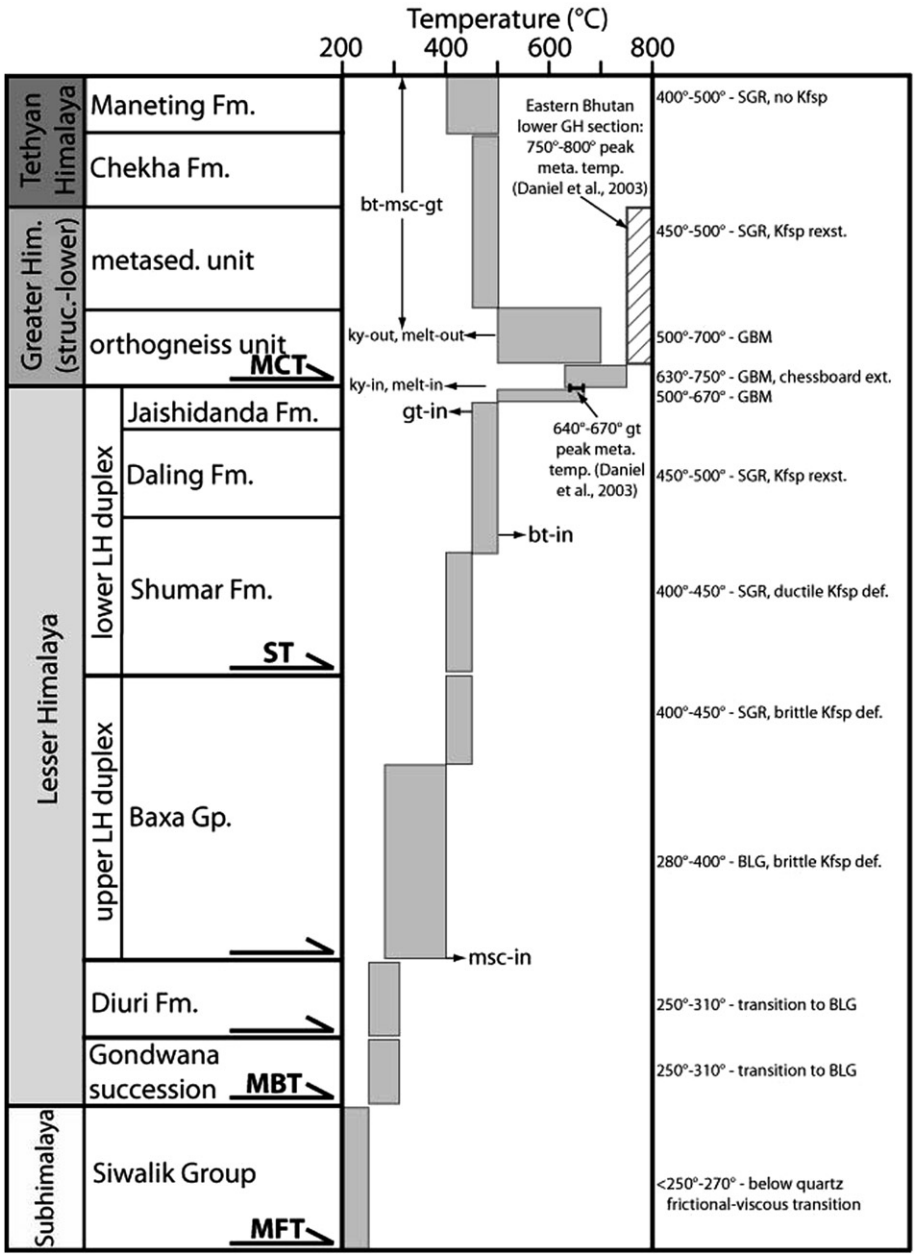

Fig. 7. Deformation temperature profile through thrust sheets of the Bhutan Himalaya, as constrained by quartz and feldspar deformation microstructure. Gray boxes show deformation temperature range for individual thrust sheets. Approximate stratigraphic positions of metamorphic mineral isograds shown. Data for Shumar, Daling, and Jaishidanda thrust sheets are composite and generalized from Fig. 6. Temperature and metamorphic mineral data from GH and TH units are generalized from the Shemgang area in central Bhutan (Long and McQuarrie, 2010). Peak metamorphic temperature estimates from structurally-lower GH section in eastern Bhutan (cross-hatched pattern) and from garnet in Jaishidanda Formation are from Daniel et al. (2003). Quartz recrystallization abbreviations: BLG – bulging, SGR – subgrain rotation, GBM – grain boundary migration.

Please cite this article in press as: Long, S., et al., Quantifying internal strain and deformation temperature in the eastern Himalaya, Bhutan: Implications for the evolution of strain in thrust sheets, Journal of Structural Geology (2011), doi:10.1016/j.jsg.2010.12.011

4.2. Baxa Group horses (upper Lesser Himalayan duplex)

Mineral assemblages and quartz and feldspar microstructure from Baxa Group samples indicate cooler deformation temperatures than the Daling–Shumar–Jaishidanda section. Baxa Group quartzite and phyllite lack neoblastic biotite, but syn-deformational growth of neoblastic muscovite up to ~0.5 mm-long is observed throughout the section, in extensional fractures in K-feldspar (Fig. 8A) and in

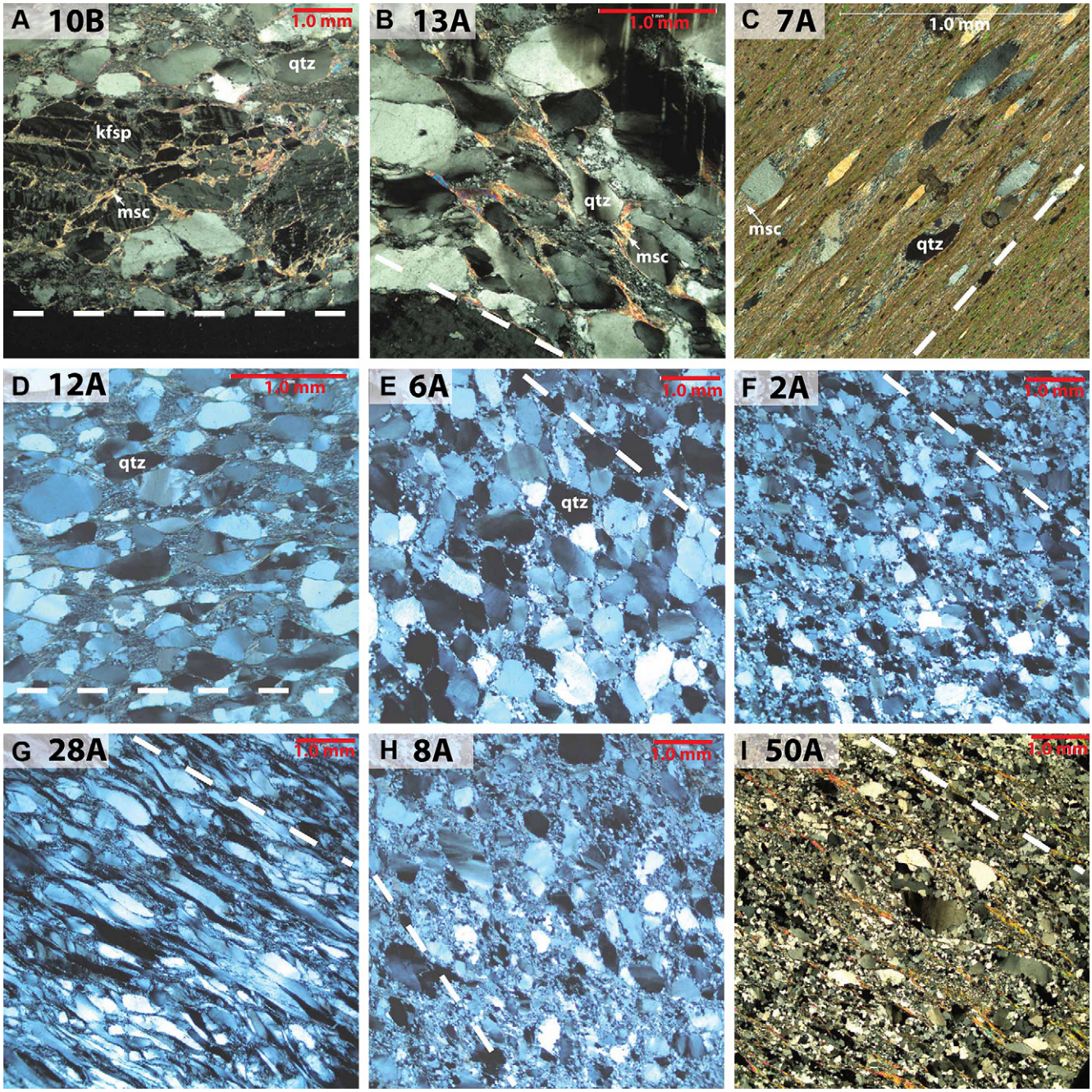

Fig. 8. Photomicrographs illustrating mineralogy and range of deformation microstructure observed in the Baxa Group (cross-polarized light). All thin sections cut perpendicular to quartzite bedding or phyllite tectonic foliation, and parallel to mineral stretching lineation, except for A, which is cut perpendicular to lineation. White dashed line shows apparent dip of quartzite bedding or phyllite tectonic foliation in plane of thin section. Strain sample numbers shown for each; refer to Fig. 3 for sample locations. A) Sample 10B: Bedding-normal extensional fracturing of K-feldspar, with syn-deformational growth of neoblastic muscovite in fractures. B) Sample 13A: Growth of syn-deformational muscovite in pressure shadows between quartz grains that are plastically-elongated parallel to bedding. C) Sample 7A: Microstructure characteristic of Baxa Group phyllite; quartz clasts are isolated within a mica-rich (typically ~10 um or greater grain size) matrix, and plastically-elongated parallel to tectonic foliation. Note neoblastic muscovite growth in quartz clast pressure shadows. D) Sample 12A: Microstructure characteristic of micaceous Baxa Group quartzite; quartz clasts are isolated within mica-rich (typically ~10 um or greater grain size) matrix (~25% volume fraction), and plastically-elongated subparallel to bedding. E) Sample 6A: Microstructure characteristic of clast-supported Baxa Group quartzite, which comprises the majority of strain samples; note formation of ~0.1 mm-diameter subgrains localized at quartz clast boundaries, characteristic of bulging recrystallization. F) Sample 2A: Core-and-mantle microstructure of strained quartz clasts surrounded at their boundaries by a matrix of ~0.1 mm-diameter recrystallized subgrains. This texture appears with a ≥25% volume fraction of subgrains, and is the approximate transition point from bulging-dominated recrystallization to subgrain rotation recrystallization (Stipp et al., 2002). G, H, I) Baxa Group quartzite displaying high volume proportions of recrystallized subgrains, between ~40% (G), ~60% (H), and ~80% (I), which forms a matrix texture that surrounds isolated ribbon porphyroclasts. These microstructures are typically observed only in the northern portions of Baxa Group exposure, near the Shumar Thrust, and indicate subgrain rotation recrystallization. Note that G (sample 28A) is the most highly-strained Baxa Group sample observed (Rs[*XZ*] = 5.1).

Please cite this article in press as: Long, S., et al., Quantifying internal strain and deformation temperature in the eastern Himalaya, Bhutan: Implications for the evolution of strain in thrust sheets, Journal of Structural Geology (2011), doi:10.1016/j.jsg.2010.12.011

pressure shadows between elongated quartz clasts (Fig. 8B and C) indicating the occurrence of mass transfer deformation.

Quartz microstructure of the Baxa Group is dominated by plastically-elongated clasts, typically 0.5–1.0 mm-long, with sweeping or undulose extinction (Fig. 8B). In phyllite and micaceous quartzite (typically up to ~25% matrix volume fraction; Fig. 8D), elongated quartz grains are isolated within a typically ~10 um or larger grain size, mica-rich matrix (Fig. 8C and D). However, the majority of Baxa Group quartzite displays dynamic recrystallization of quartz through formation of subgrains, typically ~0.1 mm in diameter, localized at grain boundaries (Fig. 8E). This texture is characteristic of bulging (BLG) recrystallization (Bailey and Hirsch, 1962; Drury et al., 1985; Stipp et al., 2002), and indicates deformation at temperatures between ~280° and 400 °C (Fig. 7) (Stipp et al., 2002). Extensive subgrain formation during BLG recrystallization corresponds to the lower temperature domain of dislocation creep regime 2 of Hirth and Tullis (1992) (Stipp et al., 2002). Our estimated temperature ranges correspond very well with ca. 350° deformation temperatures obtained from Raman spectroscopy on carbonaceous material in Baxa Group rocks south of Trashigang (Whynot et al., 2010).

When the volume proportion of recrystallized grains is ≥25%, quartz microstructure takes on a core-and-mantle appearance (Fitzgerald and Stunitz, 1993; Stipp et al., 2002), with strained quartz clasts surrounded by a matrix of recrystallized subgrains (Fig. 8F). Subgrain volume proportions as high as ~40–80% are observed in Baxa Group quartzite, typically only in the northern extent of exposure, near the ST. This texture forms a matrix of subgrains that surrounds isolated ribbon porphyroclasts (Fig. 8G–I). Stipp et al. (2002) documented that the transition from BLG to SGR recrystallization, which represents temperature conditions of ~400 °C, occurs at a ~25% subgrain volume proportion. The highly-recrystallized (>25%) Baxa Group quartzite samples we observe were likely dominated by SGR, which occurs between 400° and 500 °C (Stipp et al., 2002). However, K-feldspar deforms through brittle fracturing (Fig. 8A) throughout the entire Baxa Group section, which indicates that SGR deformation temperatures were likely less than ca. 450 °C (Fig. 7), the lower temperature limit of feldspar recrystallization (Voll, 1976; Tullis and Yund, 1980; Pryer, 1993). These higher deformation temperatures, which are observed only in close proximity to the ST, could be the result of emplacement of hotter Daling–Shumar rocks above, and/or shear heating associated with emplacement of the ST.

4.3. Diuri Formation thrust sheet

In thin section, Diuri Formation diamictite displays a distinct bimodal grain size of sand-size (typically ~0.25–2 mm) quartz and K-feldspar clasts suspended in a mica-rich matrix (Fig. 9A–C). The matrix material is dominantly composed of ~10 um or larger-size mica and calcite, exhibits schistosity, and often displays flattening fabrics arranged around larger quartz and feldspar clasts (Fig. 9B and C). Matrix volume fractions can be as high as 75%. Quartz clasts exhibit sweeping and undulose extinction, and are generally elongated subparallel to tectonic foliation (Fig. 9A and B). Foliation-parallel pressure shadows up to ~0.5–1.0 mm-long are developed adjacent to many of the larger quartz and feldspar clasts, and are often filled with syn-deformational calcite (Fig. 9A–C). K-feldpsar clasts exhibit foliation-normal extensional brittle fractures, which are often filled with calcite (Fig. 9D), indicating syn-deformational mass transfer deformation. Quartz grain-to-grain boundaries in Diuri Formation quartzite generally show sharp, sutured contacts, with a small number of grain boundaries displaying zones of bulging and subgrain formation, which we interpret as incipient BLG recrystallization (Fig. 9E). This likely indicates deformation at the minimum temperature conditions necessary for BLG recrystallization, which ranges from ca. 250° to 310 °C (Fig. 7) (Stipp et al., 2002). This type of BLG microstructure corresponds with dislocation creep regime 1 of Hirth and Tullis (1992) (Stipp et al., 2002).

4.4. Gondwana succession thrust sheet

Temperature conditions indicated by the metamorphic grade and quartz microstructure of the Gondwana succession vary along-strike in eastern Bhutan. North of Samdrup Jongkhar, quartzite near the top of the section displays sharp, sutured quartz grain-to-grain contacts, with isolated zones of BLG recrystallization at a small number of boundaries (Fig. 9F). This texture is similar to that observed in Diuri quartzite, and is interpreted to represent a temperature range of 250°–310 °C (Fig. 7) (Stipp et al., 2002). In argillite at the top of the section on the Kuru Chu transect, isolated quartz grains suspended in a mica-rich matrix exhibit undulose extinction and plastic elongation, indicating that temperatures above the frictional-viscous transition for quartz [ca. 250°–270 °C minimum (Dunlap et al., 1997; van Daalen et al., 1999; Stipp et al., 2002)] were obtained.

Along the Manas Chu (Fig. 3), sandstone, siltstone, and shale of the Gondwana succession are not metamorphosed. Sandstone in Fig. 9G shows a texture typical of these strata, with a very weak quartz grain preferred orientation, a significant volume proportion (ca. 25%) of micaceous matrix material, non-sutured quartz grain-to-grain contacts, and no sign of plastic quartz deformation. This indicates that temperatures of ca. 250–270 °C (Dunlap et al., 1997; van Daalen et al., 1999; Stipp et al., 2002) were most likely not obtained here.

4.5. Siwalik Group thrust sheet

Conglomerate, sandstone and siltstone of the Siwalik Group display no evidence of metamorphism through their exposed thickness. In thin section, Siwalik Group sandstone is dominated by ~0.5–1.0 mm-diameter quartz clasts, and is generally clast-supported, but contains a significant volume percentage (ca. 10–25%) of matrix, consisting dominantly of mica and calcite (Fig. 9H). The majority of quartz clasts show evidence of plastic strain, and often exhibit subgrains and sweeping or undulose extinction. However, all quartz plastic strain in these detrital grains is interpreted to be inherited from deformation of source rocks that pre-dates Siwalik Group deposition. A very weak grain preferred orientation indicating low-magnitude strain (Section 5.2.5), a lack of schistosity in matrix material, non-sutured quartz grain-to-grain contacts (Fig. 9H), and a lack of evidence for post-depositional quartz plastic deformation collectively indicate that temperatures of ca. 250°–270 °C (Dunlap et al., 1997; van Daalen et al., 1999; Stipp et al., 2002) were not obtained in the Siwalik Group thrust sheet (Fig. 7).

4.6. Greater-Tethyan Himalayan section

Long and McQuarrie (2010) presented metamorphic mineral assemblages and deformation temperature constraints from quartz and feldspar microstructure for the structurally-lower GH section and depositionally-overlying TH section in the Shemgang region in central Bhutan (Figs. 1 and 2). Their observations are briefly discussed here, and are summarized on Fig. 7. In central Bhutan, kyanite and partial melt textures are only present in the lower-mid parts of the GH orthogneiss unit. The overlying parts of the GH and TH sections are dominated by a melt-free, biotite–muscovite–garnet mineral assemblage.

Please cite this article in press as: Long, S., et al., Quantifying internal strain and deformation temperature in the eastern Himalaya, Bhutan: Implications for the evolution of strain in thrust sheets, Journal of Structural Geology (2011), doi:10.1016/j.jsg.2010.12.011

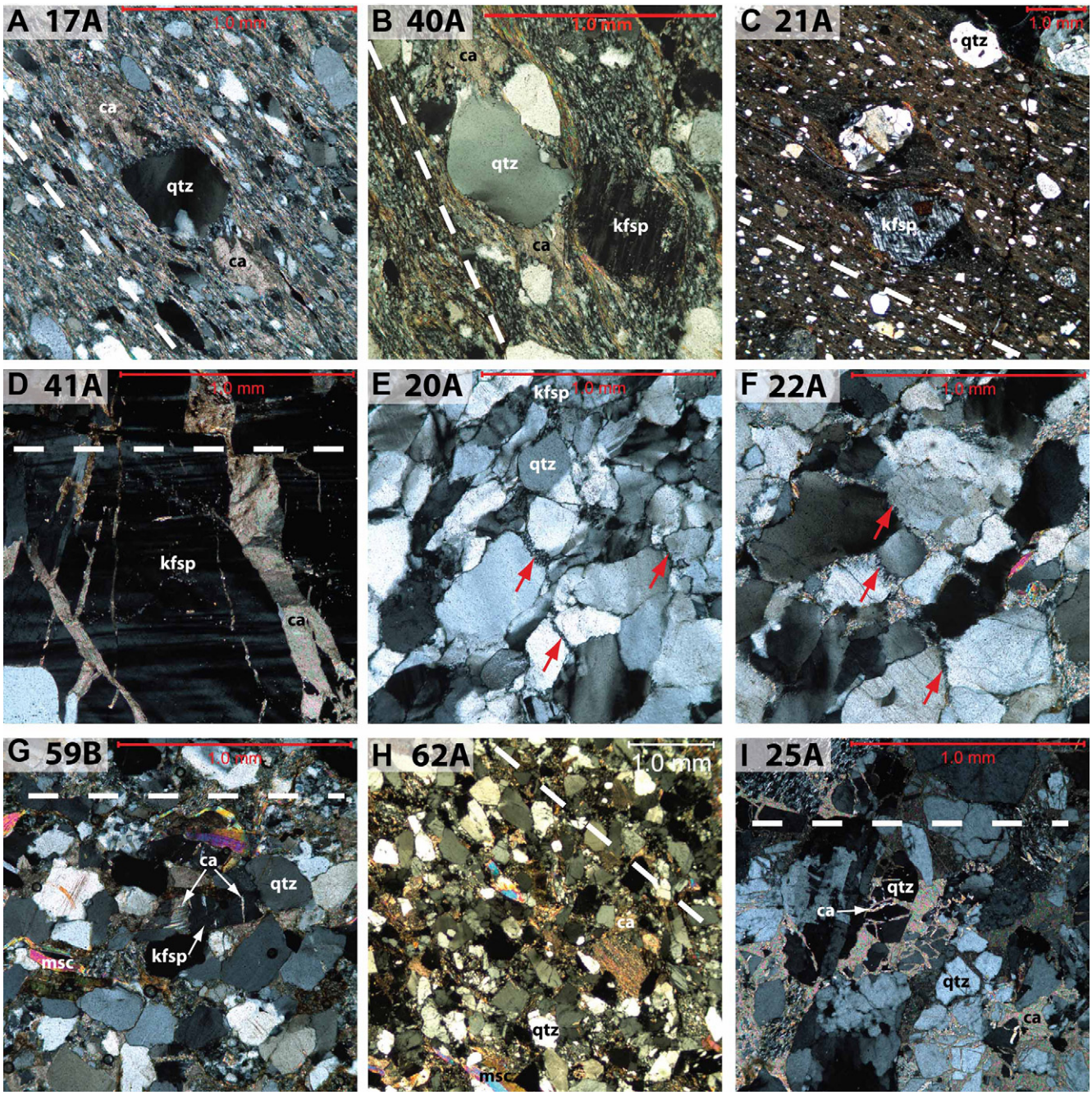

Fig. 9. Photomicrographs illustrating range of deformation microstructure observed in the Diuri Formation, Gondwana succession, and Siwalik Group (cross-polarized light). All thin sections cut perpendicular to bedding or tectonic foliation. White dashed line shows apparent dip of bedding or tectonic foliation in plane of thin section. Strain sample numbers shown; refer to Fig. 3 for sample locations. A–C) Diuri Formation diamictite samples, displaying bimodal grain size distribution of sand-size (~0.25–1.0 mm-diameter) quartz and K-feldspar clasts suspended in mica-rich matrix (~10 um or greater grain size). Quartz clasts are plastically-elongated subparallel to foliation. Matrix displays schistosity, which is arranged in flattening fabrics around larger clasts (B, C). Pressure shadows adjacent to quartz and K-feldspar clasts are often filled with calcite (A, B). Thin sections cut parallel to lineation. D) Foliation-normal, calcite-filled, extensional fractures in K-feldspar in Diuri Formation diamictite. Thin section cut parallel to dip direction. E) Diuri Formation quartzite, with sharp, sutured contacts at most grain boundaries and evidence for BLG recrystallization at some grain boundaries (marked with arrows). F) Gondwana succession quartzite north of Samdrup Jongkhar displaying sharp, sutured contacts and evidence for BLG recrystallization at some grain boundaries (marked with arrows). Thin section cut parallel to lineation. G) Unmetamorphosed Gondwana succession sandstone from the Manas Chu exposure, showing low-strain microstructure, including weak quartz grain preferred orientation, non-sutured quartz grain-to-grain contacts, significant volume proportion of matrix (ca. 25%), and a lack of undulose extinction in quartz. Note that K-feldspar exhibits bedding-normal, calcite-filled fractures. Thin section cut east-west. H) Siwalik Group sandstone from Manas Chu exposure. Note weak grain preferred orientation (low-magnitude strain), a lack of schistosity in matrix material, and non-sutured quartz grain-to-grain boundaries. Crystal–plastic deformation of quartz grains is interpreted as inherited from deformation of source rocks. Thin section cut north-south. I) Calcite-filled fractures in quartz grains from Siwalik Group sandstone; most fractures are orientated at a low angle to bedding.

GH rocks directly above the MCT underwent GBM recrystallization (~500°–700 °C; Stipp et al., 2002). Southeast of Shemgang (Gonphu transect of Long and McQuarrie, 2010), melt-bearing schist 100 m above the MCT displays 'chessboard extinction' (~630°–750 °C; Lister and Dornsiepen, 1982; Mainprice et al., 1986; Stipp et al., 2002). An upsection transition to SGR quartz recrystallization (~400°–500 °C; Stipp et al., 2002) occurs between 2000 and 5000 m structural distance above the MCT. This transition is observed both

Please cite this article in press as: Long, S., et al., Quantifying internal strain and deformation temperature in the eastern Himalaya, Bhutan: Implications for the evolution of strain in thrust sheets, Journal of Structural Geology (2011), doi:10.1016/j.jsg.2010.12.011

below and above the orthogneiss-metasedimentary unit contact on different transects. Everywhere above this transition, GH and TH rocks display SGR recrystallization microstructure (~400°–500 °C; Stipp et al., 2002) through their full exposed thickness. K-feldspar recrystallization is observed through the full thickness of the Chekha Formation, and when combined with SGR recrystallization, indicates deformation temperatures between ~450° and 500 °C (Fig. 7) (Voll, 1976; Tullis and Yund, 1980; Pryer, 1993; Stipp et al., 2002). Since no K-feldspar is observed in the overlying Maneting Formation, the deformation temperature can only be constrained between ~400° and 500 °C, the full temperature range of SGR recrystallization (Fig. 7) (Stipp et al., 2002).

In eastern Bhutan, partial melt textures (deformed leucosomes) are observed throughout the GH section, and metasedimentary rocks distributed through the section often display kyanite and sillimanite (Grujic et al., 1996, 2002; Davidson et al., 1997; Daniel et al., 2003). Peak metamorphic pressure and temperature conditions for GH rocks in eastern Bhutan are estimated at 8–12 kbar and 750–800 °C from 500 m structural distance above the MCT up through the full section to the KT (Fig. 7) (Daniel et al., 2003). These data indicate a ca. 250°–300 °C difference between GH deformation temperatures in central Bhutan and peak metamorphic temperatures in eastern Bhutan (Fig. 7) (Long and McQuarrie, 2010).

5. Finite strain data

5.1. Methods of strain analysis

To estimate 3-D internal strain of SH, LH, and GH–TH thrust sheets, we performed thin section-scale fabric analyses that quantify plastic elongation of sand-size quartz clasts. We performed single strain analyses on 207 thin sections, which were cut from 109 different samples in eastern and central Bhutan (Figs. 2–4 and 10). In general, two oriented thin sections were cut from each sample, and all thin sections were cut perpendicular to bedding or tectonic foliation (Fig. 11A; see Table SM1 for detailed summary of all samples, thin sections, and strain analyses; see Figs. SM1 and SM2 for individual data from each strain analysis). On Table SM1, thin section cuts marked 'A' strike approximately N-S and thin section cuts marked 'B' strike approximately E-W. The following features were used to orient the principal strain axes for each rock sample: 1) For the 70 samples that exhibited mineral stretching lineation, the 'A' thin section was cut parallel to lineation, and the 'B' thin section was cut perpendicular to lineation (Fig. 11A). By assuming that the foliation- or bedding-normal and lineation-parallel plane contains the principal stretch and shortening directions (e.g. Ramsay and Huber, 1983; Passchier and Trouw, 1998), the 'A' thin-sections correspond to the *XZ* strain plane, and the 'B' thin-sections, cut normal to this plane, correspond to the *YZ* strain plane; 2) for 12 samples that lacked stretching lineation but exhibited crenulation cleavage, the 'A' thin section was cut perpendicular to crenulation axial planes, and the 'B' thin section was cut parallel to crenulation axial planes (Fig. 11A). Assuming that the trend of crenulation folds approximates the lineation-normal direction, the 'A' cuts correspond to the *XZ* strain plane and the 'B' cuts correspond to the *YZ* strain plane; 3) for 20 samples that did not exhibit lineation or crenulation cleavage, the lineation-parallel (*XZ*) plane was approximated by cutting an N-S oriented thin section, and the lineation-normal (*YZ*) plane was approximated by cutting an E-W oriented thin section; 4) for 7 samples that did not exhibit lineation or crenulation cleavage, the *XZ* plane was approximated by cutting an oriented thin section parallel to the dip direction, which approximates N-S, and the *YZ* plane was approximated by cutting an oriented thin section parallel to the strike direction, which approximates E-W. The interpretations for cases 3 and 4 are supported by an overall average N-S trend of mineral stretching lineation (Fig. 2 inset), an overall average E-W trend of crenulation cleavage axial planes (Fig. 2 inset), and the regional E-W strike of thrust faults and fold axial traces in Bhutan, which collectively indicate an N-S transport direction (Long and McQuarrie, 2010; Long et al., 2011b). Finally, note that single *XZ* thin sections were cut from 11 samples (Table SM1), and that *XZ* and *YZ* thin sections were cut from 12 non-oriented samples (Table SM1). For the non-oriented samples, lineation-parallel (*XZ*) cuts are projected onto Figs. 2–4, and 10 with a N-S orientation, and lineation-normal (*YZ*) analyses are projected onto Figs. 2 and 3 with an E-W orientation. Note that stratigraphic-up, N versus S, and E versus W cannot be determined for these non-oriented samples (see Table SM1 caption).

To justify the assumptions we have made above in assigning principal strain directions to the rocks analyzed in this study, we note that the relative ratios of Rs values predicted with these techniques are reflected in our strain data (Section 5.2, Table SM1). For example, out of 75 total 3-D ellipsoids obtained from lineation- or crenulation-bearing samples, 60 (80%) contain similar or larger Rs values in the lineation-parallel or crenulation-normal (~N-S) direction. For the 23 3-D ellipsoids obtained from strain samples that did not exhibit lineation or crenulation, 19 (83%) contain a similar or larger Rs value in the N-S thin section.

Three photomicrographs were taken of each thin section, with the stage rotated 30° between each photo so the same clasts were captured at different levels of extinction. The three images were then matched with each other and overlain with the top two translucent, to increase the relief and clarity of individual grain boundaries (Fig. 11G). All photomicrographs were rotated by the angle of apparent dip of bedding or tectonic foliation within the plane of the thin-section cut, so that a horizontal line on all photomicrographs represents horizontal in space (Fig. 11B). This means that all of the strain plots in Figs. SM1 and SM2 can be directly compared with each other. For each analysis, we define φ, the angle of inclination of the long axis of the strain ellipse (Ramsay and Huber, 1983), relative to a horizontal reference line (Fig. 11D, Table SM1). For each analysis, we also calculate θ', the angle between the long axis of the ellipse and the apparent dip of bedding or tectonic foliation in the cut plane (e.g. Ramsay and Huber, 1983) (Fig. 11D). The sign convention we use for θ' is: clockwise from bedding/foliation in the view plane is positive, and counterclockwise from bedding/foliation is negative (see Table SM1 caption). Finally, the 2-D ellipses from each 'A' and 'B' thin section were combined to form a 3-D strain ellipsoid (Fig. 11E). For nearly all of our samples, the *Z* axis was in the same orientation (sub-normal to bedding/foliation) in both analyses, so it was assigned an Rs (tectonic ellipticity) of 1.0 in both ellipses, and the Rs values of the long axes of both ellipses were then directly compared to assign the *X* and *Y* strain directions ($X > Y$).

For phyllite and schist, in which quartz porphyroclasts are isolated among matrix minerals, and for micaceous or partially-recrystallized quartzite that is not dominated by quartz grain-to-grain contacts, the Rf-φ method (Ramsay, 1967; Dunnet, 1969; Dunnet and Siddans, 1971; Ramsay and Huber, 1983) of strain analysis was utilized (175 out of 207 total analyses; Table SM1; Fig. 11G, H). The orientation of the long axis relative to horizontal (φ), and the ratio of the long to short axes (final ellipticity, Rf) of approximately 30 isolated, non-recrystallized, plastically-elongated quartz porphyroclasts were measured for each analysis. The resulting Rf-φ plots are shown for individual analyses in Fig. SM1. For further discussion of the methods utilized in calculating Rs and φ for each sample, see the captions for Table SM1, Fig. SM1, and Fig. 11.

Please cite this article in press as: Long, S., et al., Quantifying internal strain and deformation temperature in the eastern Himalaya, Bhutan: Implications for the evolution of strain in thrust sheets, Journal of Structural Geology (2011), doi:10.1016/j.jsg.2010.12.011

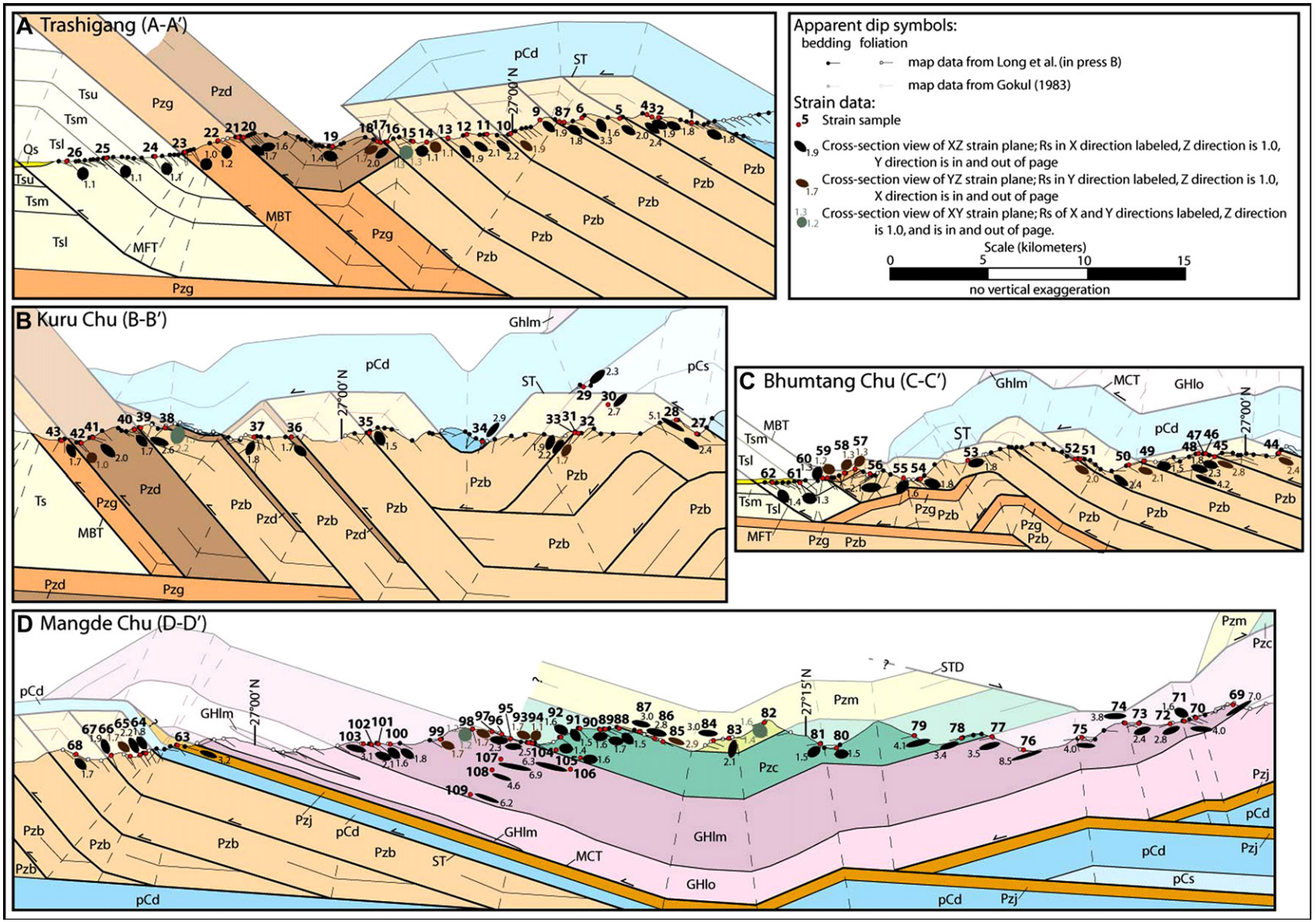

Fig. 10. A–D) Detailed insets of deformed cross-sections, referenced to Fig. 4 (cross-sections are areas of Fig. 3 of Long et al., 2011b). Translucent areas represent rock that has passed through the erosion surface. See Fig. 2 for unit abbreviations; see Fig. 1 caption for structure abbreviations. Strain ellipses from approximately N-S striking thin sections (lineation-parallel, crenulation axial plane-perpendicular, dip direction-parallel, or N-S; see Section 5.1), the majority of which represent the *XZ* strain plane, are projected directly onto the cross-sections. The 3-D ellipsoids defined by these analyses are all scaled to constant volume (see Figs. 2 and 3), and the 2-D ellipses on this figure are scaled accordingly. All ellipses are oriented in the view plane by rotating them by the 'normalized φ' plunge angle listed in Table SM1. 'Normalized φ' is a plunge angle calculated from the difference between the assigned dip domain angle for a specific area of the cross-section and θ', the angle between bedding or tectonic foliation and the long direction of the strain ellipse in the plane of the thin section. Utilizing 'normalized φ' values on the cross-sections instead of φ values removes the effects of variable dip angle, allowing for a better visual representation of strain data (see Table SM1 caption). Black ellipses represent the *XZ* strain plane, brown ellipses represent the *YZ* strain plane and gray strain ellipses represent the *XY* strain plane. (For interpretation of the references to colour in this figure legend, the reader is referred to the web version of this article).

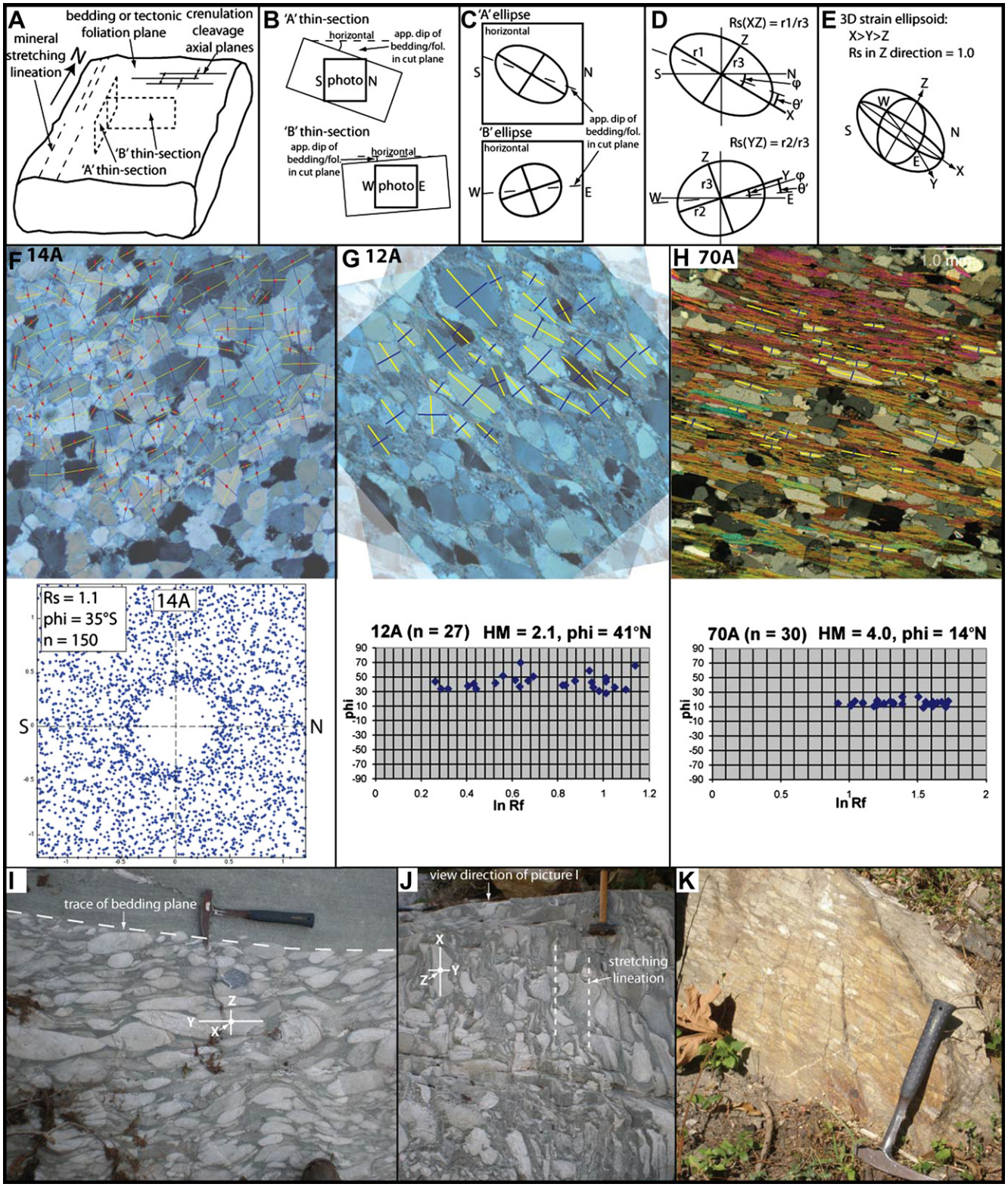

Fig. 11. Diagrams and photographs illustrating strain calculation techniques. A) Orientations of 'A' and 'B' thin-section cuts relative to bedding or tectonic foliation, mineral stretching lineation, and crenulation cleavage axial planes. B) Thin sections are rotated by the apparent dip angle of bedding to tectonic foliation in the cut plane, so that horizontal on the photo represents horizontal in space. C–D) Strain ellipsoids on 'A' and 'B' thin sections from Rf-φ or Normalized Fry analysis; Rs(*XZ*) is ratio of longest and shortest axes (r1/r3), and Rs(*YZ*) is ratio of middle and shortest axes (r2/r3). φ is angle between horizontal and long axis of ellipse (down to N or S in 'A' cuts; down to E or W in 'B' cuts); θ' is angle between long axis of ellipse and the apparent dip of bedding of tectonic foliation in the cut plane (e.g. Ramsay and Huber, 1983); sign convention for θ' is: clockwise from bedding/foliation is positive, counterclockwise from bedding/foliation is negative. E) 3-D strain ellipsoid resulting from combining 2-D 'A' and 'B' strain ellipses; $X > Y > Z$, Rs of $Z = 1.0$. F) Example of Normalized Fry method; grain axial ratios and center positions of ~150 quartz clasts are input to make Normalized Fry plot. The ratio of long and short axes of the ellipse defined by the shape of the outside edge of the vacancy field is used to obtain Rs value, and φ is the orientation of the long axis relative to horizontal. G) Example of Rf-φ method; axial ratios (Rf) and long axis orientations relative to horizontal (φ) of ~30 quartz clasts are input to make Rf-φ plot (for this sample, positive φ is down to the N). Harmonic mean (HM) of all Rf values is used to estimate Rs, and median of all φ values is used as φ for the sample. Sample photo illustrates that 3 overlapping photomicrographs are used to

Please cite this article in press as: Long, S., et al., Quantifying internal strain and deformation temperature in the eastern Himalaya, Bhutan: Implications for the evolution of strain in thrust sheets, Journal of Structural Geology (2011), doi:10.1016/j.jsg.2010.12.011

We calculated 2σ (95%) uncertainties for Rs and φ for each Rf-φ analysis (Table SM1; Figs. 12–14), using methods described in Robin and Torrance (1987). For low-strain analyses (Rs = 1.0–1.5, $n = 31$), Rs and φ had typical 2σ uncertainties ±0.1 and ±9–11°. For moderate-strain analyses (Rs = 1.6–2.5, $n = 110$), which comprise the majority of our analyses, typical Rs and φ uncertainties were ±0.2 and ±5°. For high-strain analyses (Rs = 2.5–8.5, $n = 34$), typical Rs and φ uncertainties were ±0.4–0.5 and ±2°. In general, angular uncertainty increases and Rs uncertainty decreases with decreasing tectonic strain, and vice versa. Using the maximum and minimum Rs values obtained from the 2σ errors assigned to the *XZ* and *YZ* thin sections for each sample, we also estimated 2σ errors for the *XY* strain plane for our 3-D ellipsoids (Table SM1; Fig. 12). Error generally increased with increasing *X*/*Y* ratio, with typical error ranges of ±0.1–0.2 for $X/Y < 1.3$ ($n = 60$), and ±0.3–0.4 for $X/Y > 1.3$ ($n = 24$).

For clast-supported sandstone and quartzite (32 out of 207 thin sections), we used the Normalized Fry Method (Erslev, 1988), which quantifies anticlustering in distributions of clast centers, to estimate the strain ellipse for each sample. The Normalized Fry Method is an improved version of the Fry Method (Fry, 1979; Ramsay and Huber, 1983), and allows more precise determination of bulk strain than the older technique by correcting for the effects of variable sorting and packing (Erslev, 1988). For a single analysis, grain center locations and the lengths of long and short axes of 100–150 closely-packed quartz clasts were measured off of the thin-section image (Fig. 11F), and input into a Matlab program. Off of the resulting Normalized Fry plot (plots shown in Fig. SM2; see Table SM1 for key to sample names), we measured: 1) the ratio of the long to short axes of the contact between the vacancy field and the ring of high point-density to obtain an Rs value, and 2) the orientation of the long axis relative to horizontal to estimate φ (Fig. 11F).

Studies comparing results of the Fry and Rf-φ methods performed on the same samples show that the two methods yield similar Rs and φ values, but that the Fry method often yields larger uncertainties (e.g. Yonkee, 2005). Since our Normalized Fry analyses typically yield low tectonic strain values (Rs = 1.0–1.5, median 1.3), we estimate approximate 2σ uncertainties of ±0.1–0.2 for Rs and ±8–12° for φ to be representative, based on the error ranges for Rf-φ analyses reported above.

5.2. Data

5.2.1. Daling–Shumar Group and Jaishidanda Formation

Since relict quartz porphyroclasts are totally replaced by recrystallized subgrains in Daling–Shumar Group and Jaishidanda Formation quartzite, phyllite, and schist, quartz grain aspect ratios could not be used to quantify strain on the majority of thin sections. However, we were able to quantify strain in three samples from these map units. Quartzite samples 29 (upper Shumar) and 34 (lower Daling) were collected in klippen in the southern Kuru Chu valley (Fig. 3), and display a ~90% volume proportion of recrystallized quartz subgrains, which form a matrix that surrounds elongated quartz ribbon porphyroclasts (Fig. 5K). Sample 63 is a garnet-bearing Jaishidanda Formation schist (Fig. 5J), which contains isolated, elongated, non-recrystallized quartz porphyroclasts surrounded by a matrix of muscovite. Using the Rf-φ method, we quantified aspect ratios and orientations of quartz porphyroclasts in these three samples (Table SM1). *X*/*Z* Rs ratios range between 2.3 and 3.2 ($n = 3$), and *Y*/*Z* Rs ratios range between 1.2 and 2.3 ($n = 2$). The strain ellipsoids indicate moderately-constrictional (29) and flattening (34) strain (Fig. 12A).

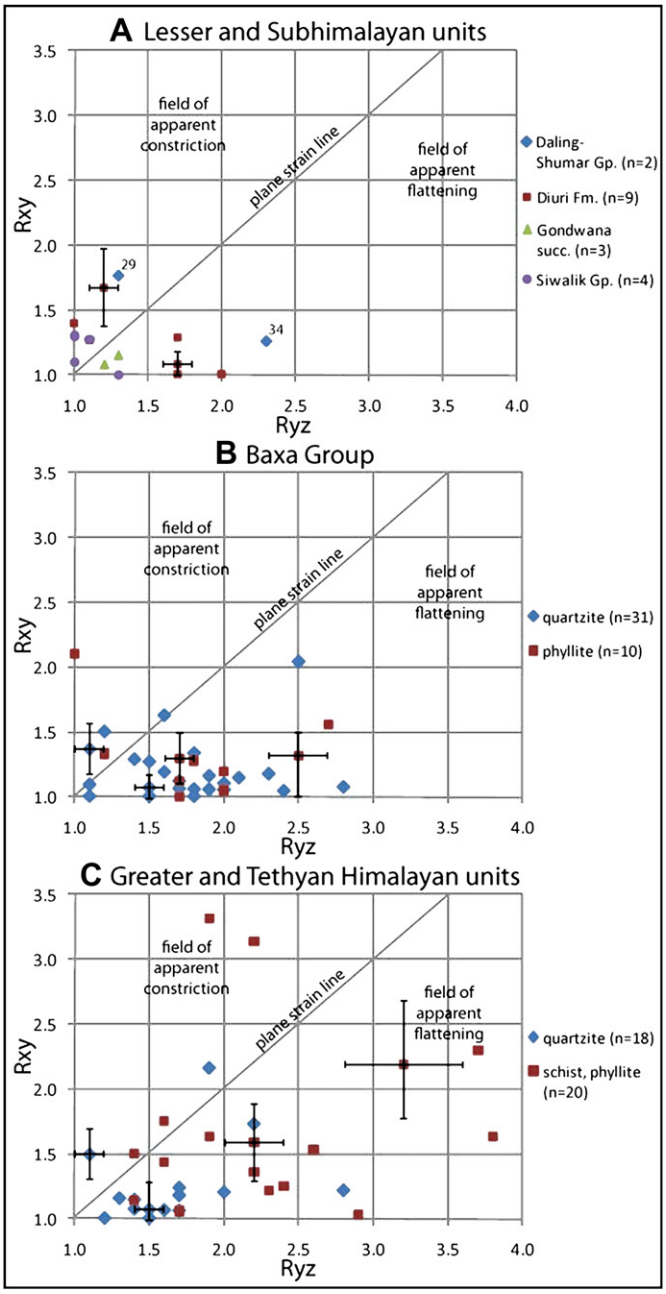

Fig. 12. Flinn diagrams (Rs[*Y*/*Z*] vs. Rs[*X*/*Y*]) of finite strain ellipsoids from: A) Lesser and Subhimalayan units, B) the Baxa Group, and C) Greater and Tethyan Himalayan units. Sample numbers of specific ellipsoids discussed in text are shown. 2σ (95%) error bars for (Rs[*Y*/*Z*] vs. Rs[*X*/*Y*]) are shown for samples with representative error (Section 5.1; Table SM1). Plots B and C show that flattening strain (oblate ellipsoids) dominates in Baxa Group and GH–TH rocks, even within the range of error. For plot C note the significant difference in strain magnitude between quartzite and schist/phyllite for GH–TH rocks.

make a composite photo, with the top two photos translucent, in order to increase the relief of grain boundaries. H) Illustrates the use of Rf-φ method in GH and TH schist where plastically-elongated quartz porphyroclasts are isolated in muscovite matrix. I–J) evidence of layer-normal flattening strain in Baxa Group conglomerate at outcrop-scale. I and J are photographs of the same rock from different perspectives; J is looking down on bedding plane (note: this is a float boulder so direction of stratigraphic-up is unknown), which is subparallel to the *XY* strain plane; lineation direction shown; note elongation of quartz cobbles in *X* and *Y* directions. I is facing in lineation direction (*X* is in and out of page), which is subparallel to the *YZ* strain plane; note bedding-subparallel elongation of quartz cobbles. K) Photograph of Chekha Formation conglomerate, showing bedding-subparallel elongation of quartz pebbles; lineation direction unknown.

Please cite this article in press as: Long, S., et al., Quantifying internal strain and deformation temperature in the eastern Himalaya, Bhutan: Implications for the evolution of strain in thrust sheets, Journal of Structural Geology (2011), doi:10.1016/j.jsg.2010.12.011

The *XY* strain plane is subparallel to bedding and tectonic foliation, with θ' values of only 1–2° (Fig. 13A).

Grujic et al. (1996) made quartz crystallographic preferred orientation (CPO) plots of thin sections of LH samples up to 2 km structural distance beneath the MCT in the Kuru Chu valley, in rocks we map as Jaishidanda and Daling formations. Quartz CPO plots were consistent with top-to-the-south motion, with no measurable increase in CPO intensity approaching the MCT (Grujic et al., 1996). Asymmetry of <c> and <a> axes indicate a moderately-rotational, plane-strain to weakly-constrictional strain regime, with the coexistence of pure- and simple-shear components (Grujic et al., 1996).

5.2.2. Baxa Group

The ubiquitous presence of plastically-elongated quartz porphyroclasts in Baxa Group quartzite and phyllite (Fig. 8) make this map unit ideal for collecting strain data. Strain ellipsoids were determined using the Normalized Fry method for clast-supported quartzite (e.g. Figs. 8E and 11F), and the Rf-φ method for phyllite and micaceous quartzite, where quartz porphyroclasts are surrounded by a mica-rich matrix (e.g. Figs. 8C–D, 11G), and for partially-recrystallized quartzite where relict quartz porphyroclasts are surrounded by a matrix of quartz subgrains (e.g. Fig. 8F–I). For the partially-recrystallized samples, the resulting Rs may be an underestimate if a significant volume proportion of the relict porphyroclasts have been recrystallized into subgrains.

In 29 out of 43 total Baxa Group samples, the longest Rs (*X* direction) is parallel to mineral stretching lineation (N-S), but 6 samples have an equal Rs in N-S and E-W thin sections, and in 8 samples the longest Rs trends E-W (Table SM1; Figs. 4 and 10). *X*/*Z* and *Y*/*Z* axial ratios vary between 1.1–5.1 and 1.0–3.0, respectively, but the majority of ellipsoids are similar, with median *X*/*Z*, *Y*/*Z*, and *X*/*Y* ratios of 1.9, 1.8, and 1.0 (Table 1; Fig. 13B). On a Flinn diagram, the majority of Baxa Group strain ellipsoids plot in the flattening field (Fig. 12B). Phyllite has a slightly longer median *X*-direction Rs than quartzite (1.9 vs. 1.8), but in general the two lithologies show little variability in strain magnitude (Figs. 12B and 13B; Table 1). The majority of θ' values in both the N-S (Fig. 13B) and E-W directions (Table SM1) are very low (median N-S θ' is ±5°, median E-W θ' is ±8°; Table 2), and decrease sharply with increasing Rs (Fig. 13B). This indicates that the *XY* strain plane is subparallel to bedding or tectonic foliation for the majority of samples (Figs. 2–4, 10).

Significant along-strike trends in strain magnitude are not observed between the four transects (Figs. 2 and 3, Table 1). An across-strike trend with lower strain magnitudes toward the foreland is observed, and is most apparent on the Bhumtang Chu transect (samples 44–49: median ellipsoid = 2.4:2.1:1.0; samples 51–57 median ellipsoid = 1.9:1.3:1.0) (Fig. 3). Although not as distinct, this trend is also observed on the Kuru Chu transect (Fig. 3), and on the Trashigang transect, where the southernmost horse in the duplex contains nearly unstrained quartzite (Fig. 3).

In summary, thrust sheets of the Baxa Group show evidence for layer-normal (±5–8° median θ') flattening strain (LNF), which can be approximated with a median strain ellipsoid of 1.9:1.8:1.0, with *X* trending approximately N-S. Evidence for outcrop-scale LNF strain of Baxa conglomerate is shown in Fig. 11I–J. Two notable

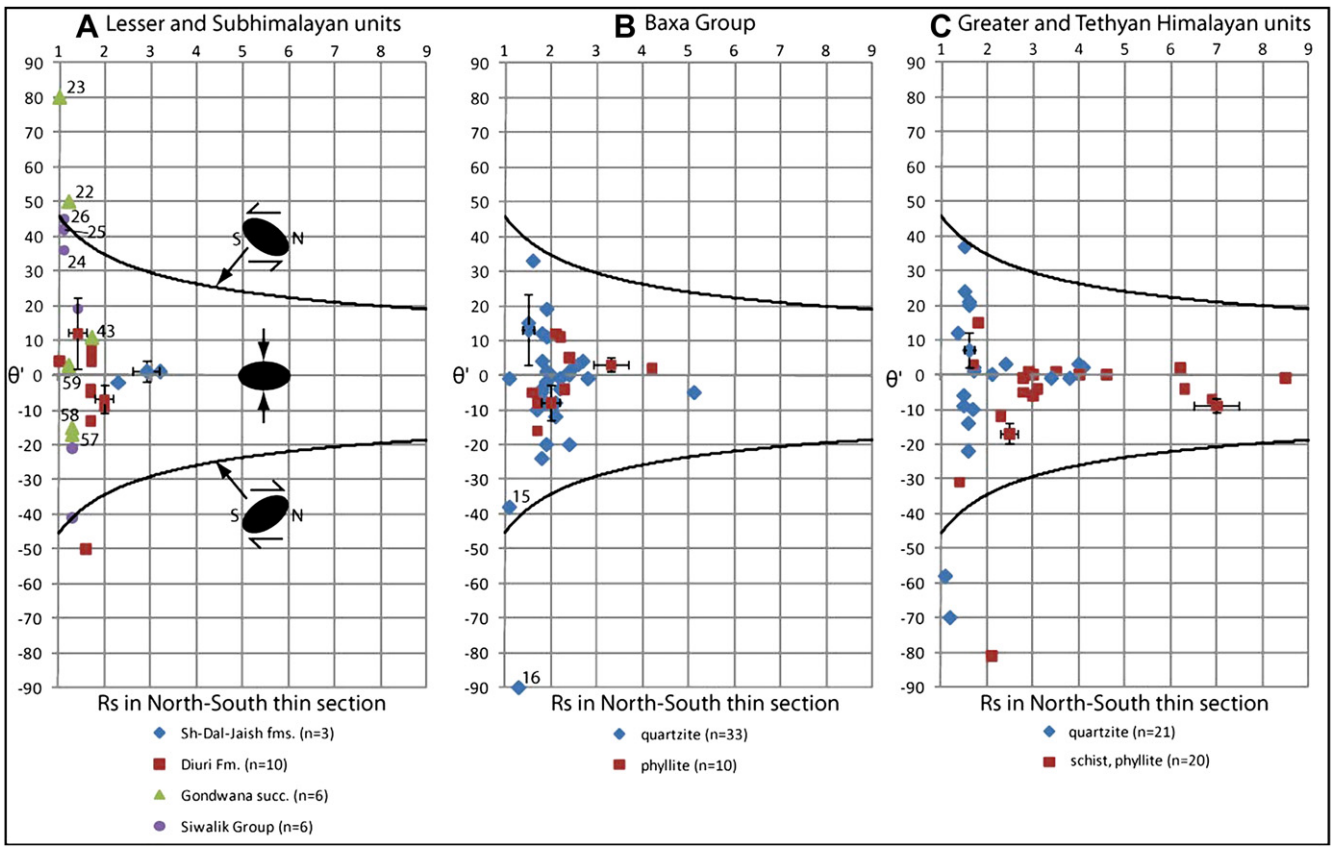

Fig. 13. Plots of Rs in N-S thin sections (generally Rs[*X*/*Z*]) vs. θ', the angle between the long axis of the strain ellipse and the apparent dip of bedding/foliation in the cut plane. Positive θ' is steeper to the N (or shallower to S) than bedding, negative θ' is steeper to the S (or shallower to the N) than bedding (Table SM1 caption). Solid black curves represent θ' values expected with idealized, plane-strain simple shear with increasing Rs; for positive θ' the curve would represent top-to-the-south sense simple shear, and for negative θ' the curve would represent top-to-the-north sense simple shear. Sample numbers of specific ellipses discussed in the text are shown. 2σ (95%) error bars for Rs and θ' are shown for samples with representative error for low (Rs<1.5), moderate (Rs = 1.6–2.5) and high (Rs>2.6) strain (Section 5.1, Table SM1).

Please cite this article in press as: Long, S., et al., Quantifying internal strain and deformation temperature in the eastern Himalaya, Bhutan: Implications for the evolution of strain in thrust sheets, Journal of Structural Geology (2011), doi:10.1016/j.jsg.2010.12.011

Table 1
Median values of strain ellipsoid axial ratios, calculated from the median of all N-S Rs values and E-W Rs values listed on Table SM1. Data listed for individual LH, GH, and TH map units. Data from individual transects listed for Baxa Group. Data is also split out by lithology for Baxa Group and GH–TH map units.

	Median *X*/*Z*	Median *Y*/*Z*	Median *X*/*Y*	n (N-S)	n (E-W)
Siwalik Group	1.2	1.1	1.1	6	4
Gondwana succession	1.5	1.3	1.2	6	3
Diuri Formation	1.7	1.7	1.0	10	9
Baxa Gp: Trashigang	1.9	1.8	1.1	15	14
Baxa Gp: Kuru Chu	2.2	1.8	1.2	9	9
Baxa Gp: Bhumtang Chu	2.1	1.8	1.1	13	13
Baxa Gp: Mandge Chu	1.8	1.7	1.1	5	5
Baxa Group quartzite	1.9	1.8	1.1	33	32
Baxa Group phyllite	2.2	1.9	1.2	10	10
Baxa Group total	1.9	1.8	1.1	43	42
Jaish–Daling–Shumar fms.	2.9	1.8	1.6	3	2
GH quartzite	1.9	1.7	1.1	8	7
GH schist/phyllite	3.8	2.2	1.7	14	12
Chekha quartzite	1.6	1.5	1.1	13	13
Maneting phyllite	2.9	1.9	1.5	6	6
GH–TH quartzite	1.6	1.5	1.1	21	20
GH–TH schist/phyllite	3.0	2.2	1.4	20	18
GH–TH total	2.1	1.8	1.2	41	38

exceptions are samples 15 and 16, which are from the southernmost Baxa Group horse on the Trashigang transect (Figs. 3, 4A and 10A, 13B). These moderate- to high-θ' analyses represent low-magnitude, layer-parallel shortening (LPS) strain, and are discussed in Section 6.2.1.

5.2.3. Diuri Formation

Strain ellipsoids for Diuri Formation diamictite were determined using the Rf-φ method for plastically-elongated quartz porphyroclasts isolated within a mica and calcite matrix (Fig. 9A–C). Of the 10 total Diuri samples, 4 have a lineation-parallel (N-S) *X* direction, 3 have an equal Rs in N-S and E-W thin-sections, and 3 have an E-W trending *X* direction (Table SM1, Fig. 3). *X*/*Z* and *Y*/*Z* axial ratios vary between 1.4–2.2 and 1.0–2.0, respectively. Axial ratios are heterogeneous; on a Flinn diagram 6 out of 9 ellipsoids plot in the flattening field, and 3 plot in the constriction field (Fig. 12A). The median strain ellipsoid (median of all N-S Rs values and E-W Rs values) is 1.7:1.7:1.0 (Fig. 13A; Table 1). The median θ' values in the N-S (Fig. 13A; Table 2) and E-W directions (Table 2) are ±7° and ±11°, respectively, indicating LNF strain (Figs. 2, 4 and 10).

5.2.4. Gondwana succession

Strain data were obtained from 6 Gondwana succession samples, and strain magnitude and orientation varies significantly along strike. In sandstone samples #22 and #23 from the Trashigang transect, quartz porphyroclasts are plastically-elongated (Fig. 9F), but yield low Rs[N-S] ratios (1.2, 1.0), with the *X* direction oriented at a high angle to bedding (θ' = ±50°, ±80°; Figs. 4, 10 and 13A). This is indicative of low-magnitude LPS strain. In shale sample #43 on the Kuru Chu transect, quartz porphyroclasts are plastically-elongated, Rs[N-S] is 1.7, and θ' is only ±11° (Figs. 4, 10 and 13A). Although Rs[E-W] is not known for this sample, this could indicate LNF strain, similar to that observed in the Baxa and Diuri thrust sheets.

On the Bhumtang Chu transect, the Gondwana succession does not exhibit evidence for quartz crystal–plastic deformation (Section 4.4, Fig. 9G). However, quartz grains in samples #57–59 do exhibit a bedding-subparallel preferred orientation. The *X* direction for all three samples trends E-W (Table SM1), *X*/*Z* and *Y*/*Z* ratios vary between 1.3–1.5 and 1.2–1.3, respectively (Fig. 3), and the ellipsoids plot in a field of moderate flattening (Fig. 12A). θ' values are low (±3–17° N-S; +2–10° E-W; Fig. 13A, Table SM1), indicating LNF strain. This strain orientation is also supported by bedding-normal fractures in K-feldspar (Fig. 9G). These low-magnitude LNF strain ellipsoids are interpreted as the result of low-temperature processes such as deformation and/or dissolution of matrix material, microfracturing of clasts (Fig. 9G), and pressure solution of quartz grains at grain-to-grain contacts (e.g. Onash et al., 1998).

5.2.5. Siwalik Group

Strain data were obtained from 6 Siwalik Group samples. On the Trashigang transect, low Rs values (1.0–1.1; Fig. 3) and moderate-high θ' values (±36–45°; Figs. 4, 10 and 13A) were obtained from samples #24–26. The combination of these θ' and Rs values could indicate top-to-the-south sense simple shear acting parallel to the top and bottom of the Siwaliks section (Fig. 13A). However, since thin sections from these samples are not oriented (note that their N-S orientation shown on Figs. 3 and 4, and 10 is arbitrary), the true *X* direction and the sign of θ' cannot be determined. Note that since the *X* direction is unknown, the θ' values should be interpreted as minima for the true *X* direction. With moderate- to high-θ' minimum values, these analyses most likely represent low-magnitude, layer-parallel shortening (LPS) strain, and are discussed further in Section 6.2.1.

On the Bhumtang Chu transect, strain ellipsoids for 3 oriented Siwalik Group samples (#60–62) yielded Rs[*X*/*Z*] and Rs[*Y*/*Z*] ratios between 1.3–1.4 and 1.0–1.3, respectively, with N-S trending *X* directions for two samples (Fig. 2), and plot in the flattening and constrictional fields (Fig. 12A). θ' values are low to moderate (+19, −21, −41° N-S; +13–20° E-W; Figs. 4, 10 and 13A). Strain orientation for these samples is difficult to characterize; the N-S θ'directions are not consistent with a dominant sense of simple shear, and the N-S θ' values are not high enough to indicate LPS strain. While not an ideal fit, these low-moderate N-S θ' values and low E-W θ' values either approximate LNF strain, or reflect some component of LPS that postdates folding (Figs. 3 and 10).

The Siwalik Group strain ellipsoids are interpreted as the result of low-temperature deformation processes, including compaction and/or dissolution of matrix material, and microfracturing (Fig. 9I)

Table 2
Median θ' values for all N-S and E-W thin sections for map units listed on Table SM1. Data is listed for all values of θ', absolute values (a.v.) of θ' (i.e. represents median deviation from bedding), positive θ' values (steeper to N or E or shallower to S or W), and negative θ' (steeper to S or W or shallower to N or E). Low θ' values in both N-S and E-W directions for all map units except Siwalik Group indicate that the *XY* strain plane is subparallel or at a low angle to bedding. Note general decrease from foreland units to hinterland units.

	Median N-S all θ'	Median N-S a.v.θ'	n	Median N-S pos θ'	n	Median N-S neg θ'	n	Median E-W all θ'	Median E-W a.v.θ'	n	Median E-W pos θ'	n	Median E-W neg θ'	n
Siwalik Group	28	39	6	39	4	−31	2	17	17	4	17	4	–	0
Gondwana succession	7	16	6	31	4	−16	2	7	7	4	7	4	–	0
Diuri Formation	−5	7	10	6	4	−8	6	5	11	8	12	5	−10	3
Baxa Group	−1	5	43	4	19	−8	24	−2	8	40	6	17	−10	23
Jaish–Daling–Shumar	1	1	3	1	2	−2	1	−4	20	2	23	1	−16	1
GH–TH	−1	6	41	3	20	−9	21	−2	8	38	7	17	−8	21

Please cite this article in press as: Long, S., et al., Quantifying internal strain and deformation temperature in the eastern Himalaya, Bhutan: Implications for the evolution of strain in thrust sheets, Journal of Structural Geology (2011), doi:10.1016/j.jsg.2010.12.011

and/or pressure solution of quartz clasts (e.g. Onash et al., 1998). The very low ellipticity values (~1.1 or less) obtained along the Trashigang transect are small enough that they could be from an initial sedimentary preferred orientation, such as clast imbrication. However, because of their high angle to bedding (ca. 36–45° minimum), we argue that this is unlikely.

5.2.6. Greater Himalayan and Tethyan Himalayan section

Long and McQuarrie (2010) presented Rs values for 21 lineation-parallel (N-S) thin sections from GH and TH rocks in the Shemgang area of central Bhutan. We add an additional 20 N-S strain analyses and 38 E-W strain analyses to this preliminary dataset (Figs. 2, 4 and 10, 12C, 13C). Quartz-dominated microlithons in GH–TH schist and phyllite are generally completely recrystallized, but quartz grains isolated within mica-dominated microlithons in these lithologies are typically plastically-elongated and non-recrystallized (Long and McQuarrie, 2010). The Rf-φ method was used on these isolated quartz porphyroclasts (Fig. 11H). Strength differences between mica- and quartz-dominated microlithons may result in heterogeneous deformation for mica-rich lithologies (e.g. Holyoke and Tullis, 2006), and we see this heterogeneous deformation expressed as a difference in strain magnitude between quartz-rich and mica-rich lithologies (Fig. 12C). Thus we argue that this technique provides a valid estimate for both bulk strain and variations in strain through these rocks. GH and TH quartzite samples are generally partially-recrystallized, with up to a ca. 60–90% subgrain volume proportion, but still exhibit plastically-elongated, relict quartz porphyroclasts (Long and McQuarrie, 2010). The Rf-φ method was used on the largest and most elongated relict porphyroclasts. As in the case of partially-recrystallized Baxa Group quartzite samples, the Rs values obtained from GH and TH quartzite may be an underestimate if a significant volume proportion of the porphyroclast was recrystallized into subgrains. Finally, the Normalized Fry method was used on three non-recrystallized GH and TH quartzite samples (Table SM1).

The *X* direction is parallel to stretching lineation (N-S) in 31 out of the 41 total GH–TH samples, but 4 samples have an equal Rs in N-S and E-W thin sections, and in 6 samples the longest Rs trends E-W (Table SM1; Figs. 2, 4 and 10). Rs varies significantly with lithology, with a general upsection decrease in strain magnitude between GH and Chekha quartzite and between GH schist/phyllite and Maneting phyllite (Fig. 14B). Rs[*X*/*Z*] and Rs[*Y*/*Z*] ratios vary between 1.2–4.1 and 1.1–2.8 for quartzite, and between 1.6–8.5 and 1.4–3.8 for phyllite and schist. Median strain ellipsoids for quartzite and schist/phyllite have axial ratios of 1.6:1.5:1.0 and 3.0:2.2:1.0, respectively (Table 1), and the median strain ellipsoid for all GH–TH samples is 2.1:1.8:1.0 (Table 1). On a Flinn diagram, the majority of GH–TH ellipsoids plot in the flattening field (Fig. 12C). The majority of θ' values in both the N-S (Fig. 13C) and E-W directions (Table SM1) are very low (median N-S θ' is ±6°, median E-W θ' is ±8°; Table 2), and decrease sharply with increasing Rs (Fig. 13C). This indicates that for the majority of GH–TH samples the *XY* strain plane is subparallel to bedding or tectonic foliation (Figs. 2,4 and 10).

A significant across-strike trend in strain magnitude is observed from north to south (Fig. 2). North of the syncline axial plane at Shemgang (samples #69–82; Trongsa transect of Long and McQuarrie, 2010), strain magnitudes in GH and TH rocks are generally higher than to the south of the syncline axial plane (samples #83–103; Sure transect of Long and McQuarrie, 2010). The lower strain magnitudes on the Sure transect coincide with the coolest-temperature GH section, which only displays partial melt textures just above the MCT. Note that high-strain samples #106–109 are from the Gonphu transect of Long and McQuarrie (2010), which displays partial melt textures as high as 4000 m above the MCT.

In summary, GH and TH rocks in central Bhutan show evidence for heterogeneous LNF strain (±6–8° median θ'), with significant lithologic control on strain magnitude. Strain can be approximated with median strain ellipsoids of 3.0:2.2:1.0 for phyllite/schist, 1.6:1.5:1.0 for quartzite, and 2.1:1.8:1.0 for all lithologies, with the *X* direction trending approximately N-S.

5.3. Kinematic vorticity of Greater-Tethyan Himalayan and Baxa Group thrust sheets

Assuming plane strain, the angle between the long axis of the strain ellipse and the shear zone boundary starts at 45° and decreases exponentially with higher Rs for the case of ideal simple shear (e.g. Ramsay, 1967). This relationship is plotted with black curves on Fig. 13 for both top-to-the-south sense (positive θ') and top-to-the-north sense (negative θ') simple shear. While measured θ' values do show a systematic decrease with increasing Rs, note that nearly all Baxa Group and GH–TH strain analyses (Fig. 13B,C) yield much smaller θ' angles than predicted by ideal simple shear. For the case of the opposite end member, ideal layer-normal pure shear deformation, θ' would be predicted to be 0°, with the *XY* strain plane perfectly parallel to bedding/foliation. Note that the median θ' of all (includes both positive and negative θ') N-S and E-W Baxa Group strain analyses are −1° and −2°, respectively, and that these values are exactly the same for the GH–TH strain analyses (Table 2). At a first approximation, this is a very good fit for pure shear deformation with an approximately layer-normal (subvertical) *Z* direction. However, the significant variability observed in θ' values indicates a combination of simple and pure shear deformation. To quantify the relative contributions of these strain end-members, mean kinematic vorticity numbers (Wm) are estimated for individual Baxa Group and GH–TH strain analyses. Wm is defined as the non-linear ratio of pure shear (Wm = 0) and simple shear (Wm = 1) end-member components of deformation (e.g. Means et al., 1980; Means, 1994). For calculation and interpretation of Wm, steady-state, plane-strain deformation is assumed. Pure and simple shear components make equal contributions at Wm = 0.71. Wm values of 0.0–0.4 correspond to ca. 70–100% pure shear, Wm values of 0.4–0.7 correspond to ca. 50–70% pure shear, and Wm values of 0.7–1.0 correspond to ca. 0–50% pure shear (Law et al., 2004).

We estimate Wm values by matching our data to lines of constant Wm on a θ' vs. log Rs[N-S] diagram (Fig. 14; curves from Sanderson, 1982 and Yonkee, 2005). We estimate uncertainties for Wm by projecting 2σ (95%) Rs and φ errors (Section 5.1, Table SM1) onto Fig. 14. For high-strain analyses (Rs>2.6, $n = 24$), typical Wm uncertainty is ±0.15. For moderate strain analyses (Rs = 1.6–2.5, $n = 43$), which comprise the majority of our data, typical Wm uncertainties are between ±0.1 and 0.2. For low-strain analyses (Rs<1.5, $n = 10$), Wm values are not well-constrained, with typical uncertainties between ±0.2 and 0.3. This illustrates the strong effect that higher errors in φ inherent in lower strain analyses has on Wm uncertainty. However, note that low-strain (Rs<1.5) analyses make up only 10 out of 77 total Baxa and GH–TH analyses.

Including estimated error, Wm values from the Baxa Group (Fig. 14A) have a total range from ca. 0.0 to 1.0 ($n = 39$), but the majority of samples ($n = 29$) yield Wm values <0.7, and nearly half ($n = 16$) of analyses are <0.4. Including estimated error, Wm values for the GH–TH section in central Bhutan (Fig. 14B) are similar, and yield a total range from ca. 0.0–1.0 ($n = 37$), with the majority of samples ($n = 26$) yielding Wm values <0.7, and about half ($n = 18$) of analyses are <0.4. For both the Baxa Group and GH–TH section, the wide range in Wm numbers indicate that strain partitioning was heterogeneous. This is particularly evident in the GH–TH data, which also shows a strong lithologic control on strain magnitude,

Please cite this article in press as: Long, S., et al., Quantifying internal strain and deformation temperature in the eastern Himalaya, Bhutan: Implications for the evolution of strain in thrust sheets, Journal of Structural Geology (2011), doi:10.1016/j.jsg.2010.12.011

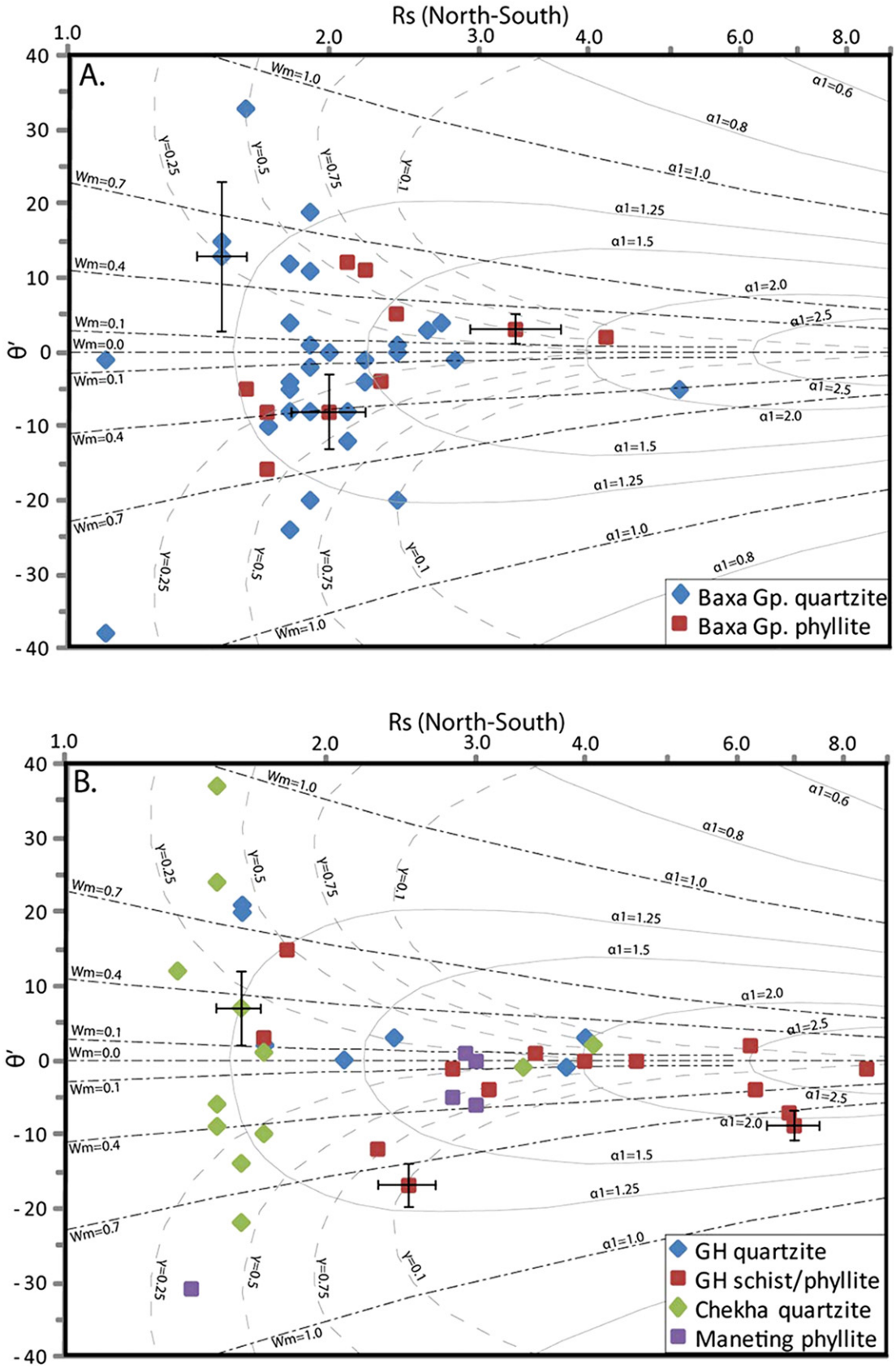

Fig. 14. Plots of log Rs in N-S direction vs. θ′ for (A) Baxa Group thrust sheets and (B) the GH–TH section in central Bhutan. Data are split out by lithology. Contours of constant layer-parallel shear strain (γ), stretch in the direction of shear (α), and mean kinematic vorticity for plane-strain deformation (Wm) are shown (modified from Sanderson [1982] and Yonkee [2005]). 2σ (95%) error bars for Rs and θ′ are shown for samples with representative error for low (Rs<1.5), moderate (Rs = 1.6–2.5) and high (Rs>2.6) strain. These errors result in typical Wm uncertainty ranges of ±0.2–0.3 (Rs<1.5, n = 10), ±0.1–0.2 (Rs = 1.5–2.6, n = 43), and ±0.15 (Rs>2.6, n = 24). Within estimated error, the majority of Baxa Group samples (n = 29) yield Wm values <0.7, with nearly half (n = 16) ≤0.4, and the majority of GH–TH samples (n = 26) also yield Wm values <0.7, with about half (n = 18) ≤0.4. Samples with θ′ values greater than ±40° are not plotted (n = 1 for Baxa Group, n = 3 for GH–TH units).

Please cite this article in press as: Long, S., et al., Quantifying internal strain and deformation temperature in the eastern Himalaya, Bhutan: Implications for the evolution of strain in thrust sheets, Journal of Structural Geology (2011), doi:10.1016/j.jsg.2010.12.011

with quartzite generally yielding a higher component of simple shear (Fig. 14B). Despite the wide overall range of Wm, the majority of values for both the Baxa Group and GH–TH section are <0.7 (approximately equal contributions of simple and pure shear; Law et al., [2004]), and nearly half are <0.4, indicating a domination of pure shear (coaxial) deformation (70–100% pure shear, 0–30% simple shear; Law et al., 2004). In summary, pure shear deformation in the form of approximately layer-normal thinning was the dominant strain mechanism for the Baxa Group and the GH–TH section in central Bhutan.

The above interpretations must be viewed with caution due to two caveats: 1) For estimation of Wm, plane strain is assumed (Means et al., 1980), and our data for both the Baxa Group and GH–TH section (Figs. 12 and 14) plot in the flattening strain field (Fig. 12), which violates this assumption. This means that layer-normal thinning must be accompanied by components of layer-parallel stretching in both transport-parallel and transport-normal directions or volume loss in the *Z* direction; 2) Another significant observation is that θ' values are both positive and negative, with approximately equal numbers and ranges of both. This range in θ' is not consistent with one dominant sense of simple shear. This raises questions about the origin and significance of the range of θ' values observed. It is possible that some of the positive and negative θ' values arise from geometries that pre-date strain, such as initial grain preferred orientations oriented at an angle to bedding (i.e. clast imbrication). The initial angle that a preferred orientation makes with bedding/foliation would be rotated to a smaller final angle during layer-normal, pure-shear flattening strain. If pre-existing orientations did exist, this would minimize the component of simple shear even further.

6. Discussion

Workers across the Himalaya have documented structural and stratigraphic evidence for Cambrian–Ordovician (ca. 490–530 Ma) tectonic activity that affected the northern Indian margin (Garzanti et al., 1986; Gehrels et al., 2003, 2006a, 2006b; Cawood et al., 2007; Martin et al., 2007), which is represented by Ordovician coarse-clastic deposits preserved in the TH section, and widespread Cambrian–Ordovician metamorphism and magmatic activity within the GH section.

It is possible that some metamorphic minerals, microstructural textures, and strain fabrics that we observe in rocks in the Bhutan GH and TH sections may, to some extent, have been produced during the Cambrian–Ordovician orogenic event (e.g. Martin et al., 2010). Since we do not present any data that allow us to quantitatively date the formation of rock microstructure and fabrics that we use to estimate deformation temperature and strain, the interpretations we make below assume that all of the microstructural deformation occurred during the Cenozoic Himalayan event.

6.1. Lesser Himalayan inverted deformation temperature gradient

The LH zone, when viewed in its entirety between the MBT and the MCT, shows an inverted gradient in metamorphic grade (Gansser, 1983) and deformation temperature (section 4, Fig. 7). Quartz and feldspar microstructure show that deformation temperatures increase from ca. 250°–310° at the MBT to ca. 500°–670° at the MCT (Fig. 7). However, with the exception of the upper part of lower LH thrust sheets directly below the MCT, there are discrete increases in deformation temperature that correspond to the positions of major thrust faults. We suggest that the inverted S-N deformation temperature gradient observed in the LH zone is primarily the result of stacking of discrete thrust sheets that were buried to and internally deformed at greater and greater depths toward the hinterland (e.g. Robinson et al., 2003; Martin et al., 2010). Assuming a geothermal gradient of 25 °C/km, thrust sheets of the Gondwana succession and Diuri Formation were internally deformed at depths of ca. 10–12 km, and thrust sheets of the Baxa Group duplex were internally deformed at depths of ca. 11–16 km. A few Baxa Group samples just under the ST record higher-temperature deformation, which could record greater depths of deformation (ca. 16–18 km) or shear heating at small structural distances below the ST.

The Daling–Shumar–Jaishidanda section shows a true inverted metamorphic and deformation temperature gradient within a single thrust sheet. Between the bottom (ST) to the top (MCT) of the section, biotite-in and garnet-in isograds are crossed (Gansser, 1983), and quartz and feldspar microstructure indicates a ca. 200–250 °C increase in deformation temperature (Figs. 6 and 7). However, the majority of deformation temperature increase (ca. 140–170 °C) occurs within ≤350 m structural distance below the MCT, which is the lowest observed transition from SGR to GBM recrystallization (Section 4.1.2, Fig. 6). In addition, shear heating associated with emplacement of the MCT could also be contributing to the high deformation temperature gradient observed here.

The approximately exponential form of the deformation temperature profiles (Fig. 6) indicates a rapid decrease in deformation temperature with structural distance just below the MCT, followed by more a gradual decrease at greater structural distances. This temperature profile is consistent with heating from the hot GH section in the hanging wall of the MCT (the 'hot-iron' effect of LeFort, 1975) (Fig. 15A). However, we suggest that the entire 'hot-iron' effect in the Bhutan LH section is limited to the Daling–Shumar–Jaishidanda thrust sheets, and therefore occupies a secondary role for creation of the inverted deformation temperature profile observed through the entire LH zone. The lowest observable thermal effects are: 1) the transition to K-feldspar recrystallization, which varies between ~1900 and 3600 m structural distance below the MCT east and west of the Kuru Chu valley (Fig. 6A, E), and 2) the biotite-in line, which varies between ~1300 and 2600 m structural distance below the MCT east and west of the Kuru Chu, to a maximum of ~5800–6000 m beneath the MCT in the Kuru Chu valley (Fig. 6C). Below these two transitions, at the base of the section, deformation temperatures are between ca. 400 and 450 °C, indicating depths of ca. 16–18 km (assuming a 25 °C/km geothermal gradient). This indicates that the GH section was emplaced above LH rocks that were originally at upper greenschist facies conditions, as originally predicted by Grujic et al. (2002) and Hollister and Grujic (2006).

Finally, another significant observation is that similar inverted metamorphic and deformation temperature profiles are repeated in both of the exposed Daling–Shumar Group thrust sheets in the Kuru Chu valley (Fig. 6C). The structural depth below the MCT of the first appearance of neoblastic biotite is very similar in both thrust sheets (5800 and 6000 m). This provides additional support for the discrete thrust fault that repeats the lower LH section (McQuarrie et al., 2008; Long et al., 2011b), which must post-date emplacement of the MCT and metamorphism of footwall LH rocks (Fig. 15A). Thus the MCT acts as the roof thrust for the lower LH duplex (Long et al., 2011b).

6.2. Strain order of operations

6.2.1. Layer-parallel shortening prior to layer-normal flattening

On the Trashigang transect, the *XY* strain plane of ellipsoids from samples in the southernmost Baxa Group horse, the Gondwana succession thrust sheet, and the Siwalik Group thrust sheet, are oriented at moderate to high angles to bedding (Figs. 4A and 10A). This is indicative of layer-parallel shortening (LPS) strain. The

Please cite this article in press as: Long, S., et al., Quantifying internal strain and deformation temperature in the eastern Himalaya, Bhutan: Implications for the evolution of strain in thrust sheets, Journal of Structural Geology (2011), doi:10.1016/j.jsg.2010.12.011

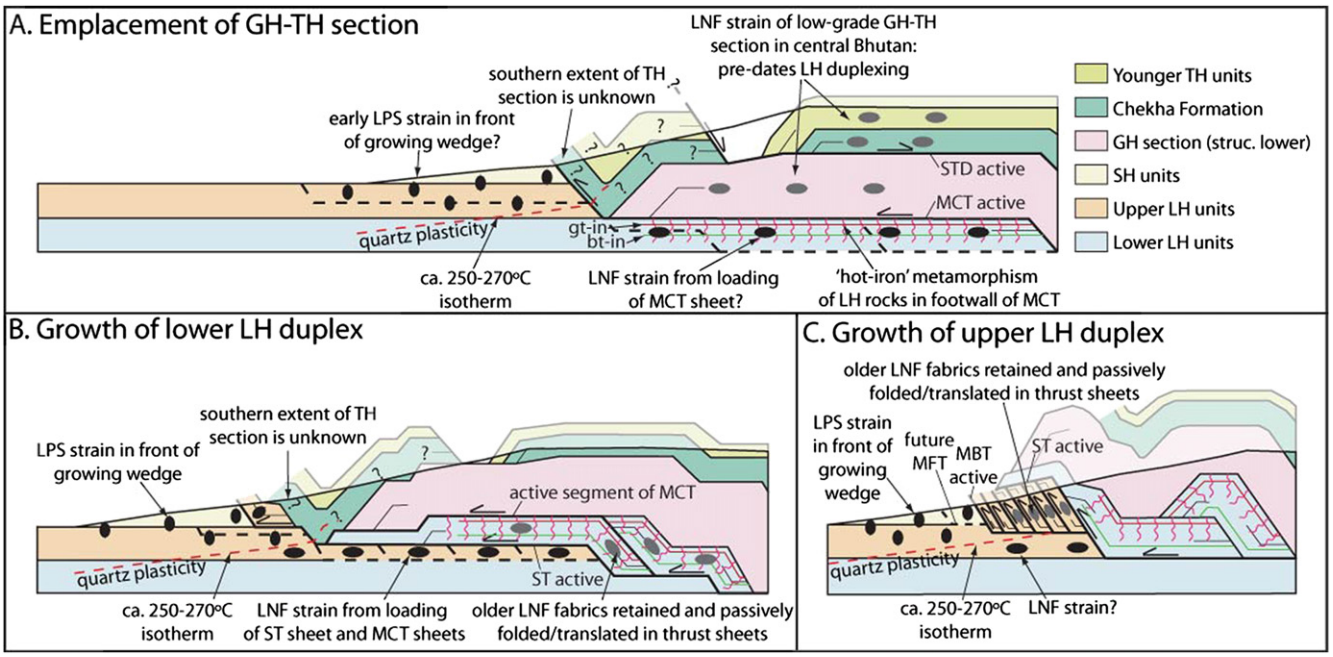

Fig. 15. Schematic cross-sections illustrating sequential development of strain patterns during specific deformation increments of the Bhutan fold-thrust belt. Active structures are shown in bold; structures that become active in next time increment are dashed. A) During emplacement of the GH–TH section (MCT and STD active), lower LH units (Shumar, Daling, Jaishidanda formations) in the MCT footwall were metamorphosed, producing the inverted metamorphic and deformation temperature gradient. Schematic positions of the biotite-in and garnet-in isograds are shown. Strain ellipsoids showing hypothetical layer-normal flattening (LNF) strain that presumably accompanied tectonic burial and metamorphism of these units are shown. LNF strain observed in the GH–TH section in central Bhutan occurred prior to lower LH duplexing, but whether it coincides with or pre-dates displacement on the MCT and STD is uncertain. Strain ellipsoids showing hypothetical layer-parallel shortening (LPS) strain in SH and upper LH units in front of the growing wedge are shown. B) During growth of the lower LH duplex (ST active), upper LH units (Baxa Group) underwent LNF strain from tectonic burial under the ST and MCT sheets. Low-magnitude LPS strain in SH and upper LH units in the foreland occurred above the ca. 250–270 °C isotherm (quartz plastic transition). The transition between LPS and LNF strain occurs approximately at this isotherm, and this is schematically shown in the subsurface. C) During growth of the upper LH duplex and subsequent deformation of foreland upper LH units and SH units, Baxa Group horses retaining older LNF strain fabrics were exhumed. Presumably, LPS strain in SH and upper LH units continued into the foreland, possibly as much as ca. 80 km south of the deformation front.

medians of Rs[*X*/*Z*] and Rs[*Y*/*Z*] ratios are 1.1 ($n = 7$) and 1.1 ($n = 3$), respectively. This median ellipsoid (1.1:1.1:1.0) restores to a sphere of the same volume with a radius of 1.07, indicating a 7% LPS magnitude. While data supporting LPS strain are only observed on this transect, this may indicate that low-magnitude LPS strain in the foreland is the earliest deformation that occurs. LPS strain most likely developed foreland-ward of the thrust deformation front (Fig. 15A–C), and preceded the LNF strain observed further to the hinterland, which we attribute to tectonic loading (Section 6.2.2). LPS strain may have been initiated from an increase in burial depth (and corresponding temperature) from subsidence and sedimentation in the foreland basin, and/or an increase in deviatoric stress near the leading edge of the growing, approaching thrust wedge (e.g. Yonkee and Weil, 2009). The importance of LPS strain in other orogenic belts, and the significance of the deformation temperature of the transition between LPS and LNF strain are discussed below in Section 6.5.

6.2.2. *Layer-normal flattening prior to thrust imbrication*

The majority of finite strain ellipsoids from the Diuri Formation, Baxa Group, and GH–TH section indicate that these map units underwent LNF strain, with the principal shortening direction (*Z*) oriented subperpendicular to bedding or tectonic foliation. The bedding/foliation-subparallel orientation of the *XY* strain plane persists regardless of the dip angle and dip direction at any given location. This is evident in areas of all four cross-sections, including: 1) the folded Diuri Formation thrust sheet on the Trashigang cross-section (Fig. 10A), 2) the foreland- and hinterland-dipping parts of the Baxa Group duplex on the Kuru Chu cross-section (Fig. 10B), 3) the southernmost exposed Baxa–Gondwana thrust sheet on the Bhumtang Chu cross-section (Fig. 10C), which exhibits multiple folds, and 4) the GH–TH section on the Mangde Chu cross-section (Fig. 10D), which is folded into a regional-scale synform. The orientations of ellipsoids are folded to the same degree as the thrust sheets in which they lie, which indicates that LNF strain preceded thrust imbrication and southward translation. We interpret this early LNF strain as the result of tectonic loading due to emplacement of thick overriding thrust sheets (Fig. 15A, B). LNF strain observed in Baxa Group horses (upper LH duplex) is attributed to burial and loading from emplacement of lower LH thrust sheets, which previously had been loaded by the GH–TH section (Fig. 15B). The strain observed in each individual Baxa Group horse had to precede the imbrication of that thrust sheet into the construction of the upper LH duplex. The minimal data that we present from the foreland exposures of the Daling, Shumar, and Jaishidanda formations suggest that LNF strain presumably occurred in these rocks as well. This is attributed to loading and burial from emplacement of the GH–TH section above the MCT (Fig. 15A).

Flattening strain recorded in the GH–TH section on the Mangde Chu transect must have preceded the construction of the lower and upper LH duplexes that fold the overlying section into a broad synform. In addition, based on Wm values calculated in this study (Section 5.3), and assuming that an approximate median Wm value of 0.4 (30% simple shear, 70% pure shear) is representative for the GH–TH section, the majority of strain the GH–TH rocks have experienced is pure-shear LNF strain. This is similar to data presented in the previous paragraph that suggest that LNF strain of LH units took place during tectonic burial that preceded thrust imbrication. If the LNF strain observed in the GH–TH section predates slip on the MCT and STD, it could be related to burial during

Please cite this article in press as: Long, S., et al., Quantifying internal strain and deformation temperature in the eastern Himalaya, Bhutan: Implications for the evolution of strain in thrust sheets, Journal of Structural Geology (2011), doi:10.1016/j.jsg.2010.12.011

earlier deformation of the TH section (e.g. Searle, 1986; Ratschbacher et al., 1994; Corfield and Searle, 2000; Murphy and Yin, 2003; Aikman et al., 2008). Implications of strain data on the style and magnitude of GH deformation is further explored in Section 6.4.

6.2.3. Strain order of operations: summary

As deformation progressed, and areas in the front of the wedge were incorporated into the foreland-propagating thrust system, the record of early LPS fabrics in hinterland units, if it was ever present, was overprinted by higher-magnitude LNF strain fabrics when units were tectonically buried by thick hinterland thrust sheets (Fig. 15A–C). Subsequently, deformation became localized along thrust faults, as these previously-strained map units were imbricated and translated in individual thrust sheets separated by discrete fault zones (Fig. 15B, C). After thrust emplacement, strata retaining older LNF fabrics were then passively folded and translated as thrusting propagated toward the foreland (Fig. 15B, C).

For the Baxa Group horses (upper LH duplex), graphs of structural distance of each strain sample above the basal horse thrust versus kinematic vorticity number (Wm) and versus Rs[N-S] (Fig. 16) show no correlation between strain magnitude and the component of simple shear with structural distance. This is in contrast to studies of internal thrust sheets that document a component of simple shear distributed throughout the hanging wall section, which increases toward the base, causing a concave-up strain profile (Wotjal, 1986; Mitra, 1994; Yonkee and Weil, 2009). The lack of this relationship in the upper LH duplex strongly supports the interpretation that internal deformation predates thrust imbrication and translation.

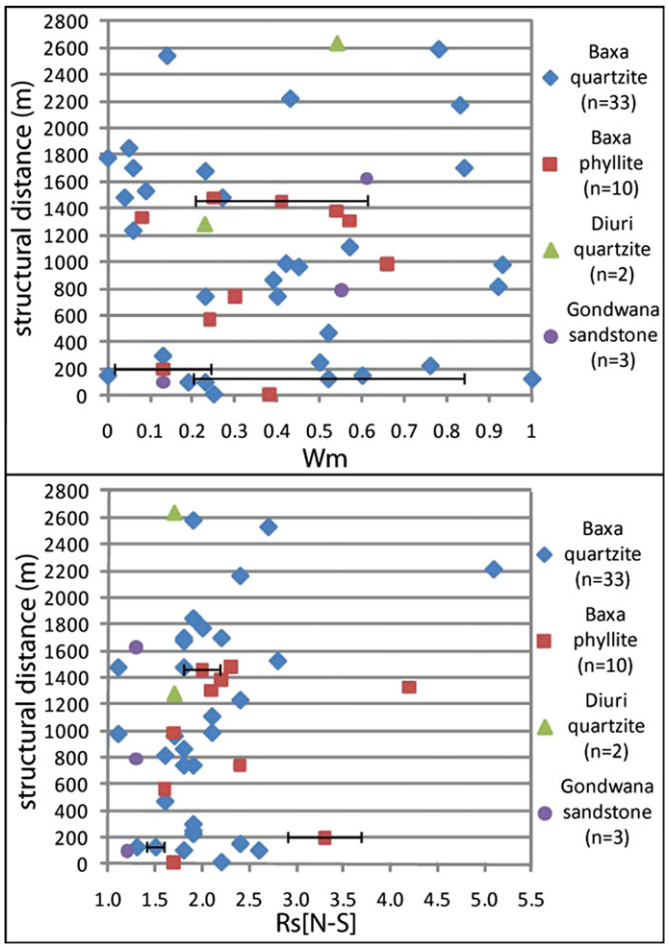

Fig. 16. Top graph plots structural distance of strain samples above the basal thrust in each horse in the upper LH duplex vs. mean kinematic vorticity (Wm), and bottom graph plots structural distance vs. Rs[N-S]. Note that there is no discernable trend in Wm or Rs[N-S] with structural distance that shows an increasing component of simple shear or strain magnitude toward the base of thrust sheets. 2σ (95%) error bars for Rs [N-S] and Wm are shown for samples with representative error for low (Rs<1.5), moderate (Rs = 1.6–2.5) and high (Rs>2.6) strain.

6.3. Implications of layer-normal flattening strain data for deformation restoration

By assigning median LPS (frontal Trashigang section only; Section 6.2.1) and LNF strain ellipsoids to the restored lengths of SH and upper LH units reported in Long et al. (2011b), we can estimate the changes in restored length that occur when internal strain is taken into account, by restoring these ellipsoids to spheres of the same volume. For the LNF domains, the restored length (in both N-S and E-W directions) decreases and thickness increases. For the LPS domain on the Trashigang transect, the restored length in the N-S direction increases. For the four cross-sections, the restored length of SH and upper LH map units collectively decreases between 22 and 42 km, which would correspond to a 15–31% decrease in shortening accommodated by SH and upper LH units on individual transects (Long et al., 2011b). This is in contrast to the common conception that not quantifying internal strain of thrust sheets results in underestimates of shortening in balanced cross-sections.

This simple restoration technique assumes that the median ellipsoids are representative of bulk strain, that LNF strain occurred entirely through pure shear deformation (Wm = 0.0), and more importantly, that there was no bulk volume change during deformation. The latter factor can be very significant in compressional environments (e.g. Ring et al., 2001 and references therein; Yonkee, 2005). Since our data show significant E-W ellipsoid elongations, and we observe no areas where this E-W strain could be accommodated (i.e. strain ellipsoids with E-W-trending *Z* axes), LNF strain of the magnitude that we document causes a significant space problem. A bulk volume decrease, such as mass loss through solution accompanying vertical thinning, would be necessary to allow for the apparent stretching in the *X* and *Y* directions that we document. Yonkee (2005) documented LNF strain in basal levels of the Willard thrust sheet in the Sevier fold-thrust belt. However, semiquantitative estimation of volume loss through analysis of fibers and seam lengths at clast boundaries indicated limited extension in the *Y* direction, which corresponded to volume losses between 10 and 40%. Ring et al. (2001) observed plane-strain vertical thinning through pure shear in greywacke above and below the Glarus Thrust in Switzerland, which is balanced by an average volume loss of 36%, through solution and cleavage development. In addition, multiple studies in convergent wedge settings have also documented significant volume loss associated with regional-scale, plane-strain, pure shear deformation (Brandon and Kang, 1995; Maxelon et al., 1998; Feehan and Brandon, 1999; Ring and Brandon, 1999; Bolhar and Ring, 2001).

Studies that quantify bulk volume change often utilize methods such as estimating the magnitude of solution mass transfer at cleavage planes (i.e. Ring et al., 2001; Yonkee and Weil, 2009). In Bhutan, the majority of examined strain samples are quartzite and sandstone, which did not exhibit cleavage planes or other solution features. As a consequence, we report no quantitative estimate of bulk rock volume change. However, in line with the studies from orogenic belts and accretionary complexes cited above (Ring et al., 2001, and references therein; Yonkee, 2005), we argue that the LNF strain ellipsoids we obtain from the Baxa Group, Diuri Formation, and GH–TH section, which in many samples display nearly equal *X*

Please cite this article in press as: Long, S., et al., Quantifying internal strain and deformation temperature in the eastern Himalaya, Bhutan: Implications for the evolution of strain in thrust sheets, Journal of Structural Geology (2011), doi:10.1016/j.jsg.2010.12.011

and *Y* elongations, require significant volume loss to maintain spatial compatibility. As a consequence, we suggest that the potential changes in restored length and shortening for SH and upper LH units calculated above should be considered maximum permissible values, and when significant flattening strain is observed, it must be accompanied by volume loss to maintain spatial compatibility.

6.4. Style and magnitude of deformation within the Greater Himalayan section

Using kinematic data through a low-temperature section of GH rocks, Long and McQuarrie (2010) documented a ~2 km-thick section immediately above the MCT exhibiting a top-to-the-south shear sense, which is overlain by an ~11 km-thick section exhibiting top-to-the-north shear, which defines the kinematic profile of a channel. They related preliminary strain data to channel flow (syn-STD and syn-MCT motion; e.g. Grujic et al., 1996, 2002) by assuming that all the strain the rocks record occurred during their exhumation path and not their burial path. Based on a preliminary strain dataset, and assuming only ideal simple shear, Long and McQuarrie (2010) estimated the top-to-the-north component of channel flow to be between ~23 and 34 km. However, based on Wm values calculated in this study (Section 5.3), and assuming that an approximate median Wm value of 0.4 (30% simple shear, 70% pure shear) is representative for the GH–TH section, the top-to-the-north component of channel flow is minimized to ~7–10 km. Under this interpretation, the majority of strain the GH–TH rocks have experienced (pure-shear LNF strain) could pre-date motion on the MCT and STD and be related to burial during earlier deformation of the TH section (e.g. Searle, 1986; Ratschbacher et al., 1994; Corfield and Searle, 2000; Murphy and Yin, 2003; Aikman et al., 2008).

Alternatively, if we assume that all LNF strain took place during channel flow (i.e. during the exhumation path rather than the burial path), and that all strain occurred through ideal pure-shear deformation, using a simple model we can calculate the magnitude of channel flow in a different way for comparison to the preliminary estimates of Long and McQuarrie (2010). By assuming that median strain ellipsoids for all GH lithologies (2.8:1.9:10) and all TH lithologies (1.6:1.5:1.0) in central Bhutan are representative of bulk strain, stretch in the *X* direction (N-S) can be calculated at 60% for GH rocks and 19% for TH rocks by restoring these median strain ellipsoids to spheres. Our strain data in GH rocks covers a final (deformed) across-strike length of ~50 km (Fig. 4E). Restoring the GH median strain ellipsoid to a sphere indicates a 31 km original length of this section, indicating that 19 km of N-S extrusion of GH rocks (central part of the channel) took place during channel flow. By assuming a similar 31 km-long original length of the overlying TH section, the final length would increase to 37 km (note that the total across-strike length of the Shemgang TH exposure is only ~25 km), indicating only 6 km of N-S extrusion of the higher part of the channel. Note that the amount of N-S extrusion increases toward the center, with a 13 km difference between GH rocks (center of channel) and TH rocks (higher part of channel, presumably near the top). These larger extrusion magnitudes toward the center of the channel would result in an overall top-to-the-north shear sense, which is supported by kinematic indicators observed across the GH–TH section (Long and McQuarrie, 2010).

Under all the above scenarios, which include: 1) all GH–TH strain is attributed to simple shear deformation during channel flow (Long and McQuarrie, 2010); 2) only a small component of simple shear (~30%) of GH–TH rocks occurred during channel flow, and the majority of strain (LNF) pre-dates channel flow; and 3) all GH–TH strain is attributed to pure-shear LNF strain during channel flow, the top-to-the-north component of channel flow shows a total range between 7 and 34 km, and is likely 19 km or less. It is important to mention that this corresponds to only 2–9% (and likely 2–5%) of the minimum total mass added to the Mandge Chu cross-section through shortening of SH, LH, and GH–TH rocks (387 km; Long et al., 2011b). In addition, since we present no quantitative estimate of volume loss in GH–TH rocks, which we argue must have accompanied the stretching in the *X* and *Y* directions that we document in order to maintain spatial compatibility, we suggest that the top-to-the-north extrusion magnitudes discussed above should be considered maximum permissible values.

For the GH–TH section in central Bhutan, we would hypothesize that an increasing component of simple shear is concentrated in the bottom ~2 km of the section, which exhibits a top-to-the-south motion sense, and likely had a low viscosity during deformation based on the presence of partial melt textures (Long and McQuarrie, 2010). However, since the majority of the GH orthogneiss unit underwent GBM quartz recrystallization, we do not have a record of strain at the base of the section, only kinematic data (Long and McQuarrie, 2010).

Our vorticity data for the GH–TH section in central Bhutan (Section 5.3) can be compared to published vorticity estimates for the GH section along-strike. Law et al. (2004) and Jessup et al. (2006) obtained mean kinematic vorticity numbers (Wm) between 0.67 and 0.98 (13–53% pure shear) from the top of the GH section at the Everest Massif in Tibet, and Carosi et al. (2006) obtained Wm values of 0.63–0.76 from the mid-upper part of the structurally-higher GH section in northwest Bhutan. Grasemann et al. (1999) and Jessup et al. (2006) obtained Wm values of 0.57–0.71 and 0.63–0.77 (44–58% pure shear), respectively, from the basal part of the GH section (MCT zone) in NW India and eastern Nepal.

These kinematic vorticity numbers indicate a substantial component of pure shear at the basal and upper parts of the GH section, which requires a degree of stretch or elongation. Grasemann et al. (1999) presented a model for extrusion of the GH section that calls for a stronger pure shear component, and thus a higher elongation, in the central part of the slab, in order to maintain the requirements of strain compatibility. Our GH–TH vorticity data from central Bhutan are from samples between 2.5 and 9.5 km structural distance above the MCT. Though the structural distance to the STD, which projects above the erosion surface on this transect (Long and McQuarrie, 2010), is unknown, these structural distances presumably occupy the majority of the middle of the GH–TH section. About half of our Wm numbers for the GH–TH section are $\leq$0.4 (within error), indicating a $\geq$70% component of pure shear. These vorticity numbers are much lower than those reported for the top (STD zone) and bottom (MCT zone) of the GH section in Tibet, Nepal, northwest Bhutan, and northwest India (Grasemann et al., 1999; Law et al., 2004; Carosi et al., 2006; Jessup et al., 2006). Thus, our data support a greater component of pure shear toward the center of the GH section, as predicted by the ductile extrusion model of Grasemann et al. (1999).

Since the peak temperatures and volume percent of partial melt in the GH section show significant along-strike changes between central and eastern Bhutan (Grujic et al., 2002; Daniel et al., 2003; Long and McQuarrie, 2010), which are presumably accompanied by significant changes in rheology (e.g. Rosenberg and Handy, 2005), we are reluctant to apply the LNF strain orientations, magnitudes, and Wm numbers that we observe for GH–TH rocks in central Bhutan to the higher-grade GH rocks in eastern Bhutan. In support of along-strike strain changes, note that Grujic et al. (1996), based on the asymmetry of <c> and <a> axes in quartz CPO plots, interpreted a moderately-rotational, plane-strain to weakly-constrictional

Please cite this article in press as: Long, S., et al., Quantifying internal strain and deformation temperature in the eastern Himalaya, Bhutan: Implications for the evolution of strain in thrust sheets, Journal of Structural Geology (2011), doi:10.1016/j.jsg.2010.12.011

strain regime, with the coexistence of pure- and simple-shear components, for the GH section in eastern Bhutan.

6.5. Comparison of Himalayan strain data to other orogens

LNF strain was accomplished with a dominant pure shear component in the Baxa Group thrust sheets and the GH–TH section in central Bhutan. This observation is similar to results from multiple studies in thrust sheets deformed at temperatures above those for quartz plasticity (ca. 250–270 °C) (Fig. 17). Ring et al. (2001) studied greywacke deformed at greenschist-facies conditions (ca. 300 °C) above and below the Glarus Thrust in Switzerland, and documented pure shear, thrust-normal thinning (30%), accompanied by significant volume loss (36%), with typical Rs values of 1.5–2, and θ' values, defined by thrust-subparallel cleavage, typically <10°. Yonkee (2005) observed simple shear dominated deformation of quartzite and micaceous strata at higher structural levels within the Willard thrust of the Idaho-Wyoming-Utah fold-thrust belt, but greywacke and slate at basal levels were dominated by thrust-subparallel foliation, extensive crystal–plastic quartz deformation, typical Rs values of 2–4, the majority of θ' values <20°, and typical Wm values <0.7. Sanderson (1982) documented large-magnitude (Rs ~ 50), thrust-subparallel (θ'<2°) strain in localized mylonite zones adjacent to the Moine thrust in Scotland, indicating significant thrust-parallel elongation and Wm values <0.7. Kligfield et al. (1981) documented high-magnitude (Rs ~ 5–10), thrust-subparallel (θ'<10°) strain in limestone deformed at ca. 400 °C in the Northern Appenines in Italy, indicating substantial thrust-normal thinning and thrust-parallel extension.

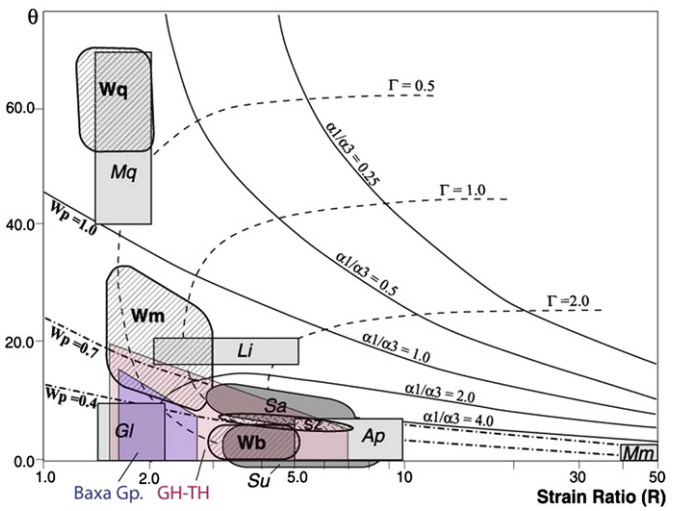

Fig. 17. Plot of Rs[*XZ*] vs. θ', showing Bhutan strain data compared to data compiled for studies of thrust sheets in different orogens (diagonally-ruled patterns; light gray patterns), transpressive belts (dark gray patterns) and shear zones (stippled patterns); modified from Yonkee (2005). Typical values for Baxa Group (blue) and GH–TH section in central Bhutan (pink) shown (absolute value of θ' was used to project our data onto this graph). Abbreviations and data sources: Wq – micaceous to arkosic quartzite at intermediate levels of Willard thrust sheet, Sevier fold-thrust belt (Yonkee, 2005); Wm – micaceous strata at lower levels of Willard thrust sheet (Yonkee, 2005); Wb – basal levels of Willard Thrust sheet (Yonkee, 2005); Mq – Moine thrust quartzite (Coward and Kim, 1981); Mm – Moine thrust mylonite zones (Sanderson, 1982); Gl – Glarus thrust greywacke (Ring et al., 2001); Ap – Northern Appenine limestone (Kligfield et al., 1981); Li – Ligurian Alps meta-conglomerate (Seno et al., 1998); Su - Superior Province belt (Czeck and Hudleston, 2003); Sa – Sambagawa belt (Wallis, 1995); SZ – examples from various shear zones (Eyster and Bailey, 2001). Contours of thrust-parallel shear strain (Γ), ratio of thrust-parallel to thrust-perpendicular stretch (α1/α3), and mean kinematic vorticity for plane strain (Wp) shown. (For interpretation of the references to colour in this figure legend, the reader is referred to the web version of this article).

The low-magnitude (7%) LPS strain observed on the Trashigang transect indicates that LPS strain in the foreland of the deformation front preceded LNF strain from tectonic loading (Section 6.2.1). Early LPS strain concentrated in front of the thrust wedge, with the *Z* direction oriented sub-normal to structural trend, and is an important deformation mechanism in many fold-thrust belts. LPS deformation is often the most significant internal strain mechanism that affects external, unmetamorphosed thrust sheets (Wotjal, 1986; Mitra, 1994; Yonkee and Weil, 2009). In the foreland parts of the Pennsylvania salient of the Appalachian orogen, LPS values between ca. 13 and 20% are reported (Nickelsen, 1963, 1983; Engelder, 1979; Gray and Mitra, 1993; Faill and Nickelsen, 1999). In exterior thrust sheets of the Idaho–Wyoming–Utah salient of the Sevier fold-thrust belt, LPS values between ca. 5–30% are reported (Crosby, 1969; Gockley, 1985; Craddock, 1992; Mitra, 1994; McNaught and Mitra, 1996; Mukul and Mitra, 1998; Yonkee and Weil, 2009). Our median value of 7% LPS falls toward the low end of values reported in these other orogens. Yonkee and Weil (2009) estimate that LPS strain preceded the Sevier thrust deformation front by a transport-parallel map distance of ca. 60 km, which is similar to the 82 km restored distance between the southernmost and northernmost LPS samples on the Trashigang transect.

The spatial transition between LNF and LPS strain observed in Bhutan, in conjunction with the results of strain studies from other orogens discussed above, illustrates the first-order control of deformation temperature on rock rheology and therefore the resulting strain mechanism. On the Trashigang transect, the transition between LPS and LNF strain occurred at an approximate deformation temperature range of ca. 250–310 °C, the minimum temperature for BLG recrystallization (Stipp et al., 2002), which coincides with the lower temperature limits for crystal–plastic quartz deformation (ca. 250–270 °C; Dunlap et al., 1997; van Daalen et al., 1999; Stipp et al., 2002). In general, external thrust sheets deformed below this temperature range will be strong, particularly if dominated by quartz-rich strata, and will exhibit limited-magnitude LPS strain, possibly combined with a component of low-magnitude simple shear toward the base (e.g. Wotjal, 1986; Mitra, 1994; Yonkee and Weil, 2009). More interior thrust sheets, if deformed at temperatures above those for quartz plasticity, will generally have higher strain magnitudes, and may exhibit a layer-normal, pure shear-dominant component of strain. Intervals of thrust sheets comprised of quartz- or mica-rich rocks at these elevated temperatures may be sufficiently weak to lose significant shear strength, causing far-field tectonic stresses inclined at a low angle to layering to rotate into a layer-subnormal orientation, resulting in layer-normal thinning and layer-parallel stretching (Means, 1989; Yonkee, 2005).

In Bhutan, strain fabrics in upper LH and GH–TH thrust sheets that were deformed at temperatures ≥ ca. 250-270 °C are dominated by pure-shear LNF strain, illustrating the strong control of deformation temperature on strain magnitude and orientation. In addition, the sequential progression from layer-normal thinning due to tectonic loading was followed by localization of deformation along discrete thrust faults. This is supported by: 1) strain ellipsoids being folded the same amount as the thrust sheets in which they lie (Fig. 10), and 2) no systematic increase in Rs or Wm with decreasing structural distance (at the scale of 10's of meters) above thrusts (Fig. 16), indicating that internal strain pre-dated thrusting, and that internal strain did not extend outside of fault zones during thrusting. This indicates that fault zones were significantly weaker than the previously-strained rocks carried in their hanging wall (e.g. Mitra and Boyer, 1999). This supports the existence of discrete faults with large translations as depicted in balanced cross-sections, even when the rocks within the thrust sheets have undergone significant internal strain.

Please cite this article in press as: Long, S., et al., Quantifying internal strain and deformation temperature in the eastern Himalaya, Bhutan: Implications for the evolution of strain in thrust sheets, Journal of Structural Geology (2011), doi:10.1016/j.jsg.2010.12.011

7. Conclusions

1. Low-magnitude (~7%) layer-parallel shortening (LPS) strain observed in the foreland part of the Trashigang transect suggests that LPS strain in front of the propagating wedge was the earliest internal deformation that occurred.
2. The majority of foreland LH thrust sheets and a composite GH–TH thrust sheet in the hinterland underwent layer-normal flattening (LNF) strain, with the *X* direction generally coinciding with N-S mineral stretching lineation. Kinematic vorticity numbers for the majority of LNF samples indicate that pure shear (≥70%) was the dominant strain mechanism. LNF strain is interpreted as the result of tectonic loading due to emplacement of thick overriding thrust sheets. As deformation propagated toward the foreland, the record of early LPS fabrics in hinterland units, if it was ever present, was overprinted by higher-magnitude LNF fabrics when units were tectonically buried.
3. The transition between low-magnitude (Rs ~ 1.1–1.2) LPS and higher-magnitude (Rs ~ 1.8–2.0) LNF strain occurs approximately at the lower temperature limits for crystal–plastic quartz deformation (ca. 250–270 °C), which illustrates the strong control of deformation temperature on strain magnitude and orientation. Thrust sheets comprised of quartz- or mica-rich rocks above this temperature range were sufficiently weak enough due to loss of shear strength to cause far-field tectonic stresses oriented at a low angle to layering to rotate into a layer-normal orientation (e.g. Means, 1989).
4. The orientations of LNF ellipsoids are folded to the same degree as the thrust sheets in which they lie, indicating that LNF strain preceded thrust imbrication and southward translation.
5. After LNF strain, deformation became more localized, as these previously-strained rocks were imbricated and translated in thrust sheets separated by discrete fault zones. After thrust emplacement, strata retaining older LNF fabrics were then passively folded and translated as thrusting propagated toward the foreland.
6. A lack of increase in Rs and Wm with decreasing structural distance above thrusts in the upper LH duplex indicates that significant internal strain did not extend more than 10's of meters outside of fault zones during thrusting. This supports the existence of discrete faults with large translations, as generally depicted in balanced cross-sections, even when the rocks within the thrust sheets have undergone significant internal strain.
7. Simple restoration of LNF strain would result in decreasing shortening estimates in Bhutan balanced cross-sections, in contrast to commonly-held views that not accounting for internal strain results in under-estimation of shortening. However, we suggest that when significant flattening strain is observed, it must be accompanied by volume loss to maintain spatial compatibility. As a consequence, strain ellipsoids become decoupled from the bulk thrust translation. Thus their strongest utility lies in illuminating the mechanisms and order of operations of strain, rather than the cumulative effect of strain in restoration of deformation.
8. The inverted gradient in deformation temperature observed in the LH zone can be attributed primarily to stacking of discrete thrust sheets of LH rocks that were deformed at progressively higher temperatures (and depths) toward the hinterland. The 'hot-iron' effect of the MCT hanging wall only affects LH thrust sheets directly below the MCT. The majority of the upsection temperature increase associated with the 'hot-iron' effect occurs within ca. 350 m structural distance of the MCT.
9. Strain data distributed through low-grade GH–TH rocks in central Bhutan that exhibit the kinematic profile of a channel (Long and McQuarrie, 2010) argue for minimal magnitudes (7–34 km range, and most likely less than 19 km) of the top-to-the-north component of channel-flow extrusion. This corresponds to only 2–9% (and likely 2–5%) of the minimum total mass added to the central Bhutan thrust belt through shortening of SH, LH, and GH–TH rocks.

Acknowledgments

The authors would like to thank the government of Bhutan for their assistance and support, in particular former Director General D. Wangda and the Department of Geology and Mines in the Ministry of Economic Affairs. We would also like to thank Chris Hepburn for assistance in the lab collecting strain data and Linc Hollister and Djordje Grujic for multiple discussions. Constructive reviews by Aaron Martin and Adolph Yonkee significantly improved the manuscript. This work was supported by NSF EAR 0738522 to N. McQuarrie.

Appendix

Supplementary data related to this article can be found online at doi:10.1016/j.jsg.2010.12.011.

References

Aikman, A.B., Harrison, T.M., Ding, L., 2008. Evidence for early (>44 Ma) Himalayan crustal thickening, Tethyan Himalaya, southeastern Tibet. Earth and Planetary Science Letters 274, 14–23.

Arita, K., 1983. Origin of the inverted metamorphism of the Lower Himalayas, central Nepal. Tectonophysics 95, 43–60.

Bailey, J.E., Hirsch, P.B., 1962. The recrystallization process in some polycrystalline metals. Proclamations of the Royal Society of London, Serial A267, 11–30.

Bhargava, O.N., 1995. The Bhutan Himalaya. In: A Geological Account. Geol. Soc. India Special Publication, vol. 39, p. 245.

Bhattacharyya, K., Mitra, G., 2009. A new kinematic evolutionary model for the growth of a duplex – an example from the Rangit duplex, Sikkim Himalaya, India. Gondwana Research 16, 697–715.

Bolhar, R., Ring, U., 2001. Deformation history of the Yolla Bolly terrane at Leech Lake Mountain, eastern belt, Franciscan subduction complex, California Coast Ranges. Geological Society of America Bulletin 113, 181–195.

Boyer, S.E., Elliott, D., 1982. Thrust systems. American Association of Petroleum Geologists Bulletin 66, 1196–1230.

Brandon, M.T., Kang, B., 1995. Exhumation processes operating above the Cascadia subduction zone, NW Washington State. Terra Nova 7, 170.

Burchfiel, B.C., Chen, Z.L., Hodges, K.V., Liu, Y.P., Royden, L.H., Deng, C.R., Xu, J.N., 1992. The South Tibetan Detachment System, Himalayan Orogen: Extension Contemporaneous with and Parallel to Shortening in a Collisional Mountain Belt. In: Geological Society of America Special Paper, vol. 269, p. 41.

Burg, J.P., 1983. Tectogenese compare de deux segments de chaine de collision: le sud du Tibet (suture du Tsangpo), la chaine hercynienne en Europe (suture du Massif Central): Thesis, Montpellier.

Carosi, R., Montomoli, C., Rubatto, D., Visona, D., 2006. Normal-sense shear zones in the core of the Higher Himalayan Crystallines (Bhutan Himalaya): evidence for extrusion? In: Law, R.D., Searle, M.P., Godin, L. (Eds.), Channel Flow, Ductile Extrusion and Exhumation in Continental Collision Zones Geolocial Society of London Special Publication, vol. 268, pp. 425–444.

Catlos, E.J., Harrison, T.M., Kohn, M.J., Grove, M., Ryerson, F.J., Manning, C.E., Upreti, B.N., 2001. Geochronologic and thermobarometric constraints on the evolution of the Main central thrust, central Nepal Himalaya. Journal of Geophysical research (Series B). Solid Earth and Planets 106, 16,177–16,204.

Cawood, P.A., Johnson, M.R.W., Nemchin, A.A., 2007. Early Paleozoic orogenesis along the Indian margin of Gondwana: tectonic response to Gondwana assembly. Earth and Planetary Science Letters 255, 70–84.

Chakungal, J., Dostal, J., Grujic, D., Duchene, S., Ghalley, K.S., 2010. Provenance of the Greater Himalayan sequence: evidence from mafic granulites and amphibolites in NW Bhutan. Tectonophysics 480, 198–212.

Corfield, R.I., Searle, M.P., 2000. Crustal shortening estimates across the north Indian continental margin, Ladakh, NW India. In: Khan, M.A., Treloar, P.J., Searle, M.P., Jan, M.Q. (Eds.), Tectonics of the Nanga Parbat Syntaxis and the Western Himalaya. Geological Society of London Special Publication, vol. 170, pp. 395–410.

Coward, M.P., Kim, J.H., 1981. Strain within thrust sheets. In: McClay, K.R., Price, N.J. (Eds.), Thrust and Nappe Tectonics. Geological Society of London Special Publication, vol. 9, pp. 275–292.

Craddock, J.P., 1992. Transpression during tectonic evolution of the Idaho-Wyoming fold-and- thrust belt. In: Link, P.K., Kuntz, M.A., Platt, L.B. (Eds.), Regional

Geology of Eastern Idaho and Western Wyoming. Geological Society of America Memoir, 179, pp. 55–81.
Crosby, G.W., 1969. Radial movements in the western Wyoming salient of the Cordilleran Overthrust Belt. Geological Society of America Bulletin 80, 1061–1077.
Czeck, D.M., Hudleston, J., 2003. Testing models for obliquely plunging lineations in transpression: a natural example and theoretical discussion. Journal of Structural Geology 25, 959–982.
Dahlstrom, C.D.A., 1969. Balanced cross-sections. Canadian Journal of Earth Sciences 6, 743–757.
Daniel, C.G., Hollister, L.S., Parrish, R.R., Grujic, D., 2003. Exhumation of the Main central thrust from lower crustal depths, eastern Bhutan Himalaya. Journal of Metamorphic Geology 21, 317–334.
Dasgupta, S., Ganguly, J., Neogi, S., 2004. Inverted metamorphic sequence in the Sikkim Himalayas: crystallization history, P-T gradient and implications. Journal of Metamorphic Geology 22, 395–412.
Dasgupta, S., 1995. Jaishidanda formation. In: Bhargava, O.N. (Ed.), The Bhutan Himalaya: a Geological Account. Geological Society of India Special Publication, vol. 39, pp. 79–88.
Davidson, C., Grujic, D.E., Hollister, L.S., Schmid, S.M., 1997. Metamorphic reactions related to decompression and synkinematic intrusion of leucogranite, High Himalayan Crystallines, Bhutan. Journal of Metamorphic Geology 15, 593–612.
DeCelles, P.G., Robinson, D.M., Zandt, G., 2002. Implications of shortening in the Himalayan fold-thrust belt for uplift of the Tibetan Plateau. Tectonics 21, 1062–1087. doi:10.1029/2001TC001322.
Drury, M.R., Humphreys, F.J., White, S.H., 1985. Large strain deformation studies using polycrystalline magnesion as rock analogue, Part II. Dynamic recrystallization mechanisms at high temperatures. Physics of the Earth and Planetary Interior 40, 208–222.
Dunlap, W.J., Hirth, G., Teyssier, C., 1997. Thermomechanical evolution of a ductile duplex. Tectonics 16, 983–1000.
Dunnet, D., 1969. A technique for finite strain analysis using elliptical particles. Tectonophysics 7, 117–136.
Dunnet, D., Siddans, A.W.B., 1971. Non-random sedimentary fabrics and their modification by strain. Tectonophysics 12, 307–325.
Edwards, M.A., Kidd, W.S.F., Jixiang, L., Yue, Y., Clark, M., 1996. Multi-stage development of the southern Tibetan detachment system near Khula Kangri; New data from Gonto La. Tectonophysics 260, 1–19.
Edwards, M.A., Pecher, A., Kidd, W.S.F., Burchfiel, B.C., Royden, L.H., 1999. Southern Tibet detachment system at Khula Kangri, eastern Himalaya: a large-area, Shallow detachment stretching into Bhutan? The Journal of Geology 107, 623–631.
Elliott, D., 1977. Some Aspects of the Geometry and Mechanisms of Thrust Belts. In: 8th Annual Canadian Society of Petrology and Geology Seminar, vol. 1, p. 17.
Engelder, 1979. Mechanisms for strain within the upper Devonian clastic sequence of the Appalachian Plateau, western New York. American Journal of Science 279, 527–542.
Erslev, E.A., 1988. Normalized center-to-center analysis of packed aggregates. Journal of Structural Geology 10, 201–209.
Eyster, E.L., Bailey, C.M., 2001. Vorticity Analyses of Extensional and Transpressional High-strain Zones; Examples from the Arizona Basin and Range and Virginia Piedmont. Geological Society of America Abstracts with Programs 33 (2), 5.
Faill, R.T., Nickelsen, R.P., 1999. Appalachian mountain section of the Valley and Ridge province. In: Schultz, C.H. (Ed.), The Geology of Pennsylvania. Pennsylvania Geological Survey Special Publication, vol. 1, pp. 268–285.
Feehan, J.G., Brandon, M.T., 1999. Contribution of ductile flow to exhumation of low T-high P metamorphic rocks: San Juan-Cascade Nappes, NW Washington State. Journal of Geophysical Research B104, 10883–10901.
Fitzgerald, J.D., Stunitz, H., 1993. Deformation of granitoids at low metamorphic grade. I. reactions and grain size reduction. Tectonophysics 221, 269–297.
Fry, N., 1979. Random point distributions and strain measurement in rocks. Tectonophysics 60, 89–105.
Gansser, A., 1964. Geology of the Himalayas. Wiley–Interscience, New York, 289 pp.
Gansser, A., 1983. Geology of the Bhutan Himalaya. Birkhauser Verlag, Boston, 181 pp.
Garzanti, E., Casnedi, R., Jadoul, F., 1986. Sedimentary evidence of a Cambro–Ordovician orogenic event in the northwestern Himalaya. Sedimentary Geology 48, 237–265.
Gehrels, G.E., DeCelles, P.G., Martin, A., Ojha, T.P., Pinhassi, G., 2003. Initiation of the Himalayan Orogen as an early Paleozoic thin-skinned thrust belt. GSA Today 13, 4–9.
Gehrels, G.E., DeCelles, P.G., Ojha, T.P., Upreti, B.N., 2006a. Geologic and U–Pb geochronologic evidence for early Paleozoic tectonism in the Dadeldhura thrust sheet, far-west Nepal Himalaya. Journal of Asian Earth Science 28, 385–408. doi:10.1016/j.jseaes.2005.09.012.
Gehrels, G.E., DeCelles, P.G., Ojha, T.P., Upreti, B.N., 2006b. Geologic and U–Th–Pb geochronologic evidence for early Paleozoic tectonism in the Kathmandu thrust sheet, central Nepal Himalaya. Geological Society of America Bulletin 118, 185–198. doi:10.1130/B25753.1.
Geiser, P.A., Engelder, T., 1983. The distribution of layer parallel shortening fabrics in the Appalachian foreland of New York and Pennsylvania; evidence for two non-coaxial phases of the Alleghenian orogeny. In: Hatcher Jr., R.D., et al. (Eds.), Contributions to the Tectonics and Geophysics of Mountain Chains. Geological Society of America Memoir, vol. 158, pp. 161–175.
Gockley, C.K., 1985. Structure and strain analysis of the Big Elk Mountain Anticline, Caribou Mountains, Idaho. M.S. Thesis, University of Colorado, Boulder, 221.
Gokul, A.R., 1983. Geological and Mineral Map of Bhutan. In: Geologicl Survey of India Map Printing Division, Hyderabad, Scale, vol. 1 500, 000, 1 sheet.
Grasemann, B., Fritz, H., Vannay, J.C., 1999. Quantitative kinematic flow analysis from the Main Central Thrust Zone (NW Himalaya, India): implications for a decelerating strain path and the extrusion of orogenic wedges. Journal of Structural Geology 21, 837–853.
Gray, M.B., Mitra, G., 1993. Migration of deformation fronts during progressive deformation: evidence from detailed studies in the Pennsylvanian Southern Anthracite region, U.S.A. Journal of Structural Geology 15, 435–450.
Grujic, D., Casey, M., Davidson, C., Hollister, L.S., Kundig, R., Pavlis, T., Schmid, S., 1996. Ductile extrusion of the Higher Himalayan Crystallines in Bhutan: evidence from quartz microfabrics. Tectonophysics 260, 21–43.
Grujic, D., Hollister, L.S., Parrish, R.R., 2002. Himalayan metamorphic sequence as an orogenic channel: insight from Bhutan. Earth and Planetary Science Letters 198, 177–191.
Guillope, M., Poirier, J.P., 1979. Dynamic recrystallization during creep of single-crystalline halite: an experimental study. Journal of Geophysical Research 84, 5557–5567.
Harrison, T.M., Ryerson, F.J., LeFort, P., Yin, A., Lovera, O., Catlos, E.J., 1997. A late Miocene-Pliocene origin for the central Himalayan inverted metamorphism. Earth and Planetary Science Letters 146, E1–E7.
Harrison, T.M., Grove, M., Lovera, O.M., Catlos, E.J., 1998. A model for the origin of Himalayan anatexis and inverted metamorphism. Journal of Geophysical Research 103, 27,017–27,032.
Heim, A., Gansser, A., 1939. Central Himalaya: Geological Observations of the Swiss Expedition, 1936. In: Memoirs of the Swiss Society of Natural Science, vol. 73 p. 245.
Hirth, G., Tullis, J., 1992. Dislocation creep regimes in quartz aggregates. Journal of Structural Geology 14, 145–159.
Hodges, K.V., 2000. Tectonics of the Himalaya and southern Tibet from two perspectives. Geological Society of America Bulletin 112, 324–350.
Hollister, L.S., Grujic, D., 2006. Pulsed channel flow in Bhutan. In: Law, R.D., Searle, M.P., Godin, L. (Eds.), Channel Flow, Ductile Extrusion and Exhumation in Continental Collision Zones. Geological Society of London Special Publication, 268, pp. 415–423.
Holyoke, C.W., Tullis, J., 2006. Formation and maintenance of shear zones. Geology 34, 105–108.
Hubbard, M.S., 1989. Thermobarometric constraints on the thermal history of the Main Central thrust zone and Tibetan Slab, eastern Nepal Himalaya. Journal of Metamorphic Geology 7, 19–30.
Jangpangi, B.S., 1974. Stratigraphy and tectonics of parts of eastern Bhutan. Himalayan Geology 4, 117–136.
Jangpangi, B.S., 1978. Stratigraphy and structure of Bhutan Himalaya. In: Saklani, P.W.S. (Ed.), Tectonic Geology of Himalaya. Todays' and Tomorrows' Publications, New Delhi, pp. 221–292.
Jessup, M.J., Law, R.D., Searle, M.P., Hubbard, M.S., 2006. Structural evolution and vorticity of flow during extrusion and exhumation of the Greater Himalayan Slab, Mount Everest Massif, Tibet/Nepal: implications for orogen-scale flow partitioning. In: Law, R.D., Searle, M.P., Godin, L. (Eds.), Channel Flow, Ductile Extrusion and Exhumation in Continental Collision Zones. Geological Society of London Special Publication, vol. 268, pp. 379–413.
Joshi, A., 1995. Setikhola formation. In: Bhargava, O.N. (Ed.), The Bhutan Himalaya: a Geological Account. Geological Society of India Special Publication, vol. 39, pp. 34–37.
Kligfield, R., Carmignani, L., Owens, W.H., 1981. Strain analysis of a Northern Apennine shear zone using deformed marble breccias. Journal of Structural Geology 16, 493–503.
Kohn, M.J., Catlos, E.J., Ryerson, F.J., Harrison, T.M., 2001. Pressure-temperature-time path discontinuity in the Main Central Thrust zone, central Nepal. Geology 29, 571–574.
Lakshminarayana, G., 1995. Damuda Subgroup. In: Bhargava, O.N. (Ed.), The Bhutan Himalaya: A Geological Account. Geological Society of India Special Publication, vol. 39, pp. 29–33.
Lakshminarayana, G., Singh, B., 1995. Siwalik Group. In: Bhargava, O.N. (Ed.), The Bhutan Himalaya: A Geological Account. Geological Society of India Special Publication, vol. 39, pp. 23–28.
Law, R.D., Searle, M.P., Simpson, R.L., 2004. Strain, deformation temperatures, and vorticity of flow at the top of the greater Himalayan slab, Everest Massif, Tibet. Journal of the Geological Society of London 161, 305–320.
LeFort, P., 1975. Himalayas: the collided range, present knowledge of the continental arc. American Journal of Science 275-A, 1–44.
Lister, G.S., Dornsiepen, U.F., 1982. Fabric transitions in the Saxony granulite terrain. Journal of Structural Geology 4, 81–92.
Long, S., McQuarrie, N., Tobgay, T., Rose, C., Gehrels, G., Grujic, D., 2011a. Tectonostratigraphy of the lesser Himalaya of Bhutan: implications for the along-strike stratigraphic continuity of the northern Indian margin. Geological Society of America Bulletin, doi:10.1130/B30202.1.
Long, S., McQuarrie, N., Tobgay, T., Grujic, D., 2011b. Geometry and crustal shortening of the Himalayan fold-thrust belt, eastern and central Bhutan. Geological Society of America Bulletin, doi:10.1130/B30203.1.
Long, S., McQuarrie, N., 2010. Placing limits on channel flow: insights from the Bhutan Himalaya. Earth and Planetary Science Letters 290, 375–390.
Mainprice, D.H., Bouchez, J.L., Blumenfeld, P., Tubia, J.M., 1986. Dominant c slip in naturally-deformed quartz: implications for dramatic plastic softening at high temperature. Geology 14, 819–822.

Please cite this article in press as: Long, S., et al., Quantifying internal strain and deformation temperature in the eastern Himalaya, Bhutan: Implications for the evolution of strain in thrust sheets, Journal of Structural Geology (2011), doi:10.1016/j.jsg.2010.12.011

Martin, A.J., Gehrels, G.E., DeCelles, P.G., 2007. The tectonic significance of (U, Th)/Pb ages of monazite inclusions in garnet from the Himalaya of central Nepal. Chemical Geology 244, 1–24. doi:10.1016/j.chemgeo.2007.05.003.

Martin, A.J., DeCelles, P.G., Gehrels, G.E., Patchett, P.J., Isachsen, C., 2005. Isotopic and structural constraints on the location of the Main Central Thrust in the Annapurna Range, central Nepal Himalaya. Geological Society of America Bulletin 117, 926–944.

Martin, A.J., Ganguly, J., DeCelles, P.G., 2010. Metamorphism of Greater and Lesser Himalayan rocks exposed in the Modi Khola valley, central Nepal. Contributions to Mineralogy and Petrology 159, 203–223. doi:10.1007/s00410-009-0424-3.

Maxelon, M., Wohlers, A., Halama, R., Ring, U., Mortimer, N., Brandon, M.T., 1998. Ductile strain in the Torlesse Wedge, South Island, New Zealand. EOS 79 (45), 889.

Mattauer, M., 1986. Intracontinental subduction, crust-mantle decollemont and crustal-stacking wedge in the Himalayas and other collision belts. In: Coward, M.P., Ries, A.C. (Eds.), Geological Society of America Special Publication, vol. 19, pp. 37–50.

McNaught, M., Mitra, G., 1996. The use of finite strain data in constructing a retrodeformable cross-section of the Meade thrust sheet, southeastern Idaho, U.S.A. Journal of Structural Geology 18, 573–583.

McQuarrie, N., Robinson, D., Long, S., Tobgay, T., Grujic, D., Gehrels, G., Ducea, M., 2008. Preliminary stratigraphic and structural architecture of Bhutan: implications for the along-strike architecture of the Himalayan system. Earth and Planetary Science Letters 272, 105–117.

Means, W.D., 1989. Stretching faults. Geology 17, 893–896.

Means, W.D., 1994. Rotational quantities in homogeneous flow and the development of small- scale structures. Journal of Structural Geology 17, 893–896.

Means, W.D., Hobbs, B.E., Lister, G.S., Williams, P.F., 1980. Vorticity and noncoaxiality in progressive deformations. Journal of Structural Geology 2, 371–378.

Mitra, G., 1994. Strain variation in thrust sheets across the Sevier fold-and-thrust belt (Idaho- Utah-Wyoming): implications for section restoration and wedge taper evolution. Journal of Structural Geology 16, 585–602.

Mitra, G., Bhattacharyya, K., Mukul, M., 2010. The Lesser Himalayan duplex in Sikkim: implications for variations in Himalayan shortening. Journal of the Geological Society of India 75, 276–288.

Mitra, M., Boyer, S.E., 1999. Strain in the Lewis thrust sheet in the Provo salient of the Sevier fold-and-thrust belt: implications for basin restoration and estimates of critical taper. Geological Society of America Abstracts with Programs 31, 237.

Mukul, M., Mitra, G., 1998. Finite strain and strain variation analysis in the Sheeprock Thrust Sheet: an internal thrust sheet in the Provo salient of the Sevier Fold-and-Thrust belt, Central Utah. Journal of Structural Geology 20, 385–405.

Murphy, M.A., Yin, A., 2003. Structural evolution and sequence of thrusting in the Tethyan fold-thrust belt and Indus-Yalu suture zone, southwest Tibet. Geological Society of America Bulletin 115, 21–34.

Nautiyal, S.P., Jangpangi, B.S., Singh, P., Guha Sarkar, T.K., Bhate, V.D., Raghavan, M.R., Sahai, T.N., 1964. A Preliminary Note on the Geology of the Bhutan Himalaya. In: Rep. 22nd International Geological Congress, New Delhi, vol. 11, pp. 1–14.

Nickelsen, R.P., 1963. Fold patterns and continuous deformation mechanisms of the central Pennsylvania Appalachians. In: Cate, A.S. (Ed.), Tectonics and Cambrian–Ordovician Stratigraphy in the Central Appalachians of Pennsylvania. Pittsburgh Geological Society and Appalachian Geological Society, Pittsburgh, Guidebook, pp. 13–29.

Nickelsen, R.P., 1983. Aspects of Alleghanian deformation. In: Nickelsen, R.P., Cotter, E. (Eds.), Silurian Depositional History and Alleghanian Deformation in the Pennsylvania Valley and Ridge. Field Conference of Pennsylvania Geologists 49th Annual, Danville, Guidebook, pp. 29–39.

Onash, C.M., Shen-tu, B., Couzens-Schultz, B.A., 1998. Strain partitioning and factorization in quartz arenite. Journal of Structural Geology 20, 1065–1074.

Ong, P.F., van der Pluijm, B.A., Van der Voo, R., 2007. Early rotation and late folding in the Pennsylvania salient (U.S. Appalachians); evidence from calcite-twinning analysis of Paleozoic carbonates. Geological Society of America Bulletin 119, 796–804.

Passchier, C.W., Trouw, R.A.J., 1998. Microtectonics. Springer, New York, 289 pp.

Pêcher, A., Le Fort, P., 1986. The metamorphism in central Himalaya: its relations with the thrust tectonics. Sciences de la Terre, Mémoire 47, 285–309.

Poirier, J.P., Nicolas, A., 1975. Deformation-induced recrystallization by progressive misorientation of subgrain-boundaries, with special reference to mantle peridotites. Journal of Geology 83, 707–720.

Powell, C.M., Conaghan, P.J., 1973. Plate tectonics and the Himalayas. Earth and Planetary Science Letters 20, 1–12.

Pryer, L.L., 1993. Microstructures in feldspars from a major crustal thrust zone: the Grenville Front, Ontario, Canada. Journal of Structural Geology 15, 21–36.

Ramsay, J.G., 1967. Folding and Fracturing of Rocks. McGraw-Hill, New York, 568 pp.

Ramsay, J.G., Huber, M.I., 1983. Techniques of Modern Structural Geology. In: Strain Analysis, vol. 1. Academic Press, London, 307 pp.

Ratschbacher, L., Frisch, W., Liu, G., 1994. Distributed deformation in southern and western Tibet during and after the India-Asia collision. Journal of Geophysical Research 99, 19,917–19,945.

Ray, S.K., Bandyopadhyay, B.K., Razdan, R.K., 1989. Tectonics of a part of the Shumar allochthon in eastern Bhutan. Tectonophysics 169, 51–58.

Ray, S.K., 1995. Lateral variations in geometry of thrust planes and its significance, as studied in the Shumar allochthon, Lesser Himalayas, eastern Bhutan. Tectonophysics 249, 125–139.

Richards, A., Parrish, R., Harris, N., Argles, T., Zhang, L., 2006. Correlation of lithotectonic units across the eastern Himalaya, Bhutan. Geology 34, 341–344.

Ring, U., Brandon, M.T., 1999. Ductile deformation and mass loss in the Franciscan Subduction complex: implications for exhumation processes in accretionary wedges. In: Ring, U., Brandon, M.T., Lister, G.S., Willett, S.D. (Eds.), Exhumation Processes: Normal Faulting, Ductile Flow and Erosion. Geological Society of London Special Publication, 154, pp. 55–86.

Ring, U., Brandon, M.T., Ramthum, A., 2001. Solution mass-transfer deformation adjacent to the Glarus Thrust, with implications for the tectonic evolution of the Alpine wedge in eastern Switzerland. Journal of Structural Geology 23, 1491–1505.

Robin, P.Y., Torrance, J.G., 1987. Statistical analysis of the effect of sample size on paleostrain calculation. I. Single face measurements. Tectonophysics 138, 311–317.

Robinson, D.M., DeCelles, P.G., Garzione, C.N., Pearson, O.N., Harrison, T.M., Catlos, E.J., 2003. Kinematic model of the Main central thrust. Geology 31, 359–362.

Robinson, D.M., DeCelles, P.G., Copeland, P., 2006. Tectonic evolution of the Himalayan thrust belt in western Nepal: implications for channel flow models. Geological Society of America Bulletin 118, 865–885.

Rosenberg, C.L., Handy, M.R., 2005. Experimental deformation of partially-melted granite revisited: implications for the continental crust. Journal of Metamorphic Geology 23, 19–28.

Sanderson, D.J., 1982. Models of strain variation in nappes and thrust sheets: a review. Tectonophysics 88, 201–233.

Schmid, S.M., 1994. Textures of geological materials: computer model predictions versus empirical interpretations based on rock deformation experiments and field studies. In: Bunge, H.J., Siegesmund, S., Skrotzki, W., Weber, K. (Eds.), Textures of Geological Materials. DGM Informations-gesellschaft, Oberursel, pp. 279–302.

Searle, M.P., 1986. Structural evolution and sequence of thrusting in the high Himalayan, Tibetan-Tethys, and Indus suture zones of Zanskar and Ladakh, western Himalaya. Journal of Structural Geology 8, 923–936.

Sengupta, S., Raina, P.L., 1978. Geology of parts of the Bhutan foothills adjacent to Darjeeling district. Indian Journal of Earth Sciences 5 (1), 20–23.

Seno, S., Dallagiovanna, G., Vanossi, M., 1998. From finite strain data to strain history: a model for a sector of the Ligurian Alps, Italy. Journal of Structural Geology 20, 573–585.

Stephenson, B.J., Waters, D.J., Searle, M.P., 2000. Inverted metamorphism and the Main central thrust: field relations and thermobarometric constraints from the Kishtwar window, NW Indian Himalaya. Journal of Metamorphic Geology 18, 571–590.

Stipp, M., Stunitz, H., Heilbronner, R., Schmid, S.M., 2002. The eastern Tonale fault zone: a 'natural laboratory' for crystal plastic deformation over a temperature range from 250° to 700°C. Journal of Structural Geology 24, 1861–1884.

Stocklin, J., 1980. Geology of Nepal and its regional frame. Journal of the Geological Society of London 137, 1–34.

Swapp, S.M., Hollister, L.S., 1991. Inverted metamorphism within the Tibetan slab of Bhutan: evidence for a tectonically transported heat source. Canadian Mineralogist 29, 1019–1041.

Tangri, S.K., Pande, A.C., 1995. Tethyan sequence. In: Bhargava, O.N. (Ed.), The Bhutan Himalaya: a Geological Account. Geological Society of India Special Publication, 39, pp. 109–142.

Tangri, S.K., 1995a. Baxa Group. In: Bhargava, O.N. (Ed.), The Bhutan Himalaya: a Geological Account. Geological Society of India Special Publication, 39, pp. 38–58.

Tangri, S.K., 1995b. Diuri formation. In: Bhargava, O.N. (Ed.), The Bhutan Himalaya: a Geological Account. Geological Society of India Special Publication, 39, pp. 59–63.

Tullis, J., Yund, R.A., 1980. Hydolitic weakening of experimentally deformed Westerly granite and Hale albite rocks. Journal of Structural Geology 2, 439–451.

van Daalen, M., Meilbronner, R., Kunze, K., 1999. Orientation analysis of localized shear deformation in quartz fibres at the brittle-ductile transition. Tectonophysics 303, 83–107.

Voll, G., 1976. Recrystallization of quartz, biotite, and feldspars from Erstlfeld to the Leventina Nappe, Swiss Apls, and it geological significance. Schweizerische Mineralogische und Petrographische Mitteilunge 56, 641–647.

Wallis, S., 1995. Vorticity analysis and recognition of ductile extrusion in the Sambagawa belt, SW Japan. Journal of Structural Geology 17, 1077–1093.

White, S., 1977. Geological significance of recovery and recrystallization processes in quartz. Tectonophysics 39, 143–170.

Whynot, N., Grujic, D., Long, S., McQuarrie, N., 2010. Apparent temperature gradient across the Lesser Himalayan Sequence: Raman spectroscopy on carbonaceous material in the eastern Bhutan Himalaya. In: Leech, M.L., Klemperer, S.L., Mooney, W.D. (Eds.), Proceedings for the 25th Himalaya-Karakoram Tibet Workshop, San Francisco, California, U.S.A.. U.S. Geological Survey, Open-File Report, p. 1. 2010-1099. http://pubs.usgs.gov/of/2010-1099/whynot/.

Wilkerson, M.S., Dicken, C.L., 2001. Quick-look techniques for evaluating two-dimensional cross sections in detached contractional settings. American Association of Petroleum Geologists Bulletin 85, 1759–1770.

Woodward, N.B., Boyer, S.E., Suppe, J., 1989. Balanced Geological Cross-Sections: An Essential Technique in Geological Research and Exploration. Washington, American Geophysical Union Short Course in Geology 6.

Wotjal, S., 1986. Deformation within foreland thrust sheets by populations of minor faults. Journal of Structural Geology 8, 341–360.

Please cite this article in press as: Long, S., et al., Quantifying internal strain and deformation temperature in the eastern Himalaya, Bhutan: Implications for the evolution of strain in thrust sheets, Journal of Structural Geology (2011), doi:10.1016/j.jsg.2010.12.011

Wu, C., Nelson, K.D., Wortman, G., Samson, S.D., Yue, Y., Li, J., Kidd, W.S.F., Edwards, M.A., 1998. Yadong cross structure and South Tibetan Detachment in the east central Himalaya (89°–90°E). Tectonics 17, 28–45.

Yin, A., 2006. Cenozoic tectonic evolution of the Himalayan orogen as constrained by along- strike variation of structural geometry, exhumation history, and foreland sedimentation. Earth Science Reviews 76, 1–131.

Yin, A., Dubey, C.S., Kelty, T.K., Webb, A.A.G., Harrison, T.M., Chou, C.Y., Celerier, J., 2010. Geologic Correlation of the Himalayan Orogen and Indian Craton (Part 2): Structural Geology, Geochronology and Tectonic Evolution of the Eastern Himalaya. Geological Society of America Bulletin 122, 360–395. doi:10.1130/B26461.1.

Yonkee, A., 2005. Strain patterns within part of the Willard thrust sheet, Idaho-Wyoming-Utah thrust belt. Journal of Structural Geology 27, 1315–1343.

Yonkee, A., Weil, A.B., 2009. Reconstructing the kinematic evolution of curved mountain belts: Internal strain patterns in the Wyoming salient, Sevier thrust belt, U.S.A. Geological Society of America Bulletin 122, 24–49.

Please cite this article in press as: Long, S., et al., Quantifying internal strain and deformation temperature in the eastern Himalaya, Bhutan: Implications for the evolution of strain in thrust sheets, Journal of Structural Geology (2011), doi:10.1016/j.jsg.2010.12.011